CENTER FOR
COMPOSITE MATERIALS
AND STRUCTURES

Development and Verification of a Resin Film Infusion/Resin Transfer Molding Simulation Model for Fabrication of Advanced Textile Composites

John Douglas MacRae
Alfred C. Loos
H. Benson Dexter
Jerry W. Deaton
Gregory H. Hasko

Virginia Tech
VIRGINIA POLYTECHNIC INSTITUTE
AND STATE UNIVERSITY

BLACKSBURG , VIRGINIA
24061

December 1994

College of Engineering
Virginia Polytechnic Institute and State University
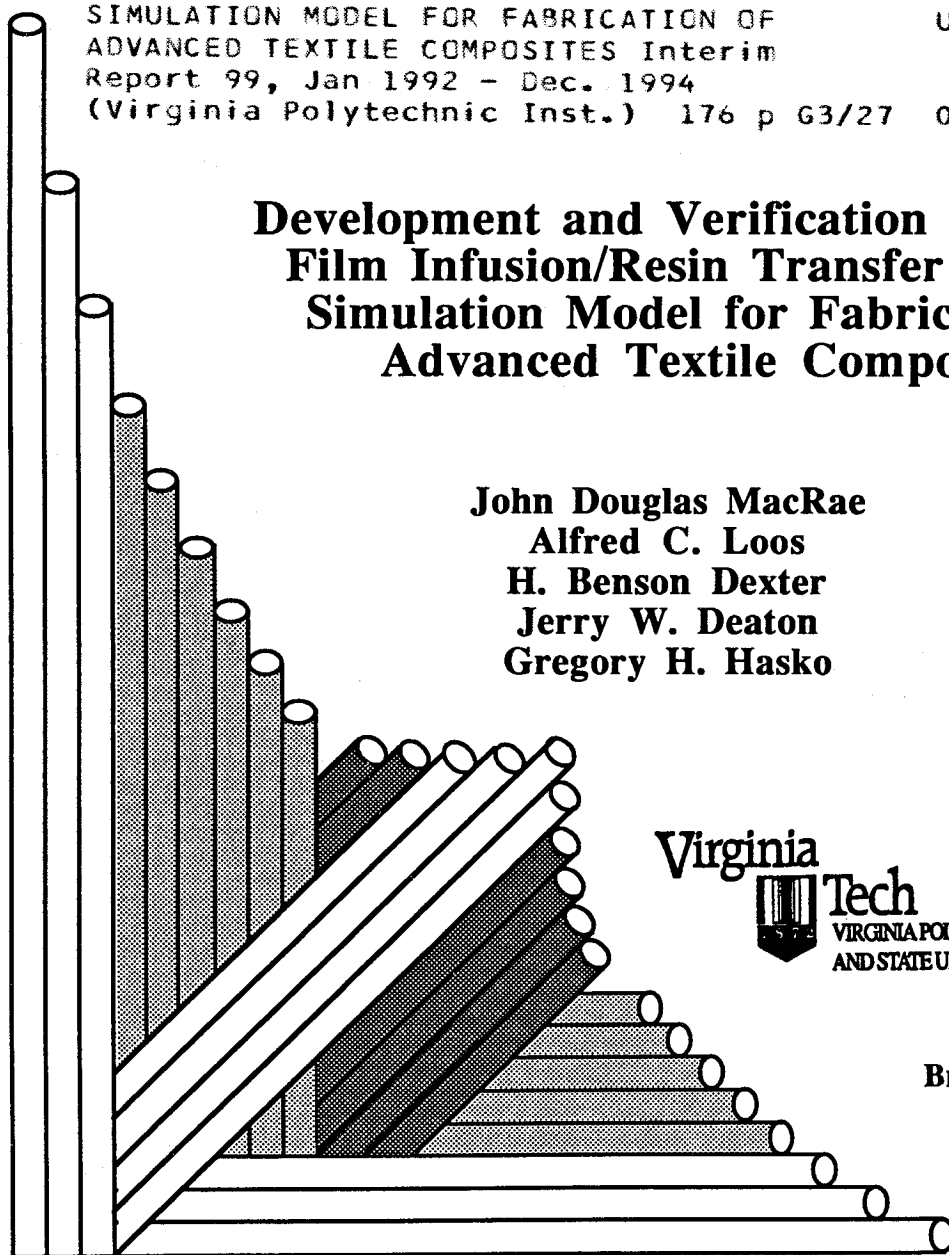Blacksburg, Virginia 24061

December 1994

CCMS-95-01
VPI-E-94-09

Development and Verification of a Resin Film Infusion/Resin Transfer Molding Simulation Model for Fabrication of Advanced Textile Composites

John Douglas MacRae[1]
Alfred C. Loos[2]
H. Benson Dexter[3]
Jerry W. Deaton[4]
Gregory H. Hasko[5]

Department of Engineering Science and Mechanics

1. Graduate Research Assistant, Department of Engineering Science and Mechanics, Virginia Polytechnic Institute and State University
2. Professor, Department of Engineering Science and Mechanics, Virginia Polytechnic Institute and State University
3. Senior Materials Research Engineer, Polymeric Materials Branch, NASA Langley Research Center, Hampton, VA
4. Senior Materials Research Engineer, Polymeric Materials Branch, NASA Langley Research Center, Hampton, VA
5. Principal Engineer, Lockheed Engineering and Sciences Company, Hampton, VA

DEVELOPMENT AND VERIFICATION OF A RESIN FILM INFUSION/RESIN TRANSFER MOLDING SIMULATION MODEL FOR FABRICATION OF ADVANCED TEXTILE COMPOSITES

ABSTRACT

The objective of this study was to develop a two-dimensional computer model for the simulation of the resin transfer molding/resin film infusion processing of advanced composite materials. This computer simulation model is designed to provide aircraft structure and tool designers with a method of predicting the infiltration and curing behavior of a composite material component. For a given specified cure cycle, the computer model can be used to calculate the resin infiltration, resin viscosity, resin advancement, heat transfer within the component/tool assembly during processing and preform compaction.

Formulations of the resin flow problem are given using the finite element/control volume technique based on Darcy's Law of flow through porous media. This technique allows for the efficient numerical calculation of the advancing resin front within the preform materials. The heat transfer in the fabric preform and tooling is analyzed using a transient finite element method which included the effects of convection on the tooling surfaces. Compaction behavior of the tooling assembly is analyzed using a simplified isotropic form of the plane elasticity equations. All of these solutions were coupled together in a quasi-steady state non-linear fashion inside the computer code.

Simulation model verifications were carried out on individual components of the computer model. A verification of the flow model is carried out by a comparison with experiments reported in literature as well as two dimensional visualization studies performed for a center-port injection of a flat plate. The heat transfer model was verified using the experimental results of a thick section composite laminate processing. Verification of the compaction model were limited to the comparison of the final part dimensions.

Two computer simulations were performed on two resin infusion cycles of a single blade-stiffened composite panel. The simulation model results of the two cycles were used to assist in the development of an alternative cycle for the composite manufacturing of a three blade stiffened panel. The results demonstrated the importance of a sufficient minimum viscosity region in the cycle in order to allow the resin to completely infiltrate the fabric preform of the structure. Predictions of the viscosities and degree of cure profiles within the single blade stiffened panel illustrated the uniformity of these parameters during the curing cycle.

ACKNOWLEDGEMENTS

Table of Contents

CHAPTER 6

CHAPTER 7

CHAPTER 8

CHAPTER 9

List of Figures

List of Figures

ix

List of Tables

CHAPTER 1

Introduction

Resin Transfer Molding (RTM) describes a manufacturing process that has been in existence since the early 1930's. Resin transfer molding developed into a viable manufacturing technique in the 1970's due to the oil embargo and the high cost of matched metal tooling.[1] Initially, resin transfer molding consisted of using polyester based resins with a chopped glass mat as the reinforcing medium. Automotive industries were the first to utilize the technique of resin transfer molding. As the techniques, resin systems, and tooling improved over the decade of the 70's, the application of resin transfer molding increased dramatically. The improvements in resin systems and reinforcements eventually generated considerable interest in the RTM process by the aerospace industry. In the early 80's, the

need for more cost efficient and lightweight structures demanded more use of fiber rein-
forced components in the aerospace and automotive industries.

Initially, aerospace industries began to manufacture components made with fiber rein-
forced tapes or fabrics using hand lay-up and forming operations. These prepreg materials
were either resin impregnated collimated tapes or woven fabrics. Today a large majority of
advanced composite components are still being manufactured from prepreg materials.
Labor costs in manufacturing components from prepreg tapes or fabrics have been high
due to the amount of hand labor and time involved.

Resin transfer molding of aerospace quality composite structures began as an effort to
reduce the high manufacturing cost of composite components. Although traditionally used
for their high specific strength, advanced composite commercial aircraft components
could not compete with metals if the cost of manufacturing those components remained
high. The resin transfer molding process offered a lower cost means of manufacturing.

A general description of the resin transfer molding process is where a fibrous component
is placed in a mold cavity which is then closed resulting in the compaction the fibrous pre-
form to the desired dimensions. A liquid resin is then injected into the mold cavity. Injec-
tion continues until all the remaining void space has been filled with resin. The mold
temperature is then raised, and the composite component is held at an elevated tempera-
ture until cured.

Aircraft structures that have been manufactured by the resin transfer molding technique
have been mainly secondary structures (which are not flight critical structures such as a
wing box or a fuselage beam). RTM has mainly been used for small detail parts where
structural integrity has not been critical or in applications where a high dimensional toler-
ance is required. However, for composite components to be utilized for flight critical

structures, the capability of designing and manufacturing these components at a competitive cost must be realized.

The RTM process offers several advantages over traditional prepregging methods. First, tight dimensional tolerances can be achieved due to the use of matched metal tooling. Second, complex shaped components can be readily fabricated. This allows for much more co-curing or integration of the structural components and not only reduces the cost of the structure but can reduce weight as well.

A variety of resin systems may be used with resin transfer molding. The only requirement is that the resin viscosity be low enough during the injection so that it is possible to effectively infiltrate the fabric preform and mold. Typical resin systems employed include epoxies, bismaleimides, polyesters, and some toughened epoxies. Also, a wide range of reinforcement types can be employed such as glass, graphite, or aramid fibers. Finally, the complete component fiber and resin volume fractions can be accurately predicted and controlled. This permits cost effective near net shape manufacturing of aircraft components.

Some of the disadvantages of the RTM process include the cost involved in the machining or fabrication of the mold. In many cases, the fabrication cost of the mold can be offset by manufacturing a large number of parts. However, in the aerospace industry, the quantities of the produced parts are relatively low, and therefore the amortization of these tooling costs is not necessarily effective in reducing the component costs to the point where they are competitive with traditional metal formed components. Another disadvantage to the RTM processing is the lack of high performance resin systems available. This issue has been partially addressed in recent years. However, most of the industry standard resin systems were designed for the prepregging process. Many of the resin suppliers are currently working towards producing high performance resin systems that have fluid viscosities that

are low enough to be resin transfer molded. Several of these new resin systems are being evaluated in non-primary aircraft structures.

In order to partially address those disadvantages described above, a new technique of resin transfer molding components has been developed by several aerospace companies. This new technique, known as resin film infusion (RFI) molding, combines the advantages of resin transfer molding with the flexibility of the traditional prepregging processing techniques. Resin infusion is performed by stacking a neat resin film and a fabric preform together inside a mold which consists of components similar to those used in autoclave processing of prepreg components. These components are then bagged and placed inside an autoclave or oven for processing at elevated temperatures. The advantages of the resin infusion technique are the ability to utilize lower cost tooling and to use many of the higher performance prepreg resin systems. The resin infusion technique was the composite processing method selected in this study.

Some of the challenges presented in the resin infusion processing of advanced composite materials include the need for a better understanding of the resin infiltration process and the effects of tooling, and the development of optimal processing cycles. The motivation for this study was to attempt to address these needs through the use of computer simulations of the resin infusion and resin transfer molding processes. The objective of this work was to provide a method by which structural and tool design engineers could analyze and predict many of the important processing variables prior to the processing of a composite component. The goal was to provide a comprehensive user friendly computer simulation model capable of meeting this objective.

CHAPTER 2

Literature Review

Previous studies of RTM processing have dealt with modeling the flow of resin through a porous medium in a variety of different manners. An important aspect of RTM modeling is the numerical techniques used to approximate the free surface location of the resin flow front. A survey of these reported moving boundary techniques and several experimental verification studies are described in this chapter.

2.1 Moving Boundary Techniques

There are many different techniques for modeling the resin boundary movement. The methods described in this section will only address those techniques which are currently

being utilized in the literature for the modeling of the resin infiltration process. There are three basic numerical methods that have been used to calculate the resin flow in a porous medium. These methods include the finite element, finite difference, and boundary element methods. A further classification of the methods can be made by grouping the techniques into either fixed or moving mesh schemes.

2.1.1   Fixed Mesh Methods

The first of the fixed mesh schemes is not currently being used for the study of RTM processing. However, it does provide the basis for a technique that is currently being used. The Marker-and-Cell method was originally developed for the study of incompressible viscous free surface flows in the field of hydraulics [2]. The technique was developed for a two-dimensional flow with simple geometries. The method uses a fixed finite element mesh and a set of marker particles that track the moving boundaries. The marker particles are started from some initial position within the mesh. Once the velocity field has been calculated the particles are then moved to a new position by using a weighted average of the four nearest cell velocities. The cells are then tagged as either full or empty, and the solution continues[2].

The finite difference/control volume technique is an extension of the Marker-and-Cell approach and is currently used in the modeling of the resin injection and RTM processes. The method, also known as FAN (Flow Analysis Network), calculates the fluxes at the cell boundaries and uses this information to calculate a fraction of the control volume that is filled at each time step. FAN also uses the lubrication approximation, which eliminates the out of plane velocities, to extend the original Marker-and-Cell method into a low Reynolds number regime. Takahasi and Matsuoka [3] have extended the FAN method to include the temperature field calculations necessary for RTM modeling. Several disadvan-

tages to this method were noted by Tucker[4]. These include the tedious lay-flat procedure used to model a 3-D part on a 2-D plane and the additional data required to connect the planes in the model.

The finite element/control volume method is another fixed mesh technique which has been applied to the resin transfer molding process [4]. This method is essentially a mixture of the finite element and the control volume approach introduced in the FAN program. The method is implemented by dividing the mold cavity into elements. At each nodal location a control volume is constructed by subdividing the elements into smaller volumes and summing the contributions of the adjacent volumes at each node. Element subdivision is carried out by breaking the element volume into smaller volumes connected at the centroid of the element. The finite element formulation is solved for the pressure distribution at the nodes. The nodal pressures are then used to calculate an elemental velocity. The flow rates into the various nodal control volumes are calculated using the velocity field. A fill factor based on the amount of the fluid present is assigned to each control volume. Flow front tracking involves finding all the partially filled control volumes[5,6]. Several advantages of the finite element control volume method were pointed out by Tucker [4]. These include the ability to handle complex geometries, numerical stability, ease of handling multiple vents and gates, and the ability to be easily extended to 3-D parts. This method was chosen as the basis for the RTM analysis reported in this document and will be discussed in greater detail in chapter 5.

2.1.2   Moving Mesh Methods

One of the current methods being used to model the flow of resin in RTM processing is the body-fitted or boundary-fitted coordinate system method [7]. The body-fitted coordinate system method is basically a finite difference method. In order to reduce the difficulty

involved in using a finite difference grid to model an irregularly shaped boundary, the method generates a curvilinear coordinate system over the physical domain. This coordinate system is then used to transform the physical domain into a regular computational domain. Remeshing occurs at each time step. The time step is calculated based on the velocity of the flow front. Smaller increments of time are used when the flow front approaches a sharp corner to maintain conservation of mass. The numerical costs of this technique are reported to be high because of the large number of time steps and the need for remeshing. The extensions of this technique to multiple injection ports and non-flat parts have presented some difficulties.[4]

The second moving mesh method that is currently being used in the simulation of the RTM process is the boundary element method. The boundary element method provides a solution to the governing equation for the fluid flow within the domain, but not the boundary conditions. Basically the method as reported in Um and Lee[8] involves the transformation of the governing differential equation into an integral equation which is valid on the boundaries of the region through the use of some "test" function. The integral equation is discritized and solved as in the finite element method. The velocity distribution on the boundary is then used to calculate a new position for the mesh at the next interval of time. Reported advantages to this method include the accuracy of both the velocity gradients and flow front positions (no interpolation of the flow front is necessary). Disadvantages include the difficulty with multiple gates and weldlines, extension to non-planar parts, and the handling of sharp corners.

2.2   RTM Experimental Verification Studies

Many examples of RTM simulation models are available in literature today. Several experimental model verification studies are discussed in this section. The studies selected give a representative cross section of the types of analyses being used in the simulation of the RTM process.

Um and Lee [8] employed the boundary element technique in modeling the flow of silicone oil through a simple rectangular mold of glass fabric. Darcy's law was employed to construct the governing differential equations. The resin front location was updated with the local velocities on the moving boundary. As the front approached the mold wall and if the newly calculated nodal position was outside the mold boundary, a corrected nodal location was placed where a line connecting the new and old nodal positions intersected the mold boundary. A "no slip" boundary condition was ignored in the analysis. The silicone oil used in Um's experimental work entered the rectangular mold through a center gate and proceeded to an exit in the far corner. Very close agreement between the calculated flow front positions and the experimentally determined values was reported.

Coulter, Smith, and Guceri [9] reported on the infiltration of a rectangular graphite panel with corn syrup. A boundary-fitted finite difference method was used to model the in-plane flow of the corn syrup from one corner of the mold across to the diagonally opposite corner. Again Darcy's law was used as the basis for the two-dimensional formulation. A stream function was included in the governing differential equation

$$\mu\left[\frac{\partial^2 \psi}{\partial x^2} + \left(\frac{K_y}{K_x}\right)\frac{\partial^2 \psi}{\partial y^2}\right] = 0 \qquad (2\text{-}1)$$

where K_x and K_y are the permeability of the fabric in the x and y directions, respectively, μ is the fluid viscosity, and ψ is the stream function. The TGIMPG computer program developed by Coulter and Guceri [9] is based on the boundary-fitted finite difference technique and uses a quasi-steady state time step during the infiltration process. The boundary conditions specified included constant velocity at the inlet, no slip along the walls of the mold, and a zero shear stress along the flow front. The new flow front position is determined from the velocities calculated along the flow front at the present time step. The contact between the resin and the mold wall is calculated with a "no-slip based relocation algorithm"[9]. Remeshing after each time step is required in the TGIMPG computer program.

The experimental results reported by Coulter, Smith, and Guceri agree well with the TGIMPG generated flow fronts except along the mold boundaries. The reason given for the discrepancy along the mold boundaries is use of the no-slip boundary condition. Measured and calculated inlet pressure versus time profiles were reported in this study. The measured and calculated pressure profiles matched well at the beginning and end of mold filling and poorly at intermediate fill times. The difference in the shape of the predicted and experimental flow front profiles was cited as the cause of this disagreement. The experimental investigation by Coulter, Smith, and Guceri will be discussed in greater detail in a latter chapter on model verification.

Finally, experimental investigations by Young et. al. [10] and Fracchia, Castro, and Tucker [6] using the finite element control volume method are discussed. The numerical formulations of the governing differential equations presented in each investigation were similar. Darcy's law was utilized in both works to replace the momentum equation. The governing differential equation was obtained by combining Darcy's law with the continuity equation

$$\frac{\partial}{\partial x}\left(\frac{K_{xx}}{\mu}\frac{\partial P}{\partial x}\right) + \frac{\partial}{\partial x}\left(\frac{K_{yy}}{\mu}\frac{\partial P}{\partial y}\right) = 0 \qquad (2\text{-}2)$$

where K_{xx} and K_{yy} are the permeabilities in the x and y directions, respectively, μ is the fluid viscosity, and P is the fluid pressure. Both Young [10] and Fracchia [6] used rectangular mold filling experiments to verify their computer models. Oil was used as the infiltrating fluid and random glass mats were used as a preform material for both investigations. A constant velocity injection of the oil was used in Young's [10] experiments whereas a varying pressure input was reported in Fracchia's case. The inlet pressure versus time profile reported by Young compared favorably to the experimentally measured pressures. Fracchia also reported the simulation results of a center gated and a twin gated resin transfer molded automotive head lamp assembly. Young's experimental investigation will be discussed in more detail in the chapter on verification latter in this document.

CHAPTER 3

Problem Definition

3.1   RTM Process

Resin transfer molding (RTM) is a process where a fibrous preform is placed in a closed mold, and a low viscosity resin is injected into the cavity until the preform and cavity have been fully saturated with resin. The injection is stopped, and the part is then cured at room or elevated temperature. This definition of RTM has changed somewhat over the years since the process was first introduced in the 70's. The term is now used to describe a variety of processes whereby a resin of some type is forced into a dry fibrous preform.

One variation of the RTM process is the resin film infusion (RFI) or resin film stacking process. In this process a neat resin film is placed along one surface of the tooling cavity and a fibrous preform is placed next to it. The mold is placed into an oven or autoclave. An external pressure is applied through either a clamping force or a hydrostatic pressure, as in the case of an autoclave. The mold is slowly allowed to close under this applied pressure. The mold assembly is heated, and the neat resin film softens and resin infiltrates the preform due to the applied pressure. The resin infiltrated part is then cured at elevated temperature and removed from the mold. During the process bulk flow of resin takes place concurrently with the resin infiltration of fiber bundles.

The flow of resin through fibrous preforms is commonly modeled as the flow of an incompressible fluid through a porous medium [11]. Flow through a porous medium can be described by Darcy's Law which states that the flow rate measured through a porous medium is linearly proportional to the pressure gradient, the permeability of the material, and inversely proportional to the fluid viscosity. Darcy's law is therefore an important part of any modeling effort of the RTM processing technique. A discussion of Darcy's law will be presented in a later chapter.

The tooling used in RTM processing generally consists of matched metal molds that provide a high degree of dimensional accuracy in the finished part. The processing is usually done in either a heated press or an oven. Generally, prior to the injection of the liquid resin, the mold is closed, and the preform is reduced to the final dimensions. Tooling used in resin infusion is generally considered "soft" tooling. "Soft" tooling consists of aluminum blocks, silicon rubber blocks, steel or aluminum caul sheets, and steel or aluminum baseplates. This type of tooling is arranged in a particular manner to produce the desired shape of the composite part. The dimensional accuracies of this type of tooling are usually

lower than the matched metal tooling used in traditional RTM processing. Also the cost of soft tooling is much lower than match metal tooling.

The resin systems used in RTM generally have a low viscosity (<0.3 Pa•s) in order to allow for easier processing. The majority of RTM processing done today is being done in the automotive industry where many different resin systems are available. The application of RTM to the aerospace industry has brought with it some additional performance requirements for the resin systems used. These requirements include higher T_g's, improved strength and toughness, and the need for good hot-wet material performance. In meeting these requirements the resin system manufacturers have formulated high molecular weight prepreg type resin systems. This in turn makes the processing by traditional resin injection difficult. The resin film infusion or resin stacking process provides a method where higher molecular weight and highly viscous resins may be used in the resin transfer molding process. The RFI process has been successfully demonstrated using resin systems designed for prepregging operations, such as Hercules 3501-6. These system have minimum viscosities in the range of 2-10 Pa•s. These viscosities are much too high for traditional RTM processing. However, resin film infusion processing allows for the use of these advanced resin systems while still retaining the benefits of the traditional RTM processing.

The resin infusion process has been utilized by the McDonnell Douglas Aircraft-West (MDA-West) as part of the NASA ACT (Advanced Composites Technology) demonstration program. Douglas used the resin infusion process to manufacture several demonstration wing box skins. The details of the use of this processing technique at Douglas and in the computer simulation effort are described in the next section.

3.2   Stiffened Panel Resin Infusion Processing

A good example of the resin infusion process is the three blade stiffened wing skin panels fabricated by MDA-West for the NASA ACT demonstration program. These wing skin panels were used to demonstrate the viability of the resin film infusion process as a cost effective means of manufacturing commercial aircraft primary structures. A description of the fabrication techniques and materials used in the resin infusion manufacturing of these three blade stiffened structures is included in this section.

Demonstration of the viability of advanced composite materials being used in a primary structure of a commercial aircraft depends largely on the ability to manufacture these structures at a low cost. The fabrication of the three blade stiffened panels by MDA-West was designed to demonstrate the ability to produce primary composite structures at low cost. The fabrication involved resin infusion of a stitched graphite preform by the RFI process. The stitched preform was manufactured using automated techniques in a further effort to reduce costs.

The fabrication of the three blade stiffened panel began with the creation of a neat resin film. One benefit of the resin infusion technique is the variety of resins which can be used. The only requirement is that the resin system chosen must have the ability to be cast into a hot-melt film. The resin system selected for use in the MDA-West panels was Hercules 3501-6. A resin film was made by taking the neat resin as supplied by Hercules in bulk form and placing required amount into a platen press. The resin was then heated in the press to lower the viscosity and pressed into a film with the desired thickness. At a future date, the resin films will be available in sheet form directly from the resin manufacturer.

Once the resin film had been prepared, it was placed on an aluminum base plate. Next, the stitched one piece fabric preform was placed on top of the resin film. Placement of the resin film and preform is shown in Figure 1. Additional aluminum tooling blocks were then placed in-between the blade stiffeners. The last phase was to place an aluminum or a graphite caul sheet over the entire assembly. The assembly at this point is shown in Figure 2. Finally, the whole assembly was then placed in a vacuum bag and into an autoclave for processing under elevated temperature and pressure.
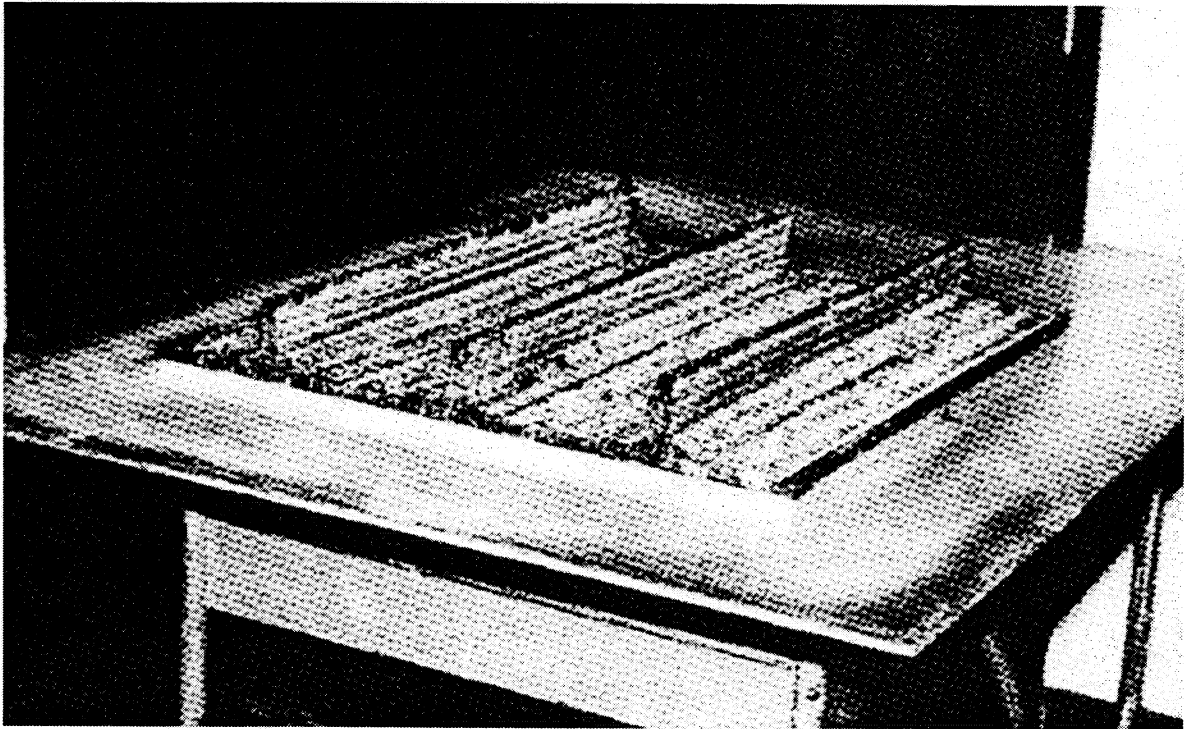
FIGURE 1 Placement of resin film and three blade stitched preform in Douglas tooling.
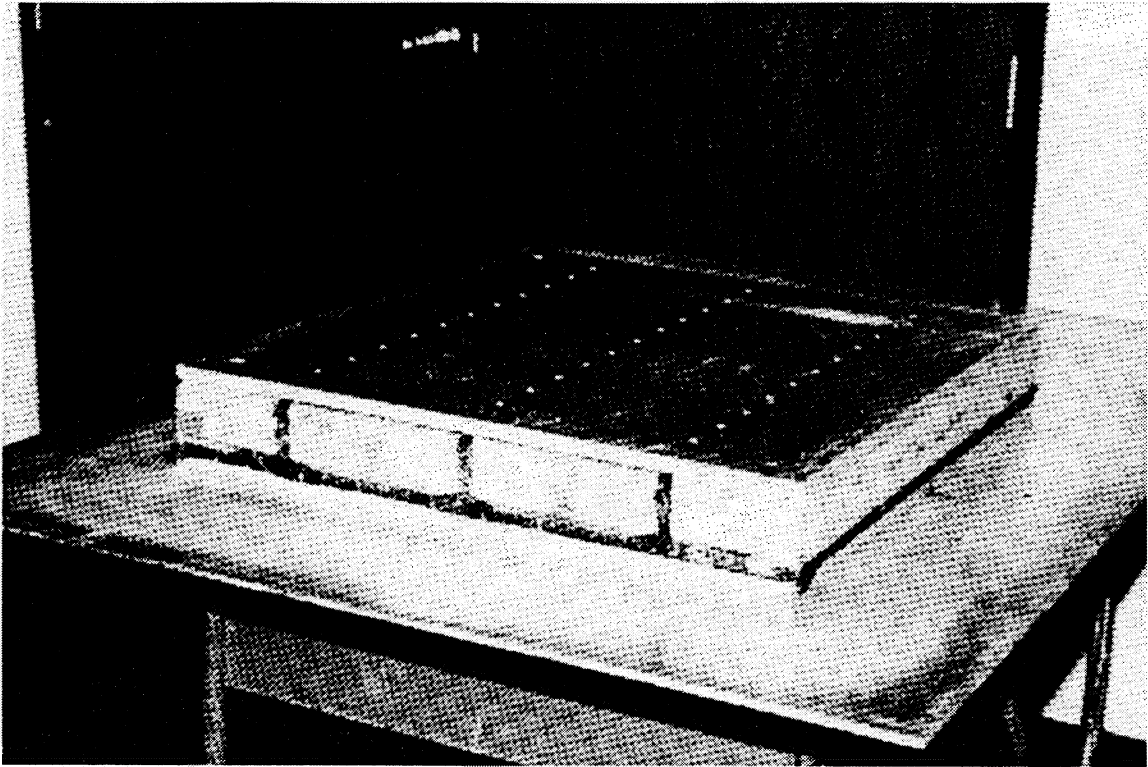
FIGURE 2 Complete three blade stiffened tooling assembly, prior to bagging.

The stitched fabric preform consisted of a 54-ply stitched preform skin and a 72-ply stitched preform blade. Each of these two sub elements of the preform were stitched together to make the three blade stiffened panel. The 72-ply blade was split into two sections at the bottom of the blade. These two sections were folded outward and then stitched down to the 54-ply skin. The folded regions of the blade, which were stitched to the skin, were allowed to taper off in 9-ply sections. A schematic of this stiffener element is shown in Figure 3 and an actual photograph of one of the single stiffeners is shown in Figure 4. Both the 54-ply skin and 72-ply blade are made up of nine-ply stitched subelements made of AS-4 uniweave fabric. Uniweave fabrics of different orientations were placed on rolls and feed into a multineedle stitching machine.
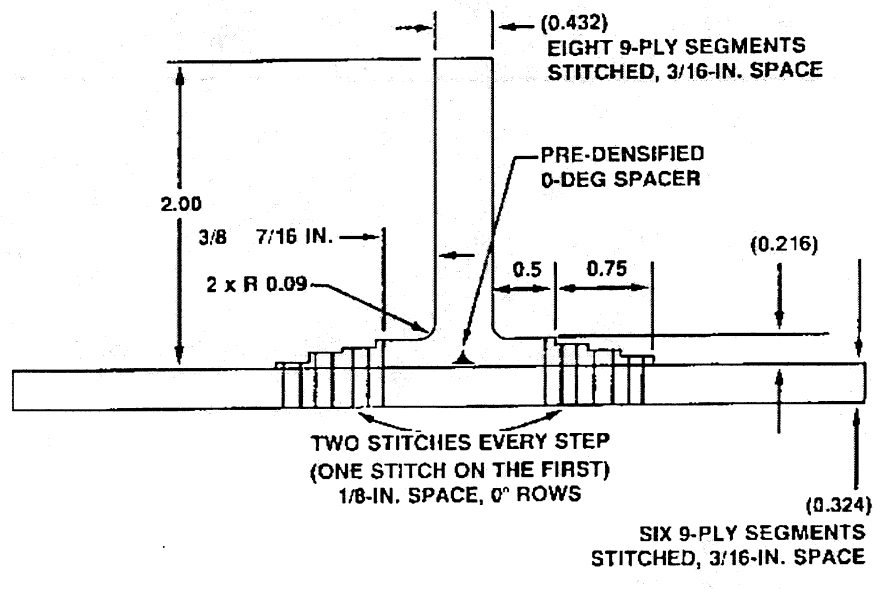
FIGURE 3 Schematic of stiffener design for the three blade panel.
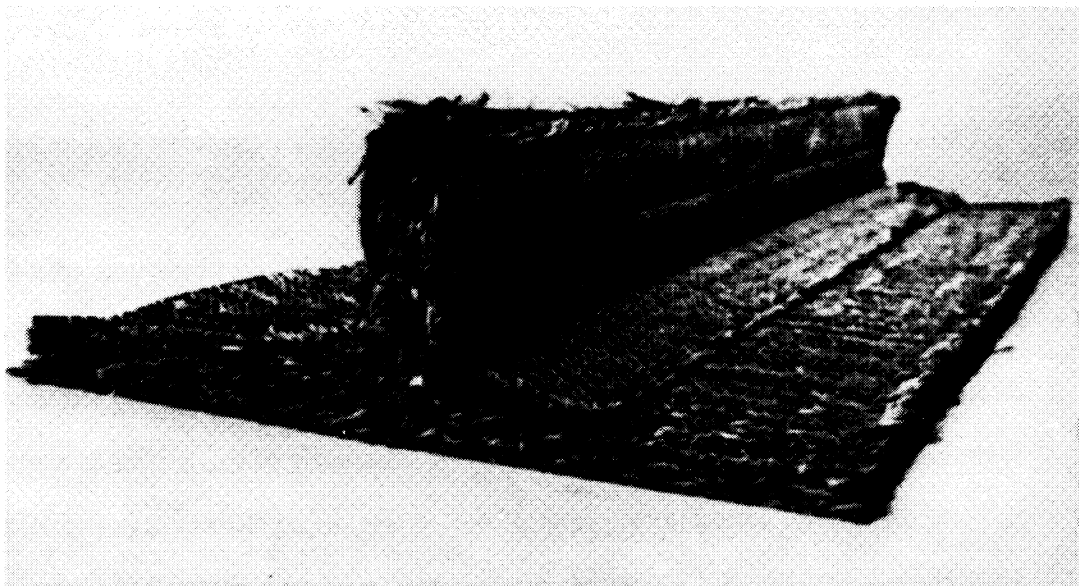
FIGURE 4 Photograph of single stitched blade stiffener.

```
0°
+45°
0°
-45°
0°
+45°
0°
-45°
90°

STORAGE
TENSION
ROLLS

LOCATING          MULTINEEDLE          STORE
ROLLS             STITCHING MACHINE    ON ROLL

0°  = 95% 0° UNIWOVEN CARBON CLOTH
45° = 95% 45° UNIWOVEN CARBON CLOTH
90° = 95% 90° UNIWOVEN CARBON CLOTH

STITCHING YARN — TBD
```
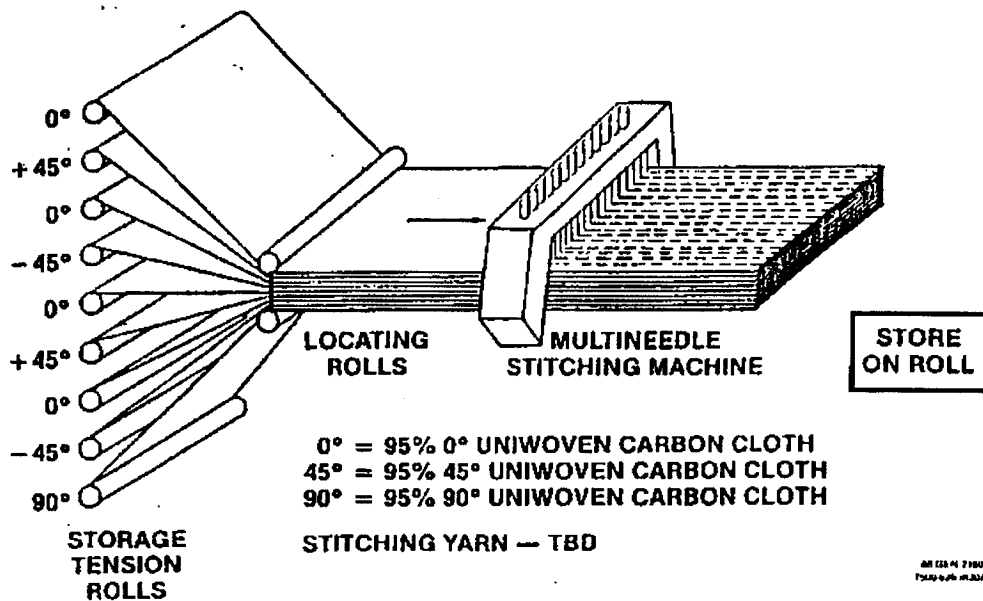
FIGURE 5 Schematic of manufacturing of nine-ply subelements.

The nine-ply stitched fabric was then stored on a roll and used later in the assembly of the skin and blade elements. A schematic of this process in shown in Figure 5. Several of these three blade stiffened panels have been manufactured by MDA-West during the course of the ACT program. A photograph of one of these panels is shown in Figure 6. During the manufacturing of these panels many different processing cycles were developed and tested. Many of the processing cycles tested were unsuccessful. An attempt was made to incorporate the lessons learned in manufacturing along with the insight gained from a computer simulation of this process into an optimum manufacturing cycle. The remaining chapters in this document illustrate the efforts to model the resin infusion processing of this three blade stiffened panel.
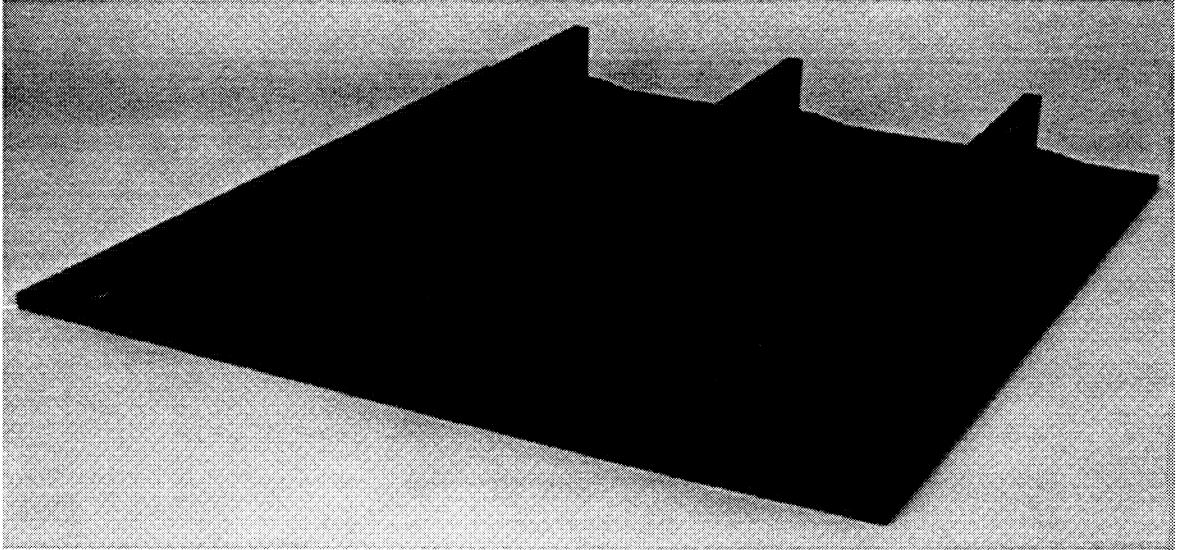
FIGURE 6 Photograph of the final three blade stiffened composite panel.

CHAPTER 4

Infiltration/Cure Model

In order to improve the cost effectiveness of the RTM process, a method by which the designer can test and validate manufacturing concepts such as tooling, processing cycles, and material compatibilities must be found. The computer simulation of this complex processing environment will allow these types of variables to be analyzed without the expensive and costly trial-and-error approach currently used in much of the advanced composite processing arena. A two-dimensional RTM process simulation model has been developed which can be used to predict the critical parameters in resin transfer molding. Parameters such as the part/mold temperature distribution, the resin kinetics and viscosity, and the resin fluid motion through the fabric preform are predicted using this model. The formula-

tion of the computer model will be discussed in this chapter. Each of the five sub-models will be introduced and the theory behind each addressed. The five sub-models which make up the computer simulation model include:

1) Flow sub-model

2) Kinetics sub-model

3) Viscosity sub-model

4) Heat Transfer sub-model

5) Compaction sub-model

4.1   Flow Sub-Model

One of the most important events in the RTM process that must be included in the computer simulation is the resin flow into the fabric preform. This information will allow tool designers to locate potential trouble spots in the infiltration of the fabric preform such as dry spots, low pressure regions, and resin rich regions. The fluid sub-model was developed for a two-dimensional complex shaped composite structure. The assumptions made in the formulation of the model include:

1) The preform material consists of a heterogeneous anisotropic porous media.

2) The resin may be modeled as an incompressible Newtonian fluid.

3) A no-slip boundary condition is not enforced along the boundaries of the tooling assembly, due to limitations in the numerical technique used to determine the flow front. (See Chapter 5)

4) Capillary and inertia effect are neglected (low Reynolds Number flow).

5) Resin must be contained inside the mold assembly.

The general expression for the continuity equation can be written as

$$\frac{\partial \rho}{\partial t} + \vec{\nabla} \bullet (\rho \vec{v}) = 0 \qquad (4\text{-}1)$$

where ρ is the density of the resin (assumed constant) and $\vec{v}$ is the average velocity of the resin. Assuming an incompressible fluid and defining the superficial velocity $\dot{v}$ for fluid flow in a porous material as

$$\dot{v} = \frac{v}{\phi} \qquad (4\text{-}2)$$

where ϕ is the porosity of the preform, the continuity equation (4-1) reduces to

$$\frac{\partial \dot{v}_x}{\partial x} + \frac{\partial \dot{v}_y}{\partial y} = 0 \qquad (4\text{-}3)$$

Since the domain into which the resin flows is a porous fabric preform, the flow sub-model uses Darcy's law as the appropriate equation of motion to predict this movement. The one-dimensional form of Darcy's law can be expressed as:

$$Q = -\frac{kA}{\mu}\frac{\partial P}{\partial x} \qquad (4\text{-}4)$$

where Q is the volumetric flow rate, k is the permeability of the material, μ is the viscosity of the resin, and A is the cross sectional area. Considering an anisotropic porous material, Darcy's Law may then be rewritten as:

$$\dot{v}_i = -\frac{k_{ij}}{\mu}\frac{\partial P}{\partial x_j} \tag{4-5}$$

where k_{ij} is the full permeability tensor. This form of the equation will allow for the prediction of the resin flow front velocity as it moves through the fabric preform. In order for Darcy's law to hold, the flow must maintain low a Reynolds number and the effects of capillary and inertia forces are assumed insignificant.

Substituting equation (4-5) into equation (4-3) one obtains a general expression which describes the pressure distribution within the fabric preform. The two-dimensional form of this equation is:

$$-\frac{\partial}{\partial x}\left[\frac{k_{xx}}{\mu}\frac{\partial P}{\partial x} + \frac{k_{xy}}{\mu}\frac{\partial P}{\partial y}\right] - \frac{\partial}{\partial y}\left[\frac{k_{xy}}{\mu}\frac{\partial P}{\partial x} + \frac{k_{yy}}{\mu}\frac{\partial P}{\partial y}\right] = 0 \tag{4-6}$$

The solution of equation (4-6) provides the pressure distribution within the saturated portion of the fabric preform. No transient terms are included in this formulation due to the piecewise linear approximation of the time dependence in the finite element control volume scheme used in the computer model for solving the moving boundary problem. The finite element control volume scheme will be addressed in detail in the next chapter.

The solution of the governing equation expressed in equation (4-6) must include the specification of boundary conditions. The boundary conditions used most frequently in the solution of RTM design problems include a constant pressure inlet, constant flow rate at the inlet, and the specification of no flow through the mold walls. Specification of inlet pressure simply means that at any time during the infiltration process the inlet pressure is known.

$$P_i = P_{applied} \qquad (4\text{-}7)$$

Specification of a constant flow at the inlet is written as follows:

$$Q_n = n_x \left(\frac{k_{xx}}{\mu} \frac{\partial P}{\partial x} + \frac{k_{xy}}{\mu} \frac{\partial P}{\partial y} \right) + n_y \left(\frac{k_{xy}}{\mu} \frac{\partial P}{\partial x} + \frac{k_{yy}}{\mu} \frac{\partial P}{\partial y} \right) \qquad (4\text{-}8)$$

Here $\hat{n}$ is the unit vector normal to the surface at the inlet. Flow through a mold wall may be restricted by requiring the boundary to be specified such that:

$$Q_n = 0 \qquad (4\text{-}9)$$

The solution of the governing equation (4-6) with the boundary conditions specified in equations (4-7) or (4-8) and equation (4-9) results in the resin pressure distribution within the preform. Once the pressure distribution is known, it is substituted into equation (4-5) for the solution of the velocity field within the resin saturated preform. Velocity field information is then used in the moving boundary technique (i.e. finite element control volume technique) to solve for the resin flow fronts.

4.2   Kinetics Sub-Model

RTM processing of advanced composite materials most often involves the use of thermo-setting resin systems. Due to the fact that these resin systems have an inherent chemical reaction that causes a network of polymer chains to crosslink, the fluid and mechanical properties of this class of materials is greatly dependent on the processing conditions. Resin systems used in RTM tend to be relatively fluid upon heating and will normally stay that way during some processing "window" in which infiltration must take place. During this processing "window", a large exothermic reaction sometimes takes place which can

generate a significant amount of heat. As time proceeds the resin system rapidly becomes less fluid and begins to solidify. In order to accurately model the RTM processing using these resin systems, some method of predicting these events is necessary.

The kinetics sub-model provides for the estimation of the curing parameters such as degree of cure and the amount of heat evolved during the curing process. In addition to directly providing values for degree of cure and heat generation, the kinetics sub-model provides input for the viscosity sub-model which calculates the viscosity of the resin system during processing.

If the assumption is made that the rate of heat generation during the curing process is proportional to the rate of the cure reaction, then the degree of cure of the resin can be defined as

$$\alpha = \frac{H(t)}{H_r} \tag{4-10}$$

where $H(t)$ is the amount of heat evolved during the curing reaction up to some time t and H_r is the total heat of reaction evolved during the entire curing process per unit mass. The degree of cure of the resin can also be defined as

$$\alpha = \int_0^t \left(\frac{d\alpha}{dt}\right) dt \tag{4-11}$$

where $\frac{\partial \alpha}{\partial t}$ is the reaction or cure rate. The heat evolved at any time $H(t)$ can be expressed as:

$$H(t) = \int_0^t \frac{dq'}{dt} dt \tag{4-12}$$

where $\dfrac{dq'}{dt}$ or $\dot{H}$ is the rate of heat generation from the reaction. H_r may be expressed in

a similar way as:

$$H_r = \int_{0}^{t_f} \frac{dq'}{dt}\, dt \tag{4-13}$$

where t_f is the time of reaction completion. The heat of reaction for the resin saturated

preform can be expressed as:

$$H_R = \frac{\rho_r}{\rho_c} v_r H_r \tag{4-14}$$

where ρ_c is the density of the resin saturated preform, ρ_r is the density of the resin, v_r is

the resin volume fraction. Combining equations (4-10) through (4-14) we get an expres-

sion for the cure rate.

$$\frac{d\alpha}{dt} = \frac{1}{H_R}\frac{dq'}{dt} = \frac{1}{H_R}\dot{H} \tag{4-15}$$

The cure rate, as well as the degree of cure of the resin system, is a function of the time

and temperature history of the resin system. These parameters are typically determined

using the Differential Scanning Calorimeter. By rearranging the expression (4-15) we can

get a relation for the source term which must be added to the expressions in the heat trans-

fer sub-models to account for the heat generated during the curing reaction.

$$\dot{H} = \frac{d\alpha}{dt}H_R \tag{4-16}$$

For the thermosetting resin system used in this work, the cure rate is expressed as a rate equation.

$$\frac{d\alpha}{dt} = A\,exp\,(\frac{-E}{RT})f(\alpha) \qquad (4\text{-}17)$$

where A is a pre-exponential factor, E is the activation energy, R is the gas constant, T is the temperature of the sample, and $f(\alpha)$ is a reaction function.

The resin system chosen for use in the experimental studies discussed in Chapter 8 was Hercules 3501-6. A kinetics model was developed for this resin system by Chiou and Letton [11]. This analytical model was incorporated into the kinetics sub-model. Chiou and Letton broke the complex reaction down into three smaller reactions which would sum to the total reaction of the resin system. The thermal analysis method chosen used a series of dynamic scanning calorimeter (DSC) scans on the 3501-6 resin system. The DSC scans were each made at a constant heating rate, $\beta = \frac{dT}{dt}$. Rewriting equation (4-17) including a constant heating rate gives:

$$\frac{d\alpha}{dT} = \frac{A}{\beta}exp\,(\frac{-E}{RT})f(\alpha) \qquad (4\text{-}18)$$

For amine-cured epoxy resins the reaction functions chosen may be of several forms. One can use either a n-th order reaction, $f(\alpha) = (1-\alpha)^n$ or an autocatalytic reaction, $f(\alpha) = \alpha^m(1-\alpha)^n$. Here m and n are the reaction orders. Chiou and Letton broke the complex reaction of 3501-6 into three independent reactions and developed a new expression for the cure rate.

$$\frac{d\alpha}{dT}_{total} = \sum_{i=1}^{3} g_i \frac{A_i}{\beta} exp\left(\frac{-E_i}{RT}\right) f_i(\alpha_i) \tag{4-19}$$

In this expression g_i is a weighting function for each of the three reactions and is defined as

$$g_i = \frac{H_i}{H_{total}} \tag{4-20}$$

where H_i is the heat of reaction for each independent reaction. H_{total} is equivalent to H_R. The sum of g_i is one for the reaction. Using equation (4-19) and the fact that

$$\frac{d\alpha}{dT} = \frac{1}{H}\frac{dH}{dT} \tag{4-21}$$

an expression for converting the experimental DSC traces into reaction components is developed.

$$\frac{dH}{dT}_{exp} = \sum_{i=1}^{3} H_i \frac{A_i}{\beta} exp\left(\frac{-E_i}{RT}\right) f_i(\alpha_i) \tag{4-22}$$

From this expression the g_i's can be calculated and the reaction orders can be determined. The reaction functions used for the 3501-6 reaction system are all n-th order. The parameters A_i, E_i, and H_i are all determined experimentally by DSC. The details of the fitting of these parameters can be found in Chiou and Letton [11]. Table 1 provides the kinetic parameters for the 3501-6 resin system used in the kinetics sub-model.

TABLE 1 Kinetic Parameters for the Complex Cure Reaction of Hercules 3501-6.

Reaction	H	lnA	E/R	n	g
	(J/g)	(1/sec)	(°K)		
Major	427.8	17.37	11220	1.06	0.85
Medium	50.0	19.16	10250	1.17	0.095
Minor	27.4	46.22	20570	3.05	0.055

4.3   Viscosity Sub-Model

In order to calculate the resin infusion into the fabric preform, the viscosity must be known as a function of position, temperature, and time. The viscosity of a thermosetting resin system is a function of the temperature of the resin, the extent of reaction of the resin, and the shear rate of the resin. The goal of the viscosity sub-model is to provide a means of predicting the viscosity of the resin system within the environment created in the resin transfer molding process. Due to the complex nature of the relationships between the viscosity parameters, analytical expressions are not available at the present time. A reasonably good approximation can be made by assuming that the resin system viscosity is not strongly dependent on shear rate in the flow regime described by RTM processing and therefore the resin may be modeled as a Newtonian fluid. This approximation may fail if the shear rates in the resin system become significantly high in areas such as the inlet to a mold. However, in a practical sense the Newtonian assumption provides a reasonable first approximation. The viscosity of the resin systems would then be measured at low shear rates and then fit to a function which includes the effects of both temperature and degree of cure. The expression for this relationship is the well known Williams-Landel-Ferry or WLF equation,

$$ln\left[\frac{\eta\,(T)}{\eta\,(T_g)}\right] = \frac{-C_1\,(T-T_g)}{C_2+(T-T_g)} \tag{4-23}$$

where $\eta\,(T)$ is the temperature dependent viscosity and $\eta\,(T_g)$ is the viscosity at the glass transition temperature T_g. C_1 and C_2 are experimental constants.

As mentioned in the previous section, the resin system used in this investigation is Hercules 3501-6. The viscosity data used for fitting the WLF equation come from the work done by Chiou and Letton [11].

In order to fit equation (4-23), the relationship between degree of cure and T_g must be established. By developing a master viscosity curve from a series of viscosity measurements made at varying isothermal and dynamic temperature profiles and correlating these results with degree of cure calculated using the kinetics modeling described in the previous section, Chiou and Letton developed a fifth-order polynomial fit of T_g vs. α.

$$T_g = 283.42 + 196.4\alpha - 925.4\alpha^2 + 3435\alpha^3 - 4715\alpha^4 + 2197\alpha^5 \tag{4-24}$$

Also, the relationship between viscosity and degree of cure was determined to be:

$$ln\,[\eta\,(T_g)] = 20.72 + 8.56\alpha - 9.69\alpha^2 + 41.17\alpha^3 \tag{4-25}$$

The constants C_1 and C_2 determined from the master curve were

$$\begin{aligned} C_1 &= 29.667 \\ C_2 &= 36.926 \end{aligned} \tag{4-26}$$

From the relationships presented in equations (4-23) through (4-26) and knowing the initial extent of reaction of the resin system it is possible to predict viscosity as a function of temperature and degree of cure.

Therefore, the viscosity sub-model uses information provided by the kinetics sub-model (the degree of cure) and the heat transfer sub-model (temperature distributions) to determine the viscosity of the resin system as a function of temperature, time, and position within the fabric preform.

4.4   Heat Transfer Sub-Model

One of the most important aspects of the modeling of the resin transfer molding process is the prediction of the temperature distribution within the part/tool assembly. The importance of an accurate solution of the temperature inside the manufactured part cannot be overstated. The temperature history that the part undergoes during processing can have a profound effect on the part's integrity. The temperature can effect the viscosity and degree of cure of the resin system, the final dimensions of the part, and the mechanical properties of the finished part. The expansion coefficients of the various types of tooling used in RTM processing must be analyzed closely since expansion can directly effect the quality of the finished part. Also, varying the thermal history of a part can influence the mechanical properties through the degrees to which the resin has been allowed to crosslink and any residual stresses have developed.

The heat transfer sub-model is based on the two-dimensional transient heat transfer equation which includes a term for heat generation [17].

$$\rho C_p \frac{\partial T}{\partial t} - \frac{\partial}{\partial x}\left(a_{xx}\frac{\partial T}{\partial x} + a_{xy}\frac{\partial T}{\partial y}\right) - \frac{\partial}{\partial y}\left(a_{yx}\frac{\partial T}{\partial x} + a_{yy}\frac{\partial T}{\partial y}\right) - u''' = 0 \qquad (4\text{-}27)$$

where:

ρ = Density of the material

C_p = Specific heat of the material

a_{ij} = Thermal conductivity of the material

$u''' = \rho\dot{H}$ = Heat generation term due to resin chemical reactions

In equation (4-27) it is assumed that the material is anisotropic and viscous heat generation due to the flowing polymer melt has been neglected. The density of the material is assumed to remain constant throughout the processing cycle. Although the density of the resin will change due to the chemical changes taking place during cure, the change is slight and a good approximation is to use a constant value. Equation (4-27) is valid for the saturated and unsaturated regions of the fabric preform and the tooling surrounding the preform. Each region (e.g. the aluminum tooling, unsaturated fabric preform) will have a different set of material properties and possibly a source term as is the case for the resin saturated fabric preform region.

The solution of equation (4-27) can be obtained only after the specification of the initial and boundary conditions. The initial conditions require that the preform/tool assembly initial temperature distribution be specified.

$$T_i = T(x, y, t) = T(x, y, 0) \qquad (4\text{-}28)$$

The only boundary condition used in the heat transfer sub-model is the convective boundary condition written as follows

$$\left[n_x \left(a_{xx}\frac{\partial T}{\partial x} + a_{xy}\frac{\partial T}{\partial y} \right) + n_y \left(a_{xy}\frac{\partial T}{\partial x} + a_{yy}\frac{\partial T}{\partial y} \right) \right] + \beta \left(T - T_\infty \right) = \hat{q} \qquad (4\text{-}29)$$

where $\vec{n}_i$ represents a unit vector normal to the boundary, β is the heat transfer coefficient, T_∞ is the autoclave air temperature and $\hat{q}$ is a specified heat flux.

The first term in equation (4-29) represents the heat transfer due to conduction, the second is the heat flux due to convection, and the third is the specified heat flux. Equation (4-29) allows not only for convective boundaries but also for the specification of several other types of conditions at the boundary. A constant temperature boundary can be approximated by setting the value of β to a very high value and setting the value of T_∞ to the specified temperature. In this manner a specified temperature profile may be input by giving T_∞ as a function of time. An adiabatic or zero heat flux boundary may be specified by setting $\hat{q}$ equal to zero. This provides some flexibility during the numerical implementation of these conditions as described in the next chapter.

The solution of equation (4-27), subject to the conditions in equations (4-28) and (4-29), will provide the temperature distribution throughout the part/tool assembly. The numerical implementation of these equations will be discussed in detail in the section on heat transfer in the next chapter.

4.5 Compaction Sub-Model

The compaction sub-model was included in the RFI process model to estimate the final part dimensions, resin and fiber mass, the amount of pressure necessary for consolidation,

and the total amount of resin needed to completely saturate the fabric preform during processing. The application of pressure is necessary in resin film infusion to ensure that the preform is compacted to the desired dimensions and fiber volume fraction. This sub-model was developed to specifically address preform compaction due to pressure application and thermal expansion during the resin film infusion process. The process, as described earlier, uses an autoclave to apply pressure to the part/tool assembly in a controlled manner. However, the autoclave pressure is also augmented by the expansion of the tooling and the initial compaction of the preform during loading. The criteria used in developing the model were that the model be compatible with the existing sub-models, use a minimum of computation time, and provide reasonable accuracy. If the geometry and loading do not vary along the length of the preform then a plane strain analysis is acceptable.

If it is assumed that the displacement in the z direction (assuming z is much larger than the x or y dimensions of the computational domain) is zero at every cross section then:

$$\varepsilon_z = \gamma_{yz} = \gamma_{xz} = 0 \tag{4-30}$$

and the remaining nonzero strain components are:

$$\varepsilon_x = \frac{\partial u}{\partial x} \qquad \varepsilon_y = \frac{\partial v}{\partial y} \qquad \gamma_{xy} = \frac{\partial u}{\partial y} + \frac{\partial v}{\partial x} \tag{4-31}$$

Here u and v are the displacements in the x and y directions respectively.

The equilibrium equations are described as follows:

$$\frac{\partial \sigma_x}{\partial x} + \frac{\partial \tau_{xy}}{\partial y} + f_x = 0$$

$$\frac{\partial \tau_{xy}}{\partial x} + \frac{\partial \sigma_y}{\partial y} + f_y = 0$$

(4-32)

where σ_i and τ_{ij} are the principal and shear stresses respectively, f_x and f_y are the body forces in the x and y directions. The thermal expansion effects of the tooling are included in the body force terms.

The materials commonly used in the RFI manufacturing process include aluminum tooling, silicon rubber tooling, resin saturated graphite preforms, dry graphite preforms, and graphite-epoxy tooling structures. As a first approximation the materials were assumed to be isotropic and linearly elastic. This would greatly simplify the necessary analysis and numerical calculations.

The constitutive relations are:

$$\sigma_x = C_{11}\varepsilon_x + C_{12}\varepsilon_y$$

$$\sigma_y = C_{12}\varepsilon_x + C_{22}\varepsilon_y$$

$$\tau_{xy} = C_{33}\gamma_{xy}$$

(4-33)

where

$$C_{11} = C_{22} = \frac{E}{1-v^2} \qquad C_{12} = \frac{vE}{1-v^2} \qquad C_{33} = \frac{E}{2(1-v)}$$

(4-34)

where v is Poisson's ratio and E is the modulus of elasticity.

The boundary conditions can be applied as either specified displacements or traction forces.

$$u = u_i$$
$$v = v_i$$

(4-35)

$$\sigma_x n_x + \tau_{xy} n_y = \hat{t}_x$$
$$\tau_{xy} n_x + \sigma_y n_y = \hat{t}_y$$

(4-36)

By substituting the strain displacement relations and the constitutive equations into the equilibrium equations an expression in terms of displacements can be found.

$$-\frac{\partial}{\partial x}(C_{11}\frac{\partial u}{\partial x} + C_{12}\frac{\partial v}{\partial y}) - C_{33}\frac{\partial}{\partial y}(\frac{\partial u}{\partial y} + \frac{\partial v}{\partial x}) = f_x$$
$$-C_{33}\frac{\partial}{\partial x}(\frac{\partial u}{\partial y} + \frac{\partial v}{\partial x}) - \frac{\partial}{\partial y}(C_{12}\frac{\partial u}{\partial x} + C_{22}\frac{\partial v}{\partial y}) = f_y$$

(4-37)

Looking at the boundary conditions including traction vectors we have:

$$(C_{11}\frac{\partial u}{\partial x} + C_{12}\frac{\partial v}{\partial y}) n_x + C_{33}(\frac{\partial u}{\partial y} + \frac{\partial v}{\partial x}) n_y = \hat{t}_x$$
$$C_{33}(\frac{\partial u}{\partial y} + \frac{\partial v}{\partial x}) n_x + (C_{12}\frac{\partial u}{\partial x} + C_{22}\frac{\partial v}{\partial y}) n_y = \hat{t}_y$$

(4-38)

Equations (4-37) and (4-38) provide a means of solving for the deflections within the part/tool assembly during the resin film infusion process given the applied pressure profile in the autoclave. These deflections are then in turn used as inputs for the flow model and also used in the finite element control volume method of tracking the free surface movement of the resin. The deflections are used in these routines to calculate new nodal control volumes

and new permeability values during the flow modeling. A further discussion of the flow

model is given the next chapter.

CHAPTER 5

Finite Element Formulation

5.1 Governing Equations

As discussed in Chapter 4 the model is broken up into five major submodels, Flow, Kinetics, Viscosity, Heat Transfer, and Compaction. Together these five submodels provide a complete description of the Resin Film Infusion (RFI) process. This chapter will address the three major portions of the model, which are formulated as a series of Finite Element Solutions. Each of the three Finite Element submodels will be defined and the application of boundary conditions will be discussed. Finally, the last section of this chapter will illus-

trate the numerical solution procedure used for the Finite Element/Control Volume Techniques in the Flow sub-model.

5.1.1   Flow Sub-Model

In Chapter 4, the governing equations for the flow portion of the model are developed using Darcy's Law and the Continuity Equation. The governing equation for two-dimensional resin mold filling is:

$$\frac{\partial}{\partial x}\left[\frac{-k_{xx}}{\mu}(\frac{\partial P}{\partial x}) + \frac{-k_{xy}}{\mu}(\frac{\partial P}{\partial y})\right] + \frac{\partial}{\partial y}\left[\frac{-k_{yx}}{\mu}(\frac{\partial P}{\partial x}) + \frac{-k_{yy}}{\mu}(\frac{\partial P}{\partial y})\right] = 0 \qquad (5\text{-}1)$$

where k_{ij} and μ are the local permeability and viscosity, respectively. The second order partial differential equation solution yields the pressure distribution $P(x,y)$ of the resin. Solution of the second order partial differential equation is obtained by the finite element variational method outlined in Reddy's text on finite elements[13]. The finite element formulation in matrix notation would be as follows:

$$\left[K^e_{ij}\right]\{P^e_i\} = \{F^e_i\} \qquad (5\text{-}2)$$

where

$$K^e_{ij} = \int_{\Omega_e}\left[\frac{\partial \psi_i}{\partial x}(\frac{-k_{xx}}{\mu}\frac{\partial \psi_j}{\partial x} + \frac{-k_{xy}}{\mu}\frac{\partial \psi_j}{\partial y}) + \frac{\partial \psi_i}{\partial y}(\frac{-k_{yx}}{\mu}\frac{\partial \psi_j}{\partial x} + \frac{-k_{yy}}{\mu}\frac{\partial \psi_j}{\partial y})\right]dxdy \qquad (5\text{-}3)$$

$$F_i = \int_{\Omega_e} f\psi_i dxdy + \oint_{\Gamma_e} q_n ds \qquad (5\text{-}4)$$

Here f represents any source or sink term present in the element, q_n represents a specified natural boundary condition or flow rate along the surface of an element, ψ_i and ψ_j are lin-

ear interpolation functions. The elements are assembled into a global matrix and solved for P_i using a half bandwidth gaussian elimination method. Due to the need to repeatedly solve this series of linear equations during the filling process, a modification was made to the gaussian solution routine that would drop all rows and columns (of the global assembly matrix) for which a pressure of zero was specified. By removing the rows with nodal pressures specified to zero, the system of equations could be reduced considerably, thus giving a large savings in computational time. The justification for specifying the nodal pressures to zero is given later in this chapter in the section on the Finite Element/Control Volume method.

The current version of the model provides only for four node linear rectangular elements.

The boundary conditions which can be specified in the Flow submodel include flow rate and applied pressure. The finite element formulation allows for the inclusion of line sources, point sources, and sinks. Boundaries such as mold walls may be specified by setting a zero pressure gradient across that surface. Inlet ports can be modeled using a specified pressure (primary variable) or flow rate (secondary variable).

5.1.2   Heat Transfer Model

The Heat Transfer model is formulated in much the same manner as the Flow Sub-model. The governing equation developed in Chapter 4 is:

$$\rho C_p \frac{\partial T}{\partial t} - \frac{\partial}{\partial x}(a_{xx}\frac{\partial T}{\partial x} + a_{xy}\frac{\partial T}{\partial y}) + \frac{\partial}{\partial y}(a_{yx}\frac{\partial T}{\partial x} + a_{yy}\frac{\partial T}{\partial y}) + u''' = 0 \qquad (5\text{-}5)$$

where:

ρ = Density of the material

C_p = Specific heat of the material

a_{ij} = Thermal conductivity of the material

u''' = Heat generation term due to resin chemical reactions

The solution of equation (5-5) provides the transient temperature distribution T(x,y,t) within the part/tool assembly. As with the Flow sub-model, variational methods are again used to provide the finite element formulation. In matrix and variational form:

$$\left[M^e \right] \{ T' \} + \left[K^e \right] \{ T \} = \{ F^e \} \tag{5-6}$$

where:

$$M^e_{ij} = \int_{\Omega_e} \rho \, C_p \psi_i \psi_j \, dxdy$$

$$K^e_{ij} = \int_{\Omega_e} \left(a_{xx} \frac{\partial \psi_i}{\partial x} \frac{\partial \psi_j}{\partial x} + a_{xy} \frac{\partial \psi_i}{\partial x} \frac{\partial \psi_j}{\partial y} + a_{yx} \frac{\partial \psi_i}{\partial y} \frac{\partial \psi_j}{\partial x} + a_{yy} \frac{\partial \psi_i}{\partial y} \frac{\partial \psi_j}{\partial y} \right) dxdy + \oint_{\Gamma_e} \beta \psi_i \psi_j ds \tag{5-7}$$

$$F^e_{ij} = -\int_{\Omega_e} u''' \psi_i \, dxdy + \beta T_\infty \oint_{\Gamma^e} \psi_i \, ds$$

Note that convective terms have been included in the equations. β represents the convective heat transfer coefficient applied at a boundary and T_∞ denotes the ambient temperature. In order to account for the time-dependent nature of the heat transfer problem, the mass matrix M has been added to the formulation. The numerical approximation scheme used in the transient heat transfer problem is the Direct Time Integration scheme [13]. The numerical scheme amounts to a linear interpolation of the temperature gradient. The theta approximation is used and is defined as follows:

$$\theta \{T'\}_{n+1} + (1-\theta) \{T'\}_n = \frac{\{T\}_{n+1} + \{T\}_n}{\Delta t} \tag{5-8}$$

where $\Delta t = t_{n+1} - t_n$ which is the time difference between the previous and current time value. The value of θ allows for the selection of the type of difference scheme used in the model. A value for θ of 0.887 was selected for use in this modeling effort. This value is based on an optimal value necessary for a reasonably accurate solution with a minimum amount of computation as reported for heat transfer problems of this type in [14]. A more complete discussion of the time integration scheme may be found in [13].

Following the approach discussed in Section 5.1.1 the elemental matrices are then assembled into global matrices (in half-bandwidth form) and solved using a half-bandwidth gaussian elimination routine.

The boundary conditions for the Heat Transfer Sub-model which can be specified include convective boundaries, heat generation sources, and temperatures.

5.1.3   Compaction Model

The governing equations for the compaction model are based on the plane elasticity equations assuming plane strain conditions. As described in Chapter 4, these equations and assumptions lead to the following governing equations.

$$-\frac{\partial}{\partial x}(C_{11}\frac{\partial u}{\partial x} + C_{12}\frac{\partial v}{\partial y}) - C_{33}\frac{\partial}{\partial y}(\frac{\partial u}{\partial y} + \frac{\partial v}{\partial x}) = f_x$$

$$-C_{33}\frac{\partial}{\partial x}(\frac{\partial u}{\partial y} + \frac{\partial v}{\partial x}) - \frac{\partial}{\partial y}(C_{12}\frac{\partial u}{\partial x} + C_{22}\frac{\partial v}{\partial y}) = f_y \tag{5-9}$$

Once again C_{ij} represent the material constants, f_i are the applied forces and u and v are the displacements in the x and y directions, respectively. The finite element formulation for these governing equations is as follows.

$$\left[K^{11}\right]\{u\} + \left[K^{12}\right]\{v\} = \{F^1\}$$
$$\left[K^{21}\right]\{u\} + \left[K^{22}\right]\{v\} = \{F^2\}$$

$$(5\text{-}10)$$

where

$$K_{ij}^{11} = \int_{\Omega_e} (C_{11}\frac{\partial\psi_i}{\partial x}\frac{\partial\psi_j}{\partial x} + C_{33}\frac{\partial\psi_i}{\partial y}\frac{\partial\psi_j}{\partial y})\,dxdy$$

$$K_{ij}^{12} = K_{ij}^{21} = \int_{\Omega_e} (C_{12}\frac{\partial\psi_i}{\partial x}\frac{\partial\psi_j}{\partial y} + C_{33}\frac{\partial\psi_i}{\partial y}\frac{\partial\psi_j}{\partial x})\,dxdy$$

$$K_{ij}^{22} = \int_{\Omega_e} (C_{33}\frac{\partial\psi_i}{\partial x}\frac{\partial\psi_j}{\partial x} + C_{22}\frac{\partial\psi_i}{\partial y}\frac{\partial\psi_j}{\partial y})\,dxdy \qquad (5\text{-}11)$$

$$F_i^1 = \int_{\Omega_e} \psi_i f_x dxdy + \oint_{\Gamma_e} \psi_i t_x ds$$

$$F_i^2 = \int_{\Omega_e} \psi_i f_y dxdy + \oint_{\Gamma_e} \psi_i t_y ds$$

f_i and t_i are the applied body and traction forces, respectively. Linear interpolation functions are used and equation (5-10) is assembled into a global matrix form and solved using gaussian elimination.

Boundary conditions for the Compaction Sub-Model include applied tractions, body forces and/or displacements.

5.2   Finite Element/Control Volume Technique

An essential part of the resin transfer molding modeling effort is the accurate prediction of the flow front movement. There are many different algorithms available for tracking the movement of the flow front. These include the Marker-and-Cell method, Finite Difference/Control Volume, Dynamic Remeshing using Body-Fitted Coordinates, Boundary Elements, and the Finite Element/Control Volume approach. Of these methods the Finite Element Control/Volume approach was selected for use in this model. The Finite Element/Control Volume approach has several advantages:

- Conservation of mass is upheld.

- It is numerically efficient.

- Complex geometries can be modeled accurately.

- It has no difficulties in tracking the flow front.

The Finite Element/Control Volume method used is based on work done by C.L. Tucker [4]. The method uses a fixed mesh which greatly simplifies the modeling aspects of complex geometries and reduces the amount of computation needed for flow front prediction. Although the technique does not have the flow front accuracy as do some of the other techniques, the Finite Element/Control Volume method can provide a good approximation with some post-processing.

5.2.1   Domain Discretization

The control volume technique is based on the assertion that each of the finite element nodes present in the mesh can be surrounded by a "control volume" which is a collection of sub-volumes from all the surrounding elements. These sub-volumes are defined by how many nodes each element contains. In this model only two dimensional elements are possible (namely, a linear triangular, and a linear quadrilateral element). Therefore, for all cases discussed, each element is of a certain unit thickness and the area is all that is needed to define the sub-volume.

The domain of interest is discretized using finite elements and is then further broken up into a collection of sub-volumes as depicted in Figure 7. The dashed lines indicate where the elements have been sub-divided and the solid lines represent the element boundaries. Figure 8 illustrates the construction of a control volume between a typical triangular and quadrilaterial element. The sub-areas contributing control volume 1 are summed from all elements which contain node 1. In this manner all the nodal control volumes are calculated using the appropriate area formula. Once the nodal coordinates are known the areas are calculated using equation (5-12). (See Figure 9)
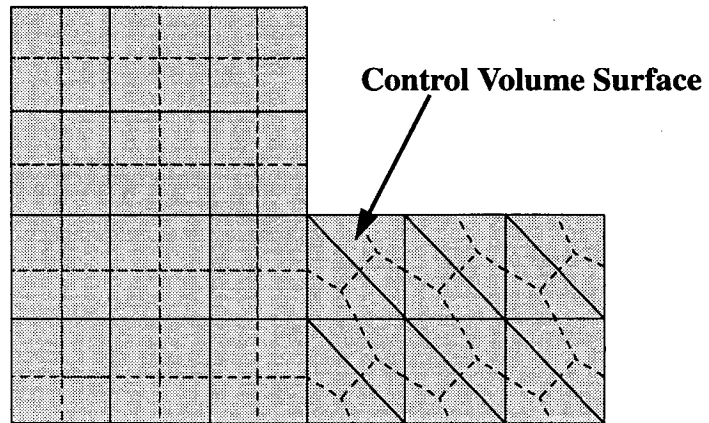
FIGURE 7 Domain divided into elements and control volumes.
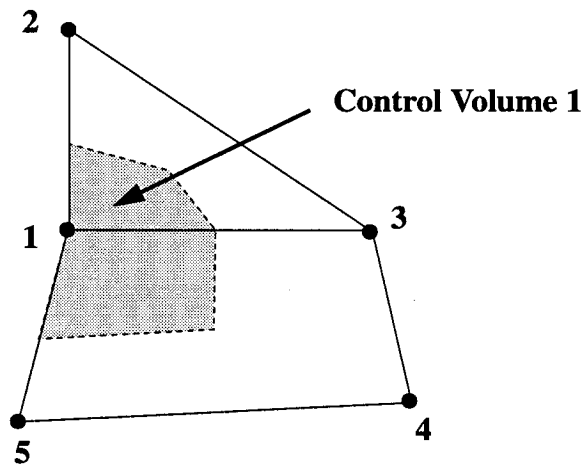
FIGURE 8 Control Volume construction
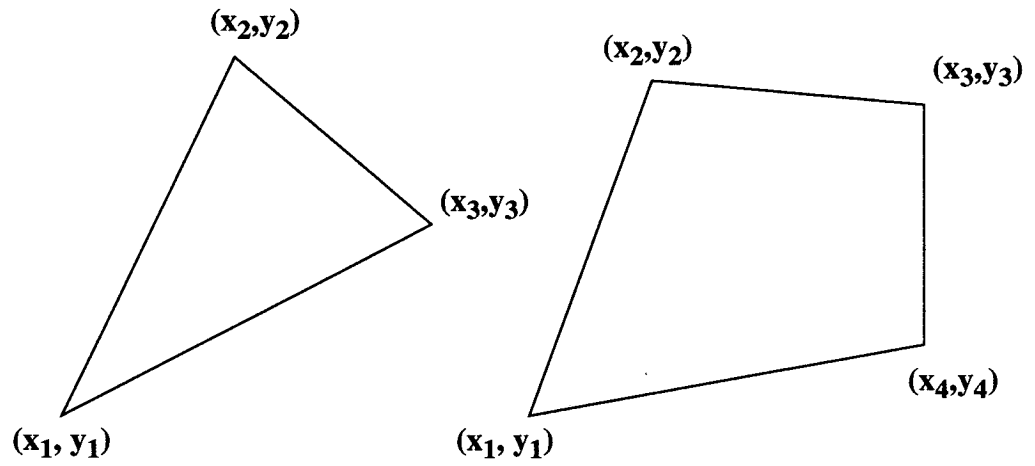
FIGURE 9 Triangular and trapezoidal element notation.

$$A = \frac{1}{2} \begin{vmatrix} x_1 \ y_1 \\ x_2 \ y_2 \\ \circ \ \ \circ \\ \circ \ \ \circ \\ x_n \ y_n \end{vmatrix} \qquad (5\text{-}12)$$

5.2.2   Resin Front Tracking

The control volume method tracks the progress of the resin front moving though the domain by monitoring the state of each nodal control volume. These control volumes can be empty, filled, or partially filled. The resin flow front is located by determining all the nodes in the computational domain that are partially filled. Thus, the accuracy of the flow front is determined by the density of the control volumes or elements in the region of interest. In order to reduce the error of the flow front location, a quadratic interpolation is done using the fill factors of the nodes surrounding the flow front. This allows for a smooth curve to be passed between the nodes and thus refines the shape of the flow front to some degree.

The amount of a control volume that is filled is represented by a quantity known as the fill factor. The fill factor is the ratio of the filled volume to the total volume of the nodal control volume. Therefore, the fill factor varies from 0 to 1.0 where 0 represents an empty control volume (no resin) and 1.0 represents a control volume completely full of resin. The flow front advances through the domain by filling these control volumes during a specified time interval.

5.2.3   Flow Rate Calculation

Once the pressure distribution has been determined and the computational domain has been discretized the flow front movement may be determined by first calculating the flow rate of the fluid into those control volumes which are partially full or empty. In order to calculate the flow rate, a flow surface is constructed across which the fluid moves with a velocity calculated at the center of the element from the pressure distribution. The flow surface is constructed by connecting the midpoints of adjacent sides of the elements. In

Figure 10 $\overline{ab}$ represents one such surface. By summing the flow rates across surfaces $\overline{ab}$,

$\overline{bc}$, $\overline{cd}$, and $\overline{da}$, the flow rate into control volume 2 can be calculated. The velocity at the

centroid of the each element is calculated using Darcy's Law and the pressure gradients.

$$v_i = \frac{-k_{ij}}{\mu} \frac{\partial P}{\partial x_j} \qquad (5\text{-}13)$$

The model assumes that the velocity of the fluid is constant within each element. A vector,

$\vec{m}_n$, normal to the flow surface is constructed which has a magnitude of the length of the

flow surface (See Figure 10). By taking the dot product of $\vec{m}_n$ and $\vec{v}_e$ the flow rate can be

calculated into the control volumes.

$$Q_{en} = \vec{v}_e \bullet \vec{m}_n \qquad (5\text{-}14)$$
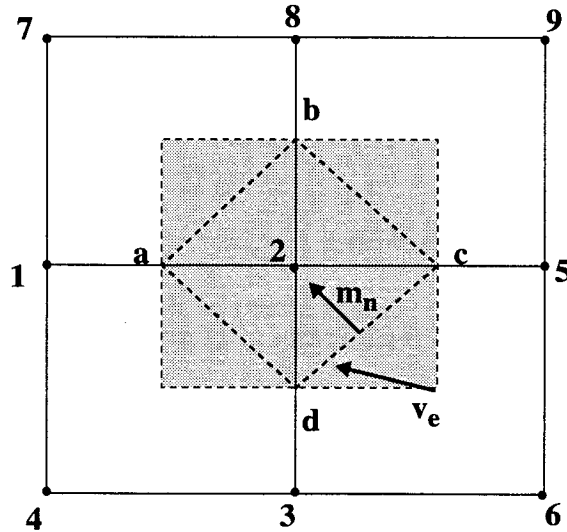
FIGURE 10 Flow rate calculation nomenclature.

5.2.4 Updating Fill Factors

Once the flow rates into each control volume have been calculated, the next quantity which must be updated is the fill factor of the associated control volume. The fill factors are updated for each time step in the flow solution. Given the fill factors at the previous time step and the time step used for that iteration, a new value for each nodal fill factor can be calculated:

$$f_n^{i+1} = f_n^i + \frac{\sum_e Q_{en} \Delta t}{V_n} \tag{5-15}$$

where f_n^{i+1} and f_n^i are the fill factors at the new and previous time steps respectively, V_n is the nodal control volume and Δt is the value of the time step which is addressed in the next section.

5.2.5 New Time Step Calculation

The solution scheme continues by calculating a new time step value to be used in the next iteration of flow solution. The magnitude of the time step chosen is based on the smallest amount of time necessary to fill one nodal control volume at the flow front. Thus, the Δt's are calculated for all the unfilled ($0 < f < 1.0$) nodal control volumes and the smallest of these is selected as the new Δt. The relation used for calculating the Δt necessary to fill a nodal control volume is:

$$\Delta t = \frac{(1 - f_n) V_n}{\sum Q_{en}} \tag{5-16}$$

Once a new time step has been determined, the finite element control volume method continues by checking to see if all nodes have been filled. If all nodes are filled the flow solution is stopped. Otherwise, the newly calculated time step would be used by the transient heat transfer sub-model which would then calculate a new temperature distribution. This new temperature distribution is then used to modify the elemental viscosities and degrees of cure. Once this has been accomplished the pressure boundary conditions are updated and the scheme returns to calculate a new temperature distribution. The finite element control volume technique is summarized in Figure

Input model geometry, material properties, and
boundary conditions.

Calculate nodal control volumes and flow surfaces

Calculate the P(x,y)

Calculate flow rates

Update Fill Factors

Find new Δt

Update pressure boundary conditions

No

Check to see if all nodal control volumes are filled

Yes

Stop
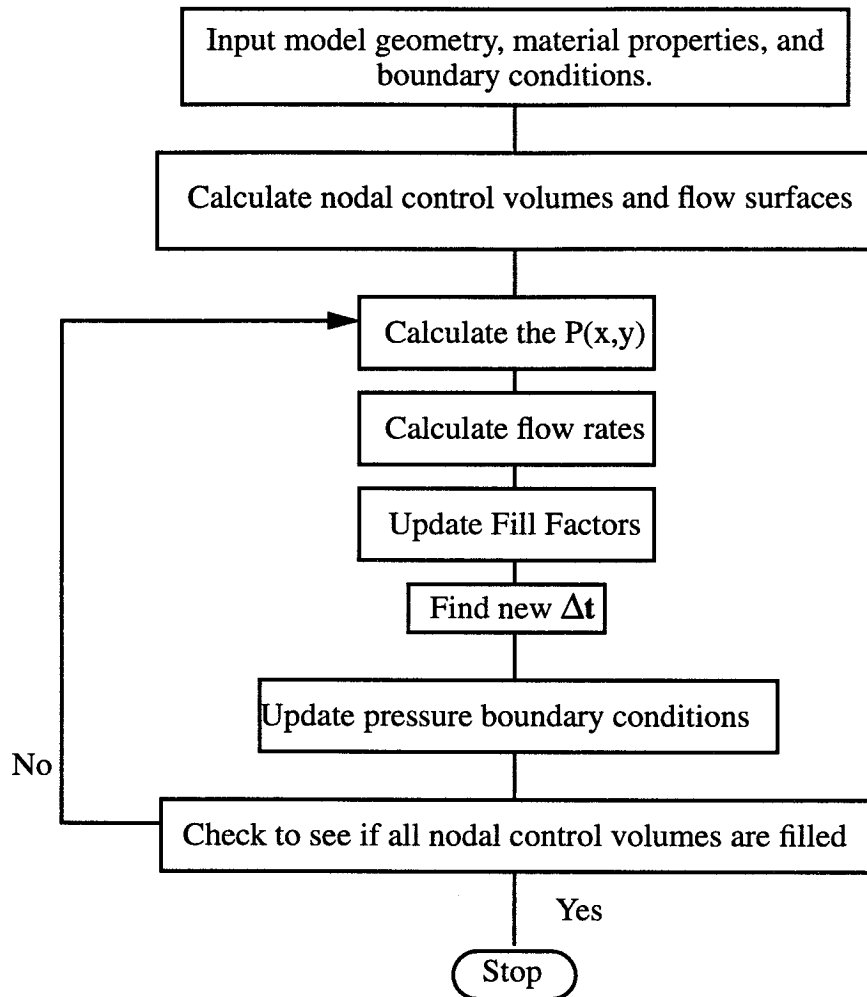
FIGURE 11 FEM Control Volume Method Flowchart.

CHAPTER 6

Computer Program

As discussed in the previous chapter the numerical implementation of the RTM model is divided into five major sub-models (flow, kinetics, viscosity, heat transfer, and compaction). This chapter describes the computer program, based on these sub-models, which was designed to numerically simulate the resin transfer molding process. Discussed in this chapter are the overall structure of the computer program and also the pre-processing, processing, and post-processing sections of the program. Also described are some of the details about what additional hardware and software are necessary for running the computer program. A listing of the program is provided in the Appendix of this document.

Although the computer model is based primarily on the five sub-models mentioned, the interaction between sub-models, as well as additional features, have been included in the computer model as separate subroutines. A schematic representation of the overall structure of the RTM computer model is shown in Figure 12. The computer code itself is broken mainly into three finite element processing routines along with many other subroutines which control and track various parameters during the computation. As shown in Figure 12, the first step taken is to input the various geometries, material properties, and boundary conditions into the problem. However, in order to get these conditions into the proper form for entry into the code some pre-processing must be done.

6.1 Pre-Processing

The first step in constructing a simulation of any resin transfer molding operation is to model the geometry of the fabricated part and the associated tooling. A commercial pre-processing code called PATRAN (developed and distributed by PDA engineering) is used as a means of constructing the geometry of the part/tool assembly. PATRAN allows the user to input the geometry, assists in the discretization of the domain into elements, and applies boundary conditions to the model. PATRAN provides the user with a graphical environment to work in and allows also for a variety of geometric description files to be converted into the proper form for the finite element processor. Relatively complex geometries can be fashioned within PATRAN itself, or if needed another commercial CAD package can provide the geometry for PATRAN through a graphical interchange file such as IGES. The flexibility of the interface and the ability to model relatively complex geometries, material types, availability, and boundary conditions were all issues in the choice of PATRAN as the preprocessor.

```
┌─────────────────────────────────────┐
│  Input Geometry, Material Properties,│
│  Cure Cycle, and Boundary Conditions │
└─────────────────────────────────────┘
             │
┌─────────────────────────────────────┐
│   Calculate Nodal Control Volumes,   │
│        and Initialize Variables      │
└─────────────────────────────────────┘
             │
┌─────────────────────────────────────┐
│ FEM Flow Solution - Calculate Pressure│
│         Distribution/Velocities       │
└─────────────────────────────────────┘
             │
┌─────────────────────────────────────┐
│  Calculate Flow Rates into Control Volumes│
└─────────────────────────────────────┘
             │
      ┌──────────────────┐
      │ Update Fill Factors│
      └──────────────────┘
             │
        ┌──────────────┐
        │ New Time Step │
        └──────────────┘
             │
   ┌─────────────────────────────────┐
   │ Update Flow Boundary Conditions │
   └─────────────────────────────────┘
             │
        ┌──────────────────┐
        │ Kinetics Submodel │
        └──────────────────┘
             │
       ┌──────────────────────┐
       │ Update Permeabilities │
       └──────────────────────┘
             │
          ┌──────────────┐
          │ Find new T_∞ │
          └──────────────┘
             │
   ┌─────────────────────────────────┐
   │    FEM Heat Transfer Solution -  │
   │ Calculate Temperature Distribution│
   └─────────────────────────────────┘
             │
 ┌──────────────────────────────────────┐
 │ Update Preform Stiffness and Resin Viscosity│
 └──────────────────────────────────────┘
             │
     ┌──────────────────────────┐
     │   FEM Compaction Solution -│
     │ Calculate Displacement Field│
     └──────────────────────────┘
             │
 ┌──────────────────────────────────────┐
 │ Update Nodal Coordinates and Control Volumes│
 └──────────────────────────────────────┘
             │
 ┌──────────────────────────────────────┐
 │ Output Data and Check if Mold is Filled│
 └──────────────────────────────────────┘
       No │         │ Yes
          │      ┌───────┐
          │      │ Stop  │
          │      └───────┘
```

FIGURE 12 RTM Simulation Program Flow Chart

Output from PATRAN to the processor takes place through a standard ASCII formatted text file called a NEUTRAL file. This file allows for the easy integration of the model input information into the processor computer program.

6.2 Processor

The processor portion of the simulation program contains the subroutines responsible for calculating and tracking the many changing variables during the RTM simulation. Routines for the processor portion were written in FORTRAN. The processor program consists of three main finite element subroutines which do the largest part of the computational work. The other subroutines included in the processor program are used for updating and tracking the many variables used in the three finite element subroutines. A modular approach was used in designing the processor routine. This approach dictated by the size and complexity of the problem being simulated and the need for flexibility in the types of problems that could be solved using the processor. The modular structure of the processor allows for smaller subset problems to be run using the same processor. For example, if a simulation of an isothermal resin transfer molding process was necessary, the same processor routines would be used except for the heat transfer sub-routines. These temperature sub-routines would return constant values of the material properties during the simulation. The same is true if compaction was not needed in the simulation.

Because of the complexity of the problem, the approach taken was to numerically solve the temperature and compaction portions of the problem with piecewise linear approximations in time, rather than attempting to solve the coupled set of non-linear governing equations. This allowed a reduction in the amount of required numerical computations and allowed a modular design. It was felt that a reasonable amount of accuracy could be

attained with this approach. An important implication of the use of a piecewise linear approximation was that the time steps must be chosen carefully in order to maintain this accuracy.

Although the modular design allowed for a reduction in the number of numerical computations, it became evident during simulation of RTM problems with complex geometries that a method for further reducing the computation time was necessary. An execution profiler was used to analyze each of the routines within the processor modules for the percentage of time spent within each subroutine. An example is shown in Figure 13. It is easily seen that the largest percentage of time was being spent in the SOLVE routine. This is the common routine used by all the finite element subroutines for solving a series of linear equations. The SOLVE routine uses a half bandwidth gaussian elimination method for solving the linear equations. It can also be seen from Figure 13 that the finite element subroutines do not necessarily call the SOLVE routine with the same frequency. In this case the temperature routine required the largest share of the computational resources. Hence, it is evident that the time steps and mesh density used in the resin transfer molding process simulations will require some tuning to increase efficiency of the processor routine. The tuning was done by running a series of test cases with different meshes and time step parameters and comparing the results with the help of the on-line execution profiler. Some improvements to the original SOLVE routine were made to eliminate the extra time spent resolving for all the nodal quantities during each time step in the flow solution. Instead of solving for the entire flow region at every time step, which included those nodes where the pressure had been specified as zero, a reduced matrix was formed which included only the unknown pressure quantities and the required boundary conditions. Effectively this was done by eliminating all the rows and columns in the global stiffness matrix where a value of zero was found for the primary variables.

```
IFLOWTRACE -- Alphabetized summary
0   Routine         Time executing  Called   Average T
  1 $MAIN           0.005  (  0.00%)      1     0.005 000000241a Called by
 11 BNDY            0.279  (  0.04%)     20     0.014 Called by      FEM FEMCOMPA
    000025253a                                                       10       10
 21 CONDUCTI        0.003  (  0.00%)     10        >  000014072a Called by      $MAIN
  6 CV              0.190  (  0.03%)     11     0.017 000021112a Called by      $MAIN
 30 DATALIST        0.179  (  0.03%)     10     0.018 000035754a Called by      $MAIN
 25 FBTIME          0.007  (  0.00%)    520        >  000015534a Called by UPDATETI
  8 FEM             0.075  (  0.01%)     10     0.008 000022407a Called by      $MAIN
 35 FEMCOMPA        0.510  (  0.08%)     10     0.051 000031376a Called by      $MAIN
 26 FEMTEMP         0.718  (  0.11%)     10     0.072 000002767a Called by      $MAIN
 16 FILL            0.004  (  0.00%)     10        >  000030373a Called by      $MAIN
 15 FLOWRATE        0.026  (  0.00%)     10     0.003 000030211a Called by      $MAIN
 17 INFILAM         0.001  (  0.00%)     10        >  000035535a Called by      $MAIN
  5 INITIALI        0.006  (  0.00%)      1     0.006 000015644a Called by      $MAIN
  2 INPUT           0.092  (  0.01%)      1     0.092 000020030a Called by      $MAIN
  3 INPUT1          0.263  (  0.04%)      1     0.263 000000626a Called by      $MAIN
  4 INPUT2          0.165  (  0.02%)      1     0.165 000001574a Called by      $MAIN
 23 KCBYU           0.006  (  0.00%)     10        >  000014441a Called by      $MAIN
 31 OUTPUTS1           >   (  0.00%)     10        >  000016610a Called by      $MAIN
 41 PATOUT          0.056  (  0.01%)      1     0.056 000017335a Called by      $MAIN
 22 PERMEABI        0.056  (  0.01%)     10     0.006 000034350a Called by      $MAIN
 33 PTIME              >   (  0.00%)     15        >  000034243a Called by UPDATEPR
 10 SHAPE          12.507  (  1.89%)  81080        >  Called by    STIFFQ  STIFFQ1  STIFFQ2   STRESS
    000027666a                                                     3920     64460    11720      980
 12 SOLVE         623.142  ( 94.02%)     75     8.309 Called by      FEM FEMCOMPA FEMTEMP
    000025544a                                                       10       10      55
 18 SOURCE          0.794  (  0.12%)     10     0.079 000007577a Called by      $MAIN
  9 STIFFQ          0.838  (  0.13%)    980        >  000023171a Called by        FEM
 28 STIFFQ1        17.175  (  2.59%)  16115     0.001 000003474a Called by    FEMTEMP
 38 STIFFQ2         3.331  (  0.50%)   2930     0.001 000032004a Called by FEMCOMPA
 13 STRESS          0.152  (  0.02%)    980        >  000026247a Called by        FEM
 19 TIMESTEP        0.016  (  0.00%)     10     0.002 000030576a Called by      $MAIN
 20 UPDATE          0.001  (  0.00%)     10        >  000031250a Called by      $MAIN
 34 UPDATEMO        2.188  (  0.33%)     10     0.219 000036115a Called by      $MAIN
 32 UPDATEPR           >   (  0.00%)     15        >  000034123a Called by      $MAIN
 24 UPDATETI        0.003  (  0.00%)     10        >  000015431a Called by      $MAIN
 40 UPDATEXY           >   (  0.00%)     10        >  000035454a Called by      $MAIN
  7 VNUPDATE           >   (  0.00%)      1        >  000035411a Called by      $MAIN
* * * TOTAL       662.789        102918 Total calls
```

FIGURE 13 Execution Profiler Output

The result was a more than 60% reduction in the amount of CPU time spent in the flow routine. Although this was a significant improvement, there still remains a need for more efficient ways of solving these equations.

The general solution procedure contained within the processor routine begins with the input of material properties and boundary conditions from the PATRAN preprocessor. The model is built in three stages or regions. The first model built includes the regions in which the flow is to take place. A mesh is generated which incorporates all the inlet or initially saturated regions. The material property data and boundary conditions are included. This information is included in the first of three PATRAN neutral files. Next, a model is built which includes the associated tooling and bagging materials required during the processing. This model includes as a subset the first PATRAN flow model and contains the initial input required for the temperature model. A PATRAN neutral file is constructed again with material property, boundary, and initial conditions. The final neutral file used as input for the processor routine contains material property and boundary conditions for the generalized plane strain finite element solution which is the third region of the model. The compaction PATRAN neutral file contains the exact same geometry that was included in the temperature input file. An additional initialization file is read by the processor routine and includes the cure cycle information and the initial reaction state of the resin system.

Once the initialization process is complete, the processor routine calculates the initial control volumes in the flow region. Next, the finite element routine for calculating the pressure distribution is triggered. The processor proceeds with the solution technique described in Chapter 5 in the discussion of the control volume method. Upon completion, the flow subroutine provides the pressure distributions and elemental velocities which are

then used for calculation of the flow rates into the nodal control volumes. Once the flow rates have been determined, the fill factors and a new time step for the flow solution are calculated. At this point the flow solution is complete for the current time step and the flow boundary conditions are updated for use in the next iteration. The next routine encountered in the processor is the kinetics routine. The resin kinetics for the present temperatures of each of the filled elements are calculated in this routine. Next, the permeabilities of the elements are updated based on the current size of the nodal control volumes and the present elemental viscosities are calculated based on the current temperatures and degree of cure. Based on the time step calculated in the flow solution, a new value of T_∞ is found by interpolation of the cure cycle information. The new value of T_∞ is then used in the transient heat transfer finite element routine. Once the new temperature distribution within the part/ tool assembly is determined, the material dependent properties such as resin viscosity are updated. Temperature information is also fed into the finite element compaction routine in order to calculate the effects of thermal expansion on the part/tool assembly. The new displacement field is then used to update the nodal control volumes for the next iteration. At this point one iteration of the processor routine is complete. The current time is checked against the cure cycle values, and if the cycle is not completed then the code returns to the finite element flow solution for the next iteration. An outline of these steps is shown in Figure 12.

At the conclusion of the cycle, the processor routine returns several data files that are used in post-processing. The returned data files include several PARTAN results formatted files for variables such as viscosity, degree of cure, temperature, and flow front. Also included in the output is an ASCII file containing the time, temperature, viscosity, degree of cure, and porosity values at specified intervals during the curing cycle. The PATRAN results file

are later used in graphically representing these variables during the resin transfer molding process simulation.

6.3 Post-Processing

The final step in the simulation process is to display the results in a manner that information or insight into the resin transfer molding process can be gained. The processor generates a large volume of information about many processing variables. Due to the transient nature of the problem being simulated, these processing variables must be tracked and displayed as a function of time. These results can be displayed as either static or dynamic images of the processing variables. The PATRAN result files contain processing variable data stored at selected times during the cure cycle. This data can be used within PATRAN to create plots of a processing variable at a selected instant in time. One such fringe plot of a "T"-stiffened panel is shown in Figure 15
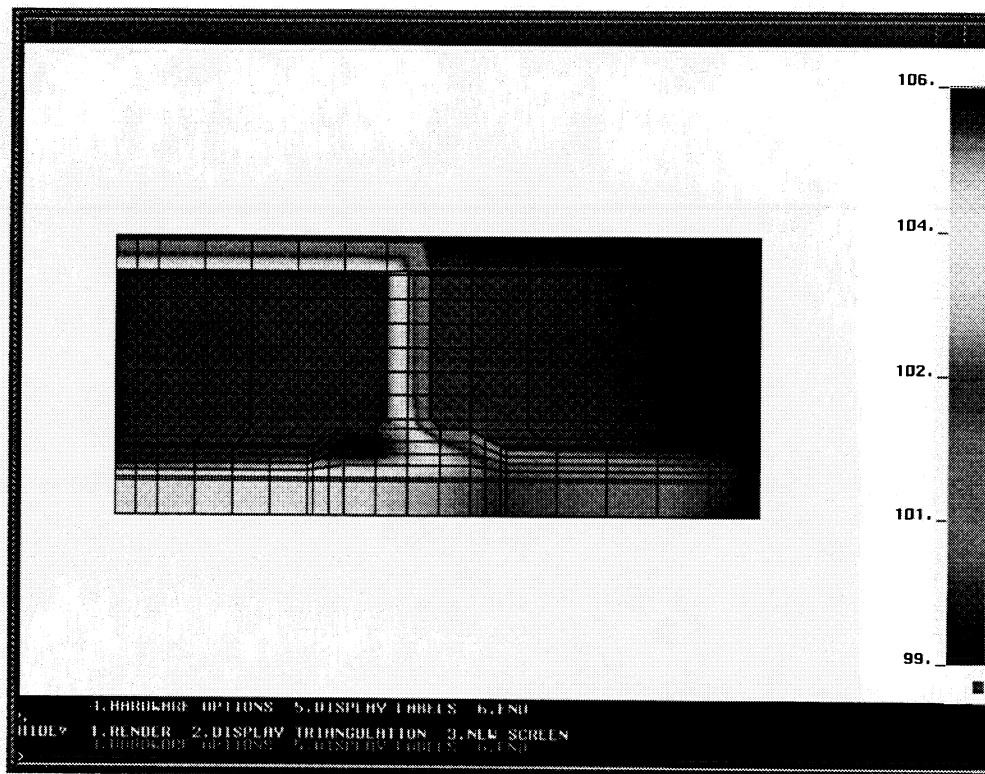
FIGURE 14 PATRAN results plot.

A series of these plots can be used to observe how the processing variables change during the RTM process.

However, in order to display multiple variables and observe changes in these variables with time, another post-processing program has been used. The AVS program marketed by Advanced Visual Systems, is currently being used to dynamically display these variables. AVS provides a graphical interface and has a modular programming paradigm which allows users to quickly create a variety of visualizations. An example of the programming paradigm and the visualizations that are possible in AVS are shown in Figure 14. AVS can display multiple variables such as viscosity and degree of cure simultaneously as well as animating the changes in these variables through the use of an animation module.
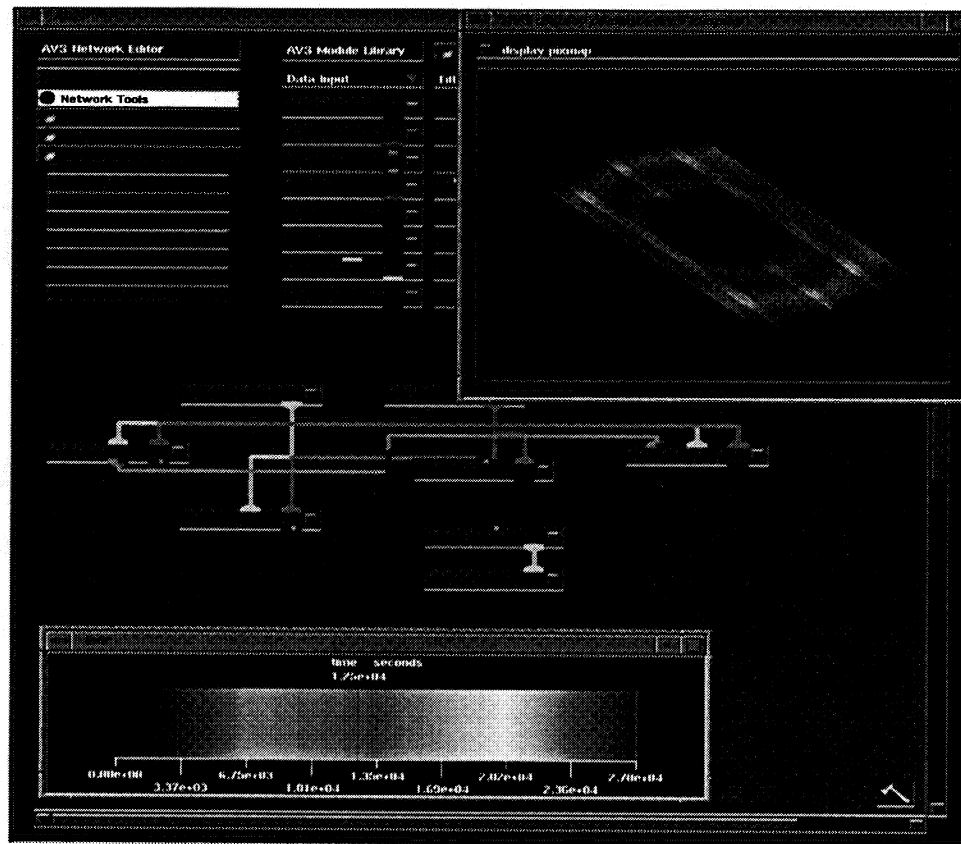
FIGURE 15 AVS display.

CHAPTER 7

Model Verification

Formulation and computer implementation of the resin transfer molding model have been addressed in the previous chapters. In this chapter a discussion of the experimental verification of the computer model will be presented. At the present time a complete experimental verification, including all elements in the computer model. However, the flow and heat transfer submodels have been individually verified. The results of these experimental investigations will be discussed in this chapter. Also included in the first section of this chapter, is a comparison of resin flow model results with those in published literature.

7.1   Flow Submodel Verification

Since a complete experimental verification of the resin transfer molding computer model, including the heat transfer, compaction and flow portions of the model, was not available, an alternative method of verifying the accuracy of the computer model was sought. The method chosen was to verify the three main components of the model independently. The first of these verification efforts involved the resin flow simulation. Two approaches were used to check the resin flow model. First, experimental results from the published literature were chosen as a comparison with the flow model. Second, several experiments using a two foot square flow visualization test fixture were carried out. These comparisons are discussed in the following sections.

7.1.1   Flow Model Comparison with Literature Results

The flow model was used to simulate two mold filling experiments described in published literature. The first of these was a study reported by Young et. al. [10]. The experimental apparatus consisted of two acrylic sheets 13.5 cm x 40 cm x 1.5 cm. A random glass fiber mat was placed between two acrylic sheets and compressed with clamps to a thickness of 0.58 cm. At that thickness the fiber volume fraction of the continuous random glass mat was 18%. An injection port was placed at the center of the upper acrylic plate to allow for injection of a nonreactive fluid. The fluid viscosity was 0.08 Pa•s and the injection flow rate was 22 ml/s. The diameter of the inlet port was not reported by Young [10]. Hence the inlet port was assumed to be 0.635 cm in diameter. A 2.5 cm hole was cut through the thickness of the mats directly beneath the center injection port to eliminate any through-the-thickness effects in the flow front. A fluid filled cylinder was placed in an Instron testing machine and the cylinder's piston was subjected to a constant displacement rate. The

fluid was then expelled from the cylinder and forced into the inlet gate on the mold at a constant flow rate. A schematic of Young's experimental apparatus is shown in Figure 16.
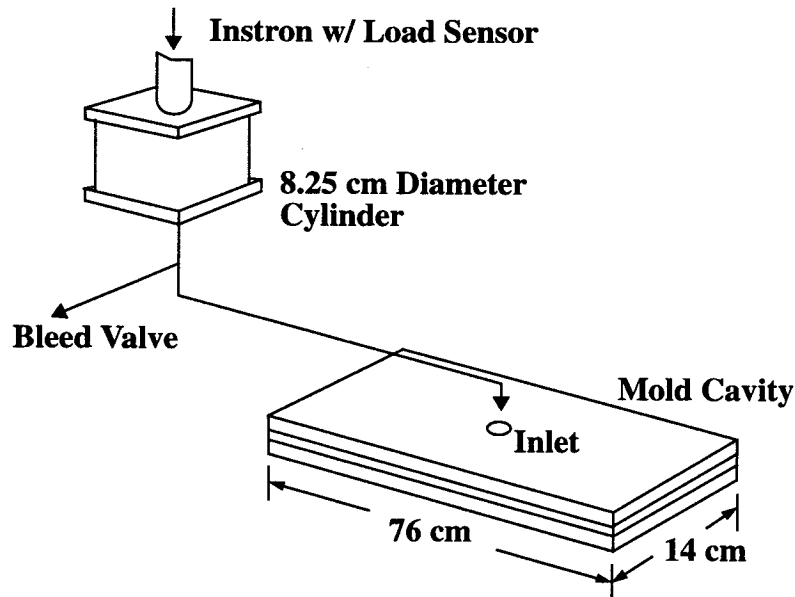
FIGURE 16 Young's Mold Filling Apparatus.

The experiments were run under isothermal conditions at room temperature. Viscous heating effects were not included due to the small mold filling rate and fluid viscosity. Six layers of random mat were used to build the thickness of the cavity.

The permeabilities used in Young's analysis were measured and reported as a function of superficial velocity and porosity of the random fiber mat. The relationship used is as follows

$$k_x = k_y = 241v' + 40e^{5.45\phi} \tag{7-1}$$

where v' is the superficial velocity and ϕ is the porosity of the random mat. In order to calculate the permeability, the superficial velocity at the 2.5 cm hole in the cloth was calculated and used along with the mat porosity in equation (7-1). Table 2 details the material constants and boundary conditions necessary for the modeling of Young's experiment.

TABLE 2 Material Constants and Boundary Conditions for Young's Experiments [10].

mold size	13.5 cm x 40 cm x 1.5 cm
porosity	0.82
cavity thickness	0.0058 m
fluid viscosity	0.08 Pa•s
flow rate (inlet)	2.24E-05 m^3/s
superficial velocity (inlet)	4.102E-03 m/s
$k_x=k_y$	4.53085E-09 m^2
inlet diameter	0.00635 m

These material constants and boundary conditions were used as input for the resin flow model. A pre-processing model was created in PATRAN. The generated mesh and the inlet boundary conditions are shown in Figure 17. At the beginning of the simulation, the inlet element was given nodal fill factors of 1.0 and a constant velocity was applied to the element. The results of the simulation are shown in Figure 18. The measured flow front values are depicted by dashed lines, and the solid lines represent the model calculated values. Agreement between the model and the experimental flow front results is reasonably good. The inlet pressure as a function of time is plotted in Figure 19.
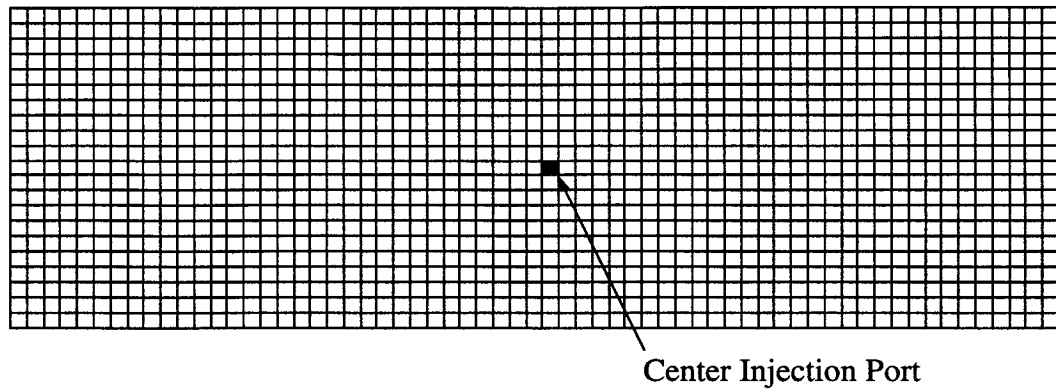
Center Injection Port

FIGURE 17 PATRAN generated mesh for Young's experiment.
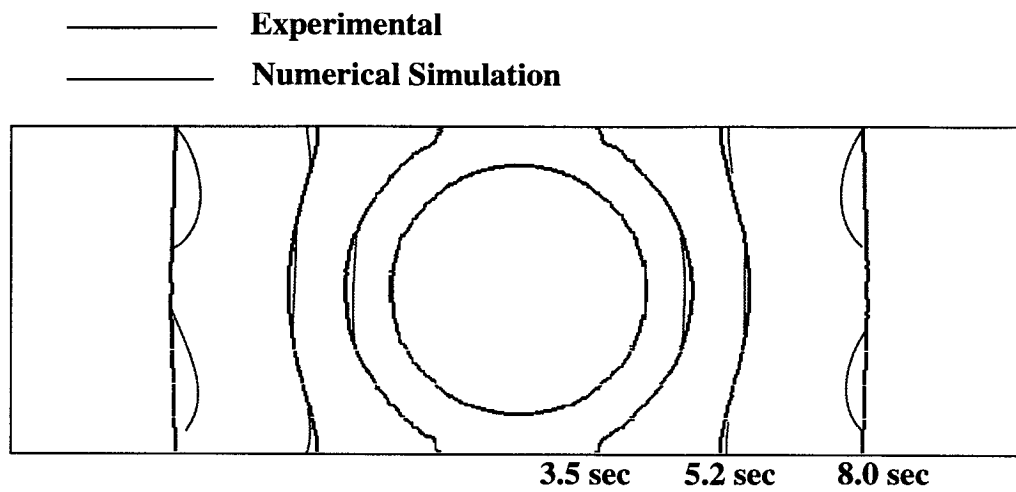
FIGURE 18 Flow front versus time results for Young's experiment [10].
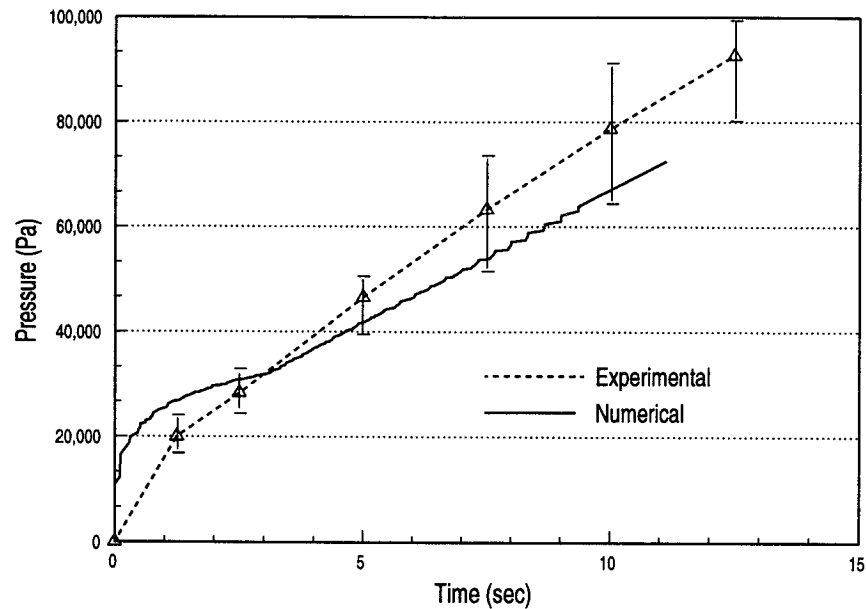
FIGURE 19 Inlet pressure versus time for Young's experiment.

Once again the solid lines indicate the model calculated values and the dashed line represent the measured values. Agreement between the calculated and measured inlet pressure versus time is reasonable except near the end of infiltration. Sources of error in the computer simulation could have come from inaccurate estimates of the mat permeabilities, the assumed dimensions of the inlet port, neglecting surface tension and capillary forces, the numerical approximations of the geometry and fluid flow, and not including the effects of the no-slip boundaries in the model. Considering the sources of error, the computer simulations approximate Young's experimental results reasonably well.

The second experimental study used for flow model verification was reported by Coulter [6]. Coulter's experimental apparatus was very similar to that described in Young's paper

which was shown in Figure 16. The mold assembly consisted of a 0.3 m x 0.2 m test specimen section which could hold a preform between 0.003 m and 0.005 m thick. The preform was surrounded by an aluminum spacer plate with the same thickness as the preform. Cutouts, 0.02 m in length, were machined in the diagonal corners of the spacer plate to allow for inlet and exit of resin. A graphite fabric preform was inserted into the mold assembly and enclosed in-between an aluminum bottom plate and a plexiglass top plate. As in Young's work, a piston and cylinder assembly was placed between the grips of an Instron machine, and a constant crosshead speed was maintained in order to provide a constant flow rate injection into the mold.

The velocity variation across the inlet region was ignored. The tests were performed at room temperature, under isothermal conditions. The test fluid chosen was corn syrup with a reported viscosity of 4.22 Pa•s. A red dye was added to the corn syrup to increase its visibility during infiltration. The fluid was considered to exhibit Newtonian behavior. The material constants and boundary conditions used for the resin flow model are reported in Table 2 .

TABLE 3 Material Constants and Boundary Conditions for Coulter's Experiments[9].

mold size	0.3 m x 0.2 m x 0.004 m
porosity	0.65
cavity thickness	0.004 m
fluid viscosity	4.22Pa•s
velocity(inlet)	0.0014 m/s
$k_x =$	2.97E-09 m^2
$k_y =$	1.12E-09 m^2
inlet length	0.02 m

Unreported in Coulter's work were the fiber volume fraction and the thickness of the fabric preform specimens. An average thickness (0.004 m) was chosen from the range of thicknesses supported by the mold assembly. The fiber volume was then approximated from reported data obtained from the manufacturer of the graphite fabric and the selected thickness. A value of 35% fiber volume was used in the flow simulation model. The material constants and boundary conditions used in Coulter's work are reported in Table 2 .

A mesh was generated using PATRAN and is shown in Figure 20.
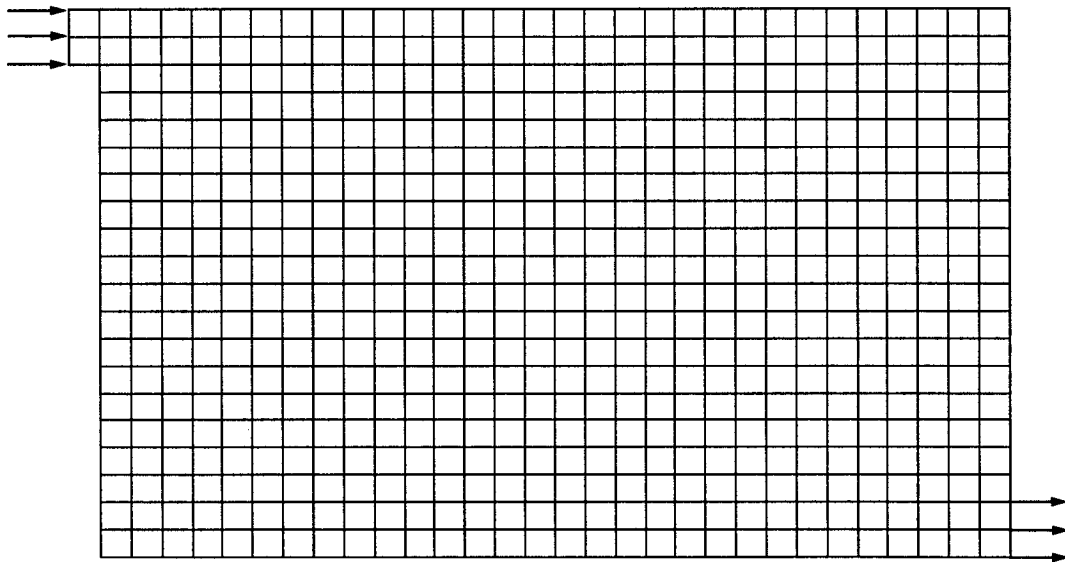
FIGURE 20 PATRAN generated mesh for Coulter's experiment.

The resin inlet port was located at the upper left hand corner of Figure 20. The resin exited at the port placed at the diagonally opposite corner of the mesh. At the start of the simulation, the elements at the inlet of the mold were fully saturated. The flow solution pro-

ceeded until all the nodal fill factors in the mesh were filled with resin. Only the flow

simulation submodel was utilized. The heat transfer and compaction submodels were not

needed during the simulation. The results of Coulter's mold filling experiments are shown

in Figure 21. The solid lines shown represent the resin front location at various mold fill-

ing times.
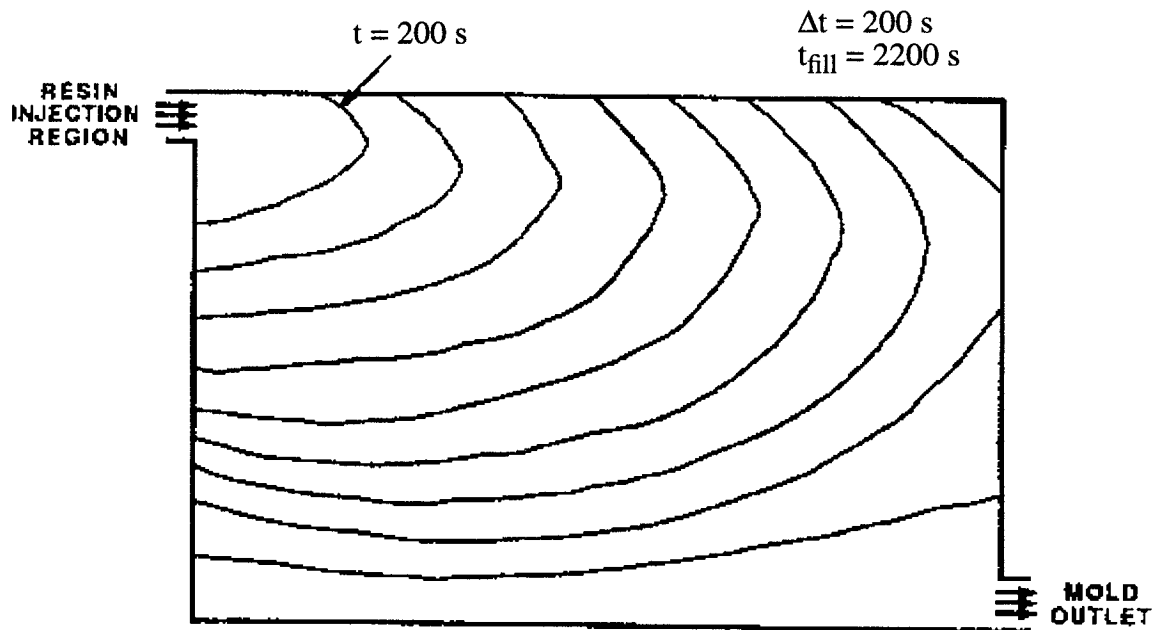
FIGURE 21 Coulter's experimental flow front results.

Mold Inlet

t = 200 s

Mold Exit

Δt = 200 s
t fill = 2053 s
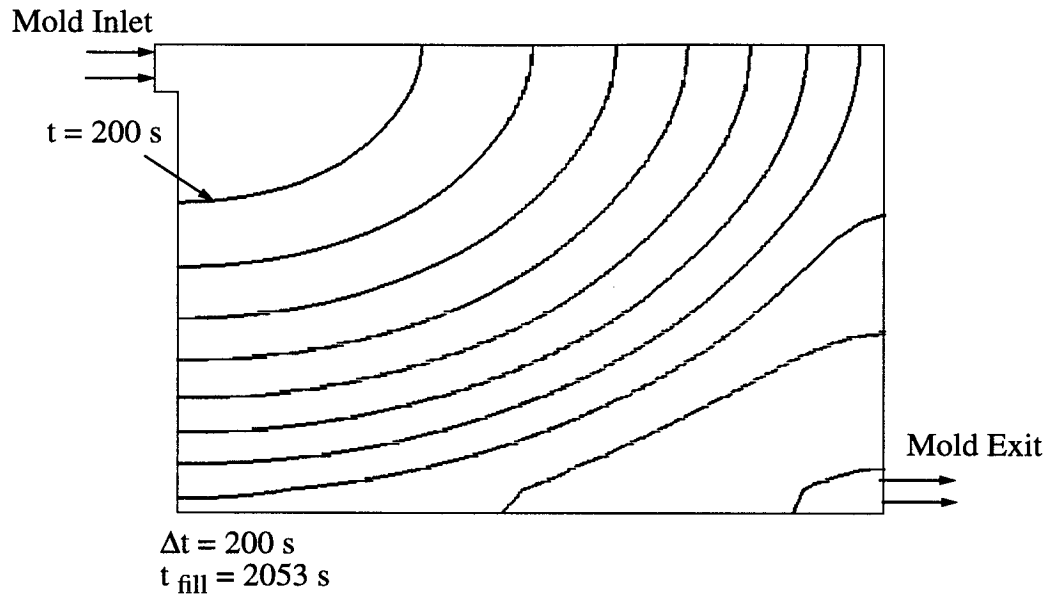
FIGURE 22 Flow front versus time results for Coulter's experiment.

The flow submodel simulation results are shown in Figure 22. Comparing Figures 21 and 22 it can be seen that the contact between the fluid and the mold walls plays an important role in determining the shape of the flow fronts. Since the flow submodel neglected the effects of a no-slip boundary condition, the fluid was allowed to slip along the mold wall. As can be seen in Figure 21, the no-slip boundary significantly affects the flow front shape along the mold wall. However, along the sides and bottom mold surface the no-slip condition played a somewhat lesser role in determining the flow front shape. Although there was a difference in shape of the flow fronts, the total infiltration time predicted by the flow submodel (2053 seconds) was fairly close to the actual value (2200 seconds).

The predicted and calculated values of the inlet pressures are compared in Figure 23. The solid lines indicate the pressure predicted by the flow simulation model, and the dashed lines represent Coulter's measured inlet pressure values. Also, included in Figure 23 are

the predicted values of inlet pressure using Coulter's simulation model. As can be seen, the predictions of inlet pressure versus time are somewhat erratic. The flow simulation model calculated inlet pressure initially overshoots the measured pressure and then begins to level off before rapidly increasing just before complete infiltration. The differences between the simulated and experimental results for inlet pressure can be attributed to many of the same factors discussed for the flow patterns. Due to the differences in saturated preform areas at the same value of time, the pressure distributions at the inlet would be expected to vary significantly. This would explain why the predicted inlet pressure is different from the measured pressures even though the values of final predicted and measured infiltration time agree reasonably well.

Several important assumptions were made in the simulation that could introduce some degree of uncertainty into the results. First, the thicknesses of the specimens tested by Coulter were not reported. Second, due to the unknown specimen thicknesses, the fiber volume fractions had to be estimated. A small variation in either of these parameters could produce a significant change in the simulation results. With the inclusion of the proper mold boundary conditions and the effects of surface tension and capillary pressure, the simulation results could be expected to improve considerably. The purpose of this verification was to prove the viability of the resin flow simulation model. Allowing for the uncertainties in the boundary conditions and material parameters reported by Coulter, the simulation results demonstrate that the resin flow submodel can provide a reasonably accurate simulations of the mold filling process.
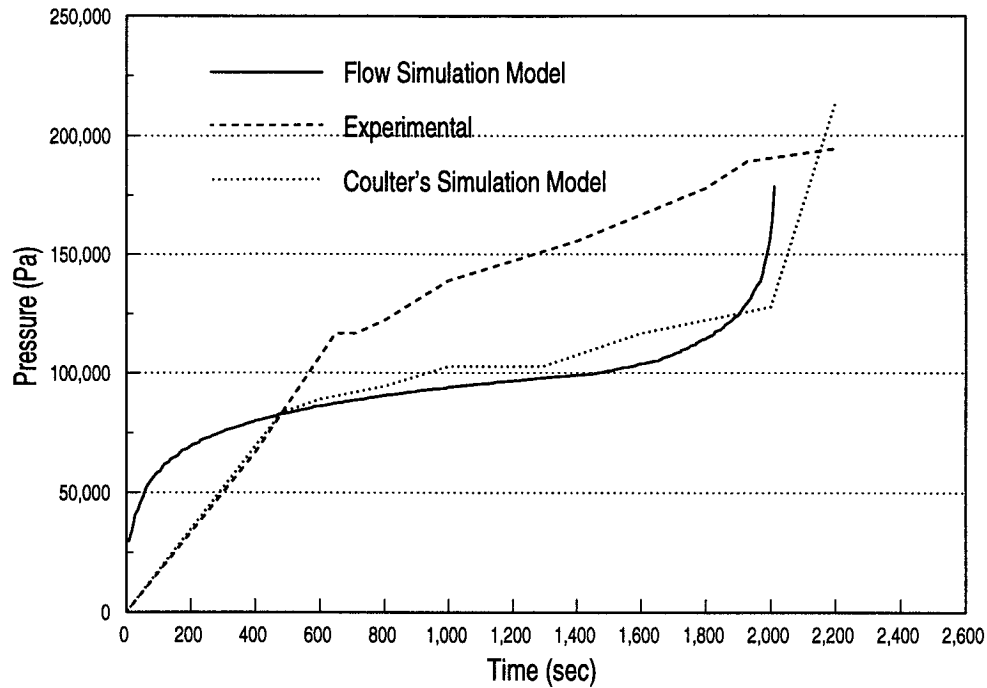
FIGURE 23 Inlet pressure versus time for Coulter's experiment.

7.1.2 Flow Model Comparison with Experimental Results

Although a comparison with reported data in the literature provides a good means of determining the viability of the flow submodel, the uncertainties in such reported data leave open the question of the model accuracy. In order to better address the question of flow model accuracy, an experimental investigation was undertaken. The purpose of this investigation was to determine how well the flow submodel could predict a simple infiltration pattern.

A mold was constructed which allowed for the infiltration of a 0.6096 m x 0.6096 m (2 ft. x 2 ft.) test specimen. The mold assembly consisted of a plexiglass upper plate and an aluminum lower plate with an aluminum frame surrounding the test specimen. A fabric specimen was placed in the fixture, and the aluminum frame was used to clamp the plexiglass lid down to the lower plate. A series of bolts along the sides of the frame were torqued down to provide the clamping force. A single injection port, 0.00635 m in diameter, was machined into the center of the lower plate of the test fixture. To control the fluid flow into the fixture, a shut-off valve with a pressure gauge was connected to the inlet. Plastic tubing was used to connect a pressurized container of fluid to the valve/gauge/fixture assembly. The pressure in the container of fluid was maintained at a relatively constant value during the infiltration of the test specimen. Figure 24 shows the apparatus used in the experiments. A video camera was used to record the resin flow patterns during the mold filling experiments.

The test specimen material consisted of a plain weave glass fabric. Eleven plies of the glass fabric were placed into the test fixture and clamped together. This provided a fiber volume fraction of approximately 43% in the test specimen. Corn oil was used as the infiltrating fluid. A red dye was added to the corn syrup in order to allow for better visibility of the resin flow front movement. Once again the experiments were carried out under room temperature, isothermal conditions. The fluid viscosity was measured prior to the test. Once the valve at the inlet to the fixture was opened pressure readings as a function of time were recorded at the mold inlet and inside the pressurized fluid container.
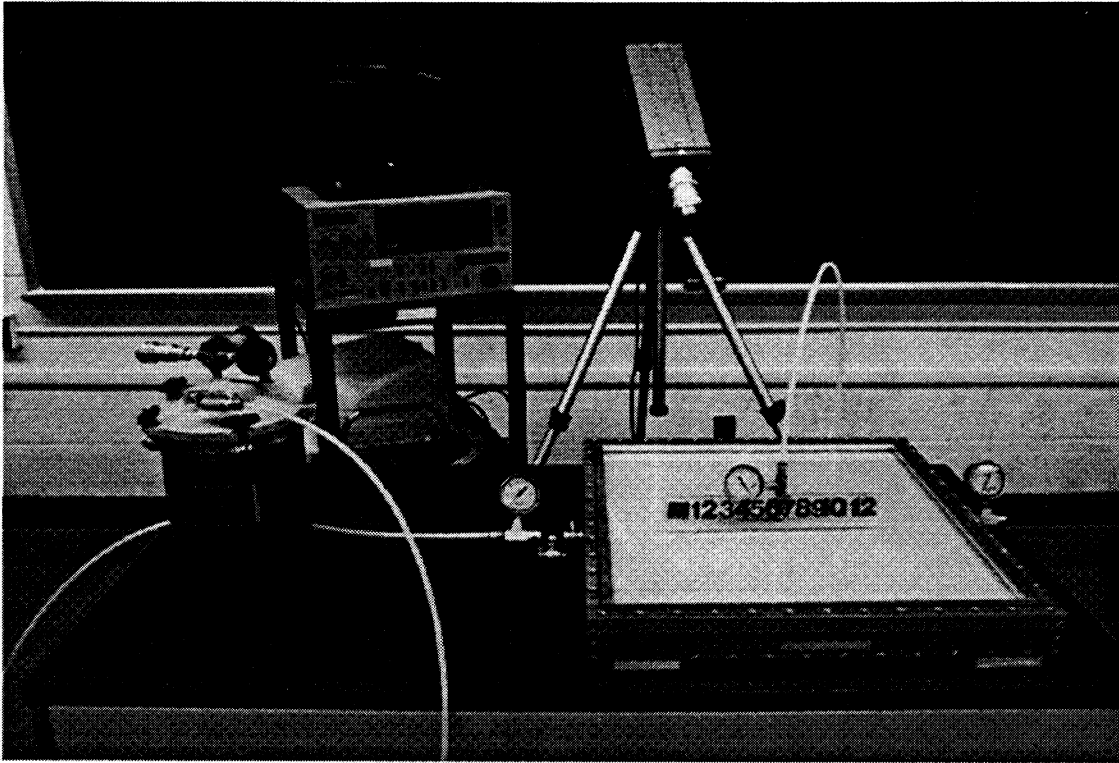
FIGURE 24 Experimental apparatus.

The pressure versus time profiles for both the pressurized container and at the mold inlet are shown in Figure 25. A nominal pressure of 103 MPa (15 psi) was maintained inside the pressurized container. Some variation in pressure did occur as is shown in Figure 25. The inlet pressure initially decreased rapidly to almost 0 Pa but then recovered and continued to measure approximately 75 MPa (11 psi) for the remainder of infiltration. The pressure versus time profiles were used as a specified pressure boundary condition in the flow simulation model. Table 2 details the material constants and boundary conditions used in the flow simulation submodel.
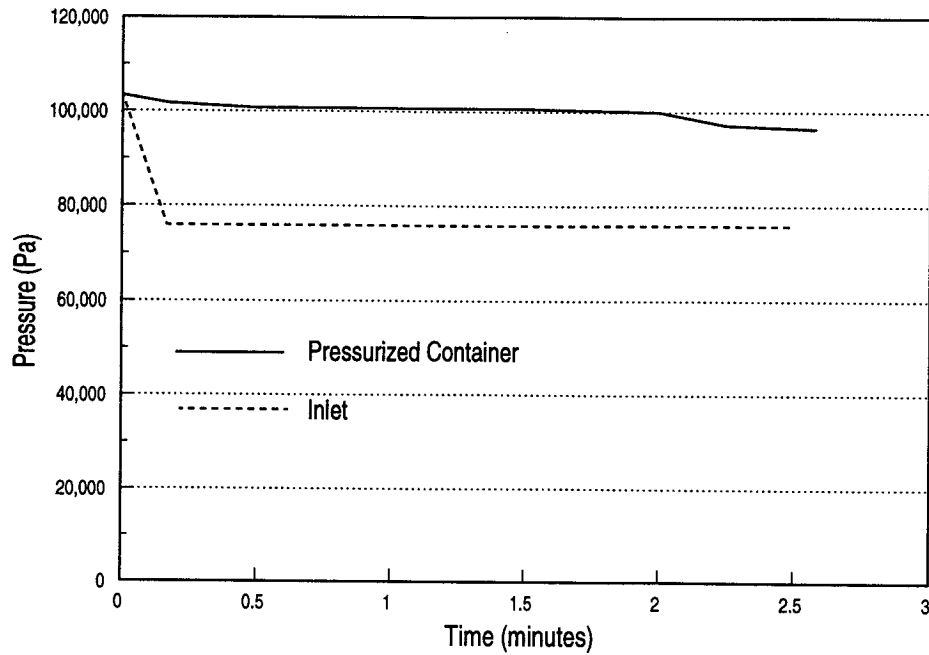
FIGURE 25 Pressure versus time for center-port injection.

TABLE 4 Material Constants and Boundary Conditions for Center-Port Experiment.

mold size	0.6096 m x 0.6096 m x 0.0038 m
porosity	0.57
cavity thickness	0.0038 m
fluid viscosity	0.0635 Pa•s
pressure (inlet)	103421 Pa
$k_x =$	1.402E-10 m^2
$k_y =$	1.946E-10 m^2
inlet diameter	0.00635 m

The permeabilities of the glass fabric were measured using a fully saturated sample under

steady state flow conditions. Details of this technique, as well as a detailed description of

the glass fabric values, can be found in Hammond [15]. It should be noted here that these permeabilities are a function of the porosity of the glass fabric specimen.

A PATRAN pre-processor model was constructed using the dimensions of the mold assembly. The PATRAN generated mesh, shown in Figure 26, also allowed for side port injections to be modeled. The higher density of elements in the center of the mesh enabled the side ports to be included. Another feature incorporated into the mesh is the ability to model a channel around the perimeter of the test specimen. This would be necessary when a side port injection test was being done with the use of a channel to distribute the fluid around the fabric specimen.

A series of still frame images were captured from the video tape of the center-port injection experiment. These images were captured at 5 second intervals during the test. The resulting flow fronts predicted from the flow submodel were plotted at the same time intervals. The video images and the PATRAN plots were superimposed on each other in order to check the accuracy of the flow submodel predictions.

Several flow submodel cases were run using the boundary conditions and material constants presented in Table 2 . It was found that the predicted and experimental flow front profiles did not agree. A reason for the discrepancy was that constant values of preform thickness and porosity were used in the calculations. It was found through a separate finite element analysis, that the plexiglass top plate deflected when the fabric preform was compressed to the thickness of the mold cavity. Furthermore, the plexiglass plate would undergo additional deflection when fluid under pressure was introduced into the mold during infiltration. This added deflection changed the thickness, the fiber volume fraction, and the permeability of the preform. The distribution in the deflections ranged from 0 at the clamped edges of the mold to a high of 3 ply thicknesses or about 0.45 mm at the center of

the mold. The resulting deflection, calculated from the finite element analysis of the plexiglass lid under uniform loading, was incorporated into the flow submodel boundary conditions to account for the variations in fiber volume fraction, element thickness, and permeability within the preform. The updated flow submodel was recalculated. Figures 27,28,29, and 30 show the PATRAN results superimposed onto the experimental patterns at 10, 30, 65, and 115 seconds, respectively.
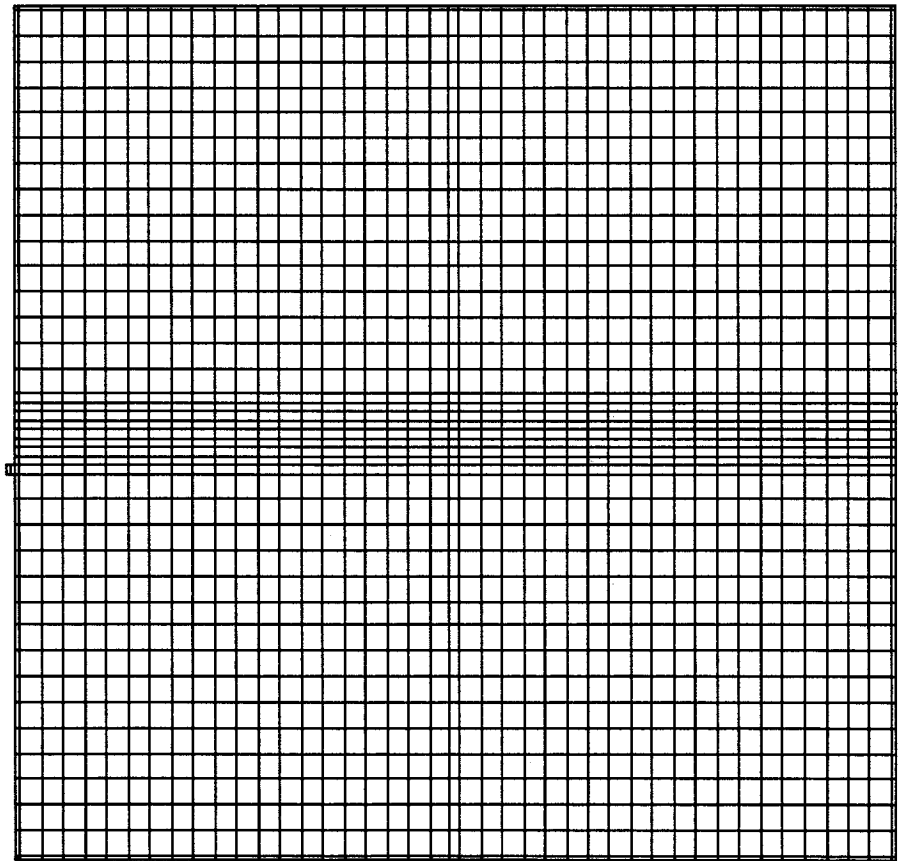
FIGURE 26 Patran generated mesh for flow visualization fixture.
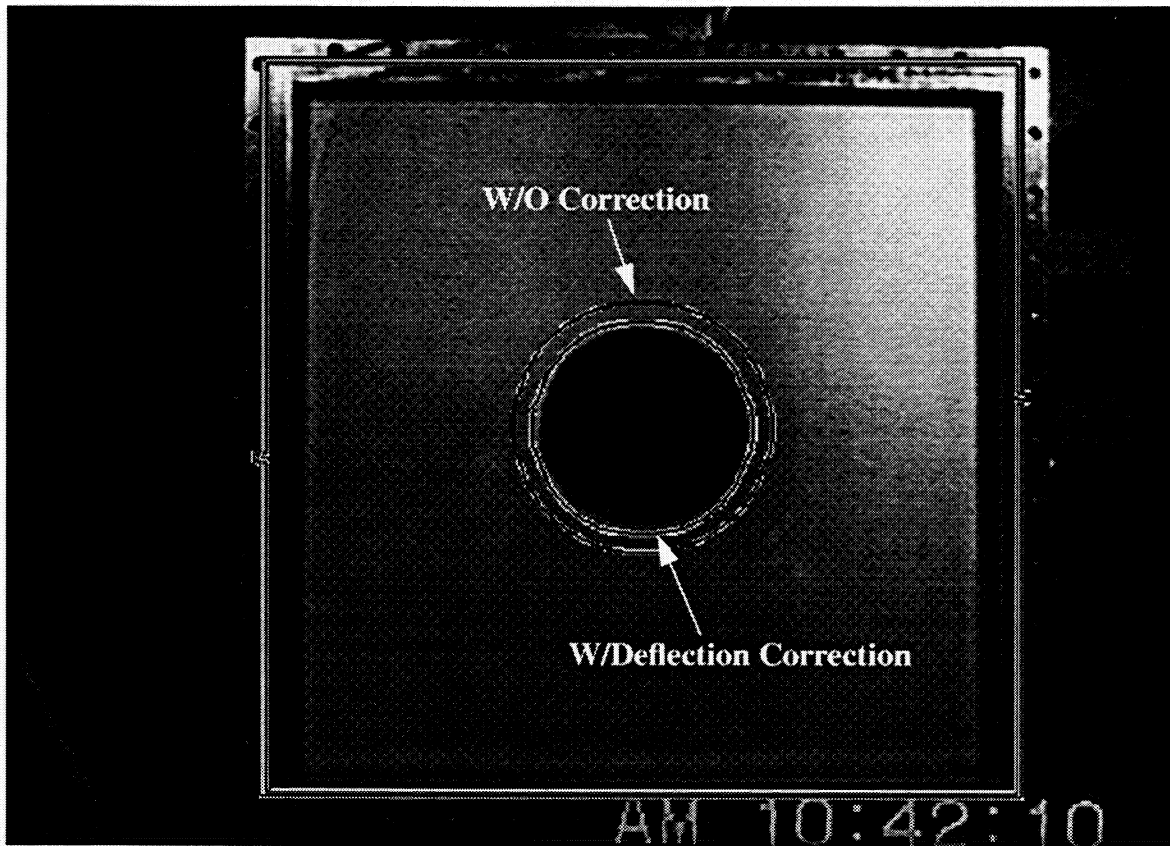
FIGURE 27 Flow model comparison with experimental data, 10 seconds.
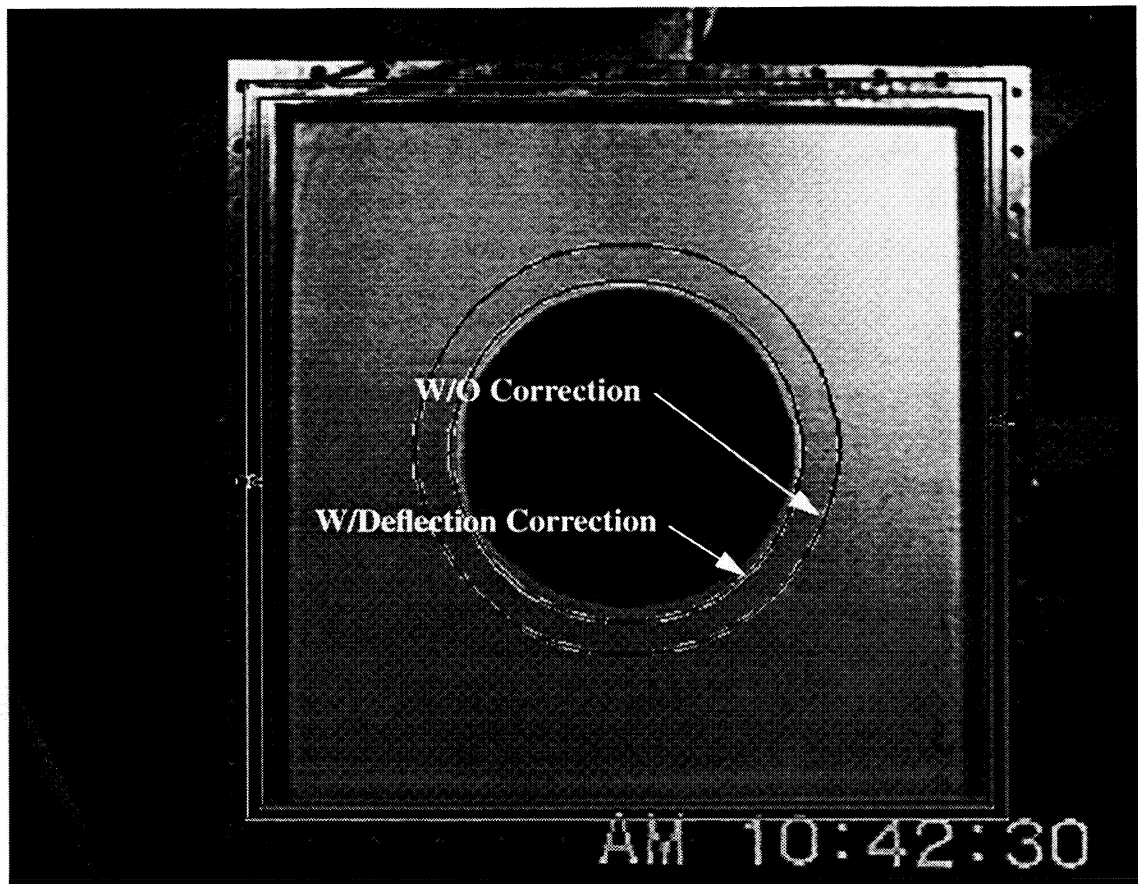
FIGURE 28 Flow model comparison with experimental data, 30 seconds.
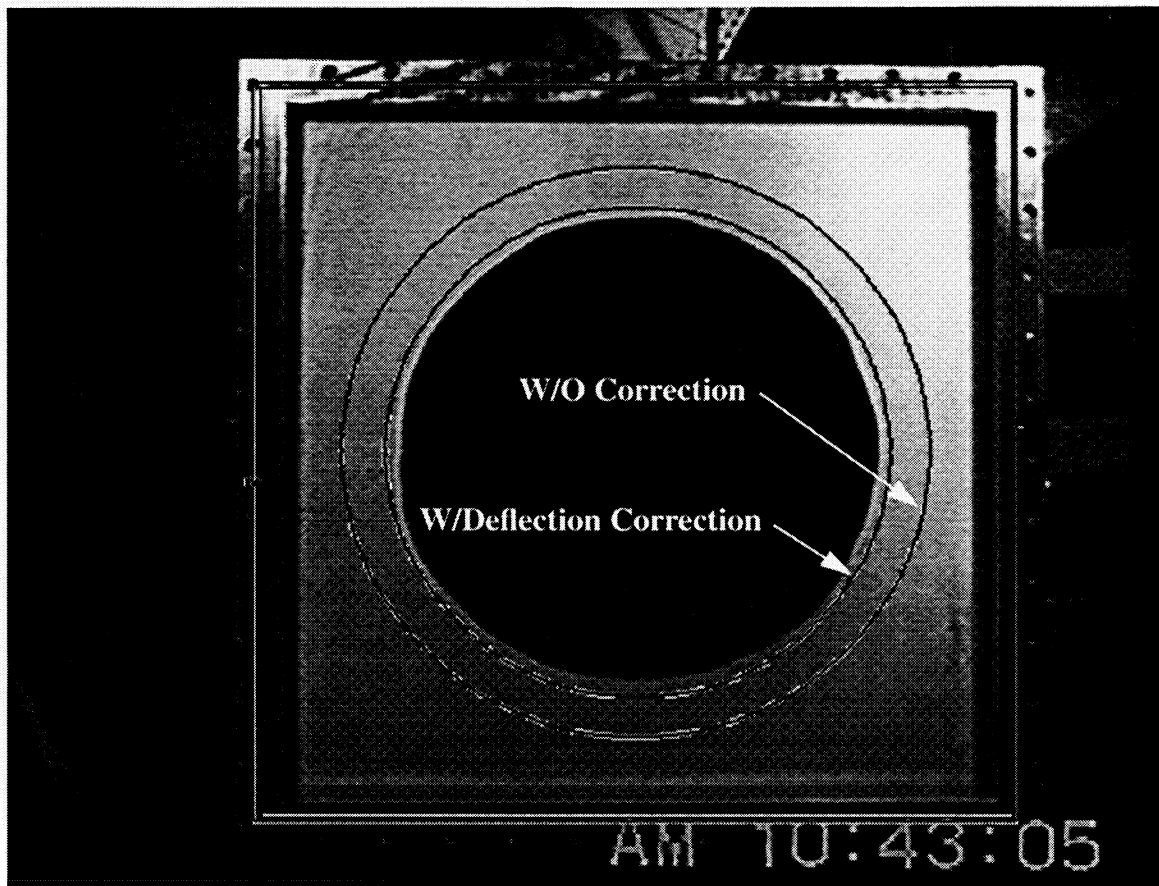
FIGURE 29 Flow model comparison with experimental data, 65 seconds.

C-2
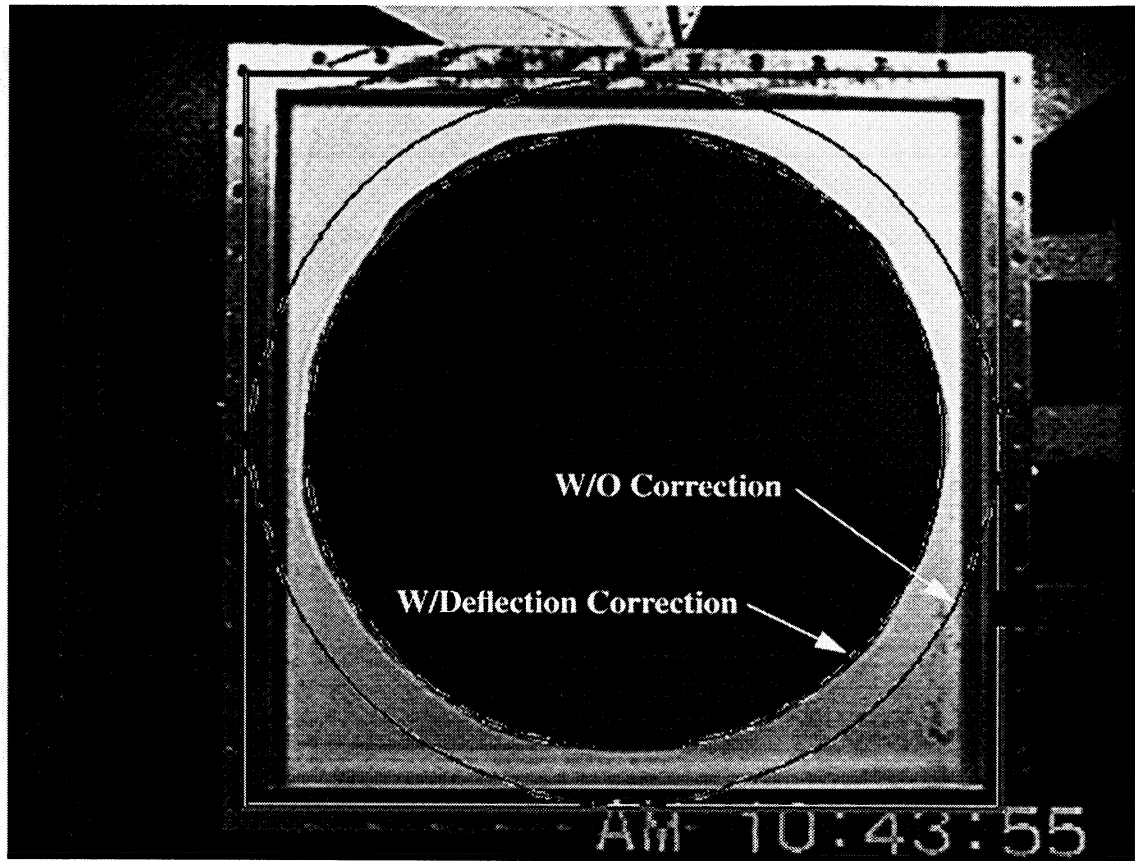
FIGURE 30 Flow model comparison with experimental data, 115 seconds.

The dark lines in these figures represent the predicted flow front. The outer lines indicate the resulting profile of an analysis that ignores the deflection of the lid. The inner lines indicate the predicted flow front positions when lid deflection is taken into account. The deflection of the lid was calculated using a finite element analysis of the plexiglass lid under a uniform applied fluid pressure. The resulting deflections were then used to calculate the distribution of permeabilities within the glass sample. As can be seen from these Figures, the flow submodel provides a good prediction of the flow front position and the flow front shape during the infiltration process. In addition to verifying the flow submodel, this experimental study helped reinforce the need for careful attention to the material con-

stants and boundary conditions used as input into the simulation model. By ignoring the effects of fabric compaction and fluid pressure on fixture deflection, a significant error was introduced into the analysis.

In addition to the center-port experiments outlined above, this fixture was used for a series of single and multiple side-port injection experiments. The flow submodel was again used in simulating the fluid flow in these experiments. A detailed discussion of this work can be found in Hammond[15].

7.2   Heat Transfer Submodel Verification

The verification of the heat transfer submodel proceeded along the same lines as the flow submodel. The purpose was to select a test case that would allow for all the elements of the heat transfer submodel to be verified without including the other submodels. The case selected was the curing of a thick section composite laminate in an autoclave. The thick section test case allowed for elements such as the resin kinetics, convective boundaries, and transient heat transfer to be analyzed. The example selected was based on work reported by Loos [16] on the processing of an 192-ply laminate. The experimental data obtained in this study were also available.

The composite lay-up used by Loos [16] consisted of six, 32-ply pre-compacted lay-ups of AS4/3501-6 graphite-epoxy. The 192-ply lay-up was trimmed to 30.48 cm x 30.48 cm. Thermocouples were distributed throughout the laminate to measure the temperature gradients during processing. The bagging schematic for the 192-ply composite laminate is shown in Figure 31. The composite panel was held under vacuum and cured according to the manufacturer's recommended cure cycle. During the cure cycle the temperatures

inside the laminate and in the autoclave were recorded. The thermocouple locations are denoted in Figure 32.

The thick-section composite laminate was constructed from a low resin content prepreg material. Due to the low resin content, the resulting resin loss during processing was less than 5%, and therefore the resin flow could effectively be neglected. The composite laminate had an initial resin mass fraction of 35%.

The composite laminate was placed on a 0.64 cm steel tool plate, and a 1.27 cm aluminum pressure plate was used atop the laminate stack. The properties for the tool and pressure plates, as well as the manufacturer's reported material properties for the AS4/3501-6 prepreg, are listed in Table 5 .
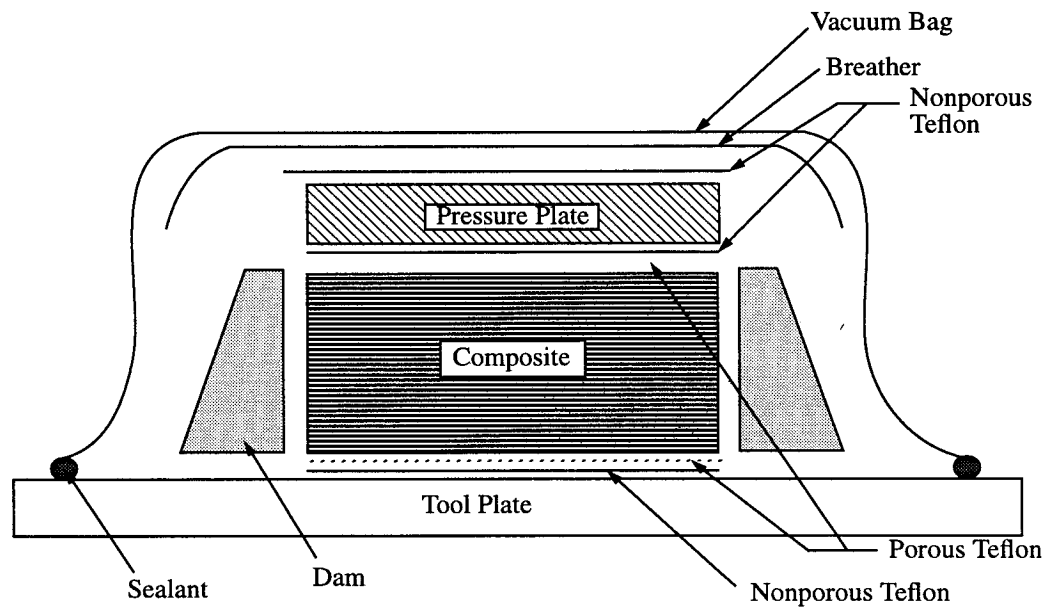
FIGURE 31 Bagging schematic for 192-ply laminate.
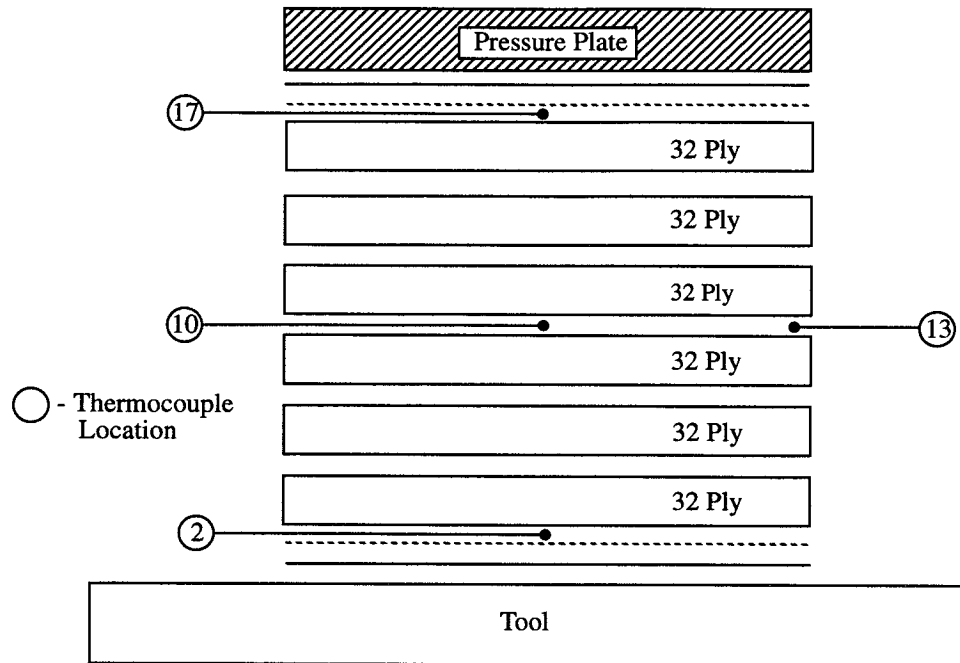
FIGURE 32 Location of Thermocouples.

TABLE 5 Material properties for 192-ply composite lay-up.

Materials	Density (kg/m³)	Specific Heat (J/kg•K)	Thermal Conductivity (W/m•K)
Steel	7.8498E+03	4.6055E+02	4.50E+01
Aluminum	2.7074E+03	8.7085E+02	2.02E+02
Resin	1.2600E+03	1.2560E+03	1.674E-01
Fiber	1.7900E+03	7.1176E+02	2.597E+01

Along with the material property information given in Table 5 , one additional piece of

information was needed in order to completely describe the boundary conditions of the

problem. That additional piece of data was the convective heat transfer coefficient. Loos

estimated this coefficient by fitting the predicted temperature values with those measured

during the experiment. The value obtained was 40 $W/m^2 \cdot K$. This method of determining

the heat transfer coefficient lumped the thermal resistance of the bagging and Teflon films

and the breather into the coefficient. The heat transfer coefficient was assumed to remain

constant during the curing process.

A two-dimensional PATRAN model was created for the 192-ply composite lay-up. The

model included the steel baseplate and the aluminum caul or pressure plate as well as the

composite laminate itself. Only the heat transfer submodel was utilized in the simulation.

The measured autoclave air temperature profile was used as the input temperature profile.

The PATRAN generated mesh for this case is shown in Figure 33.
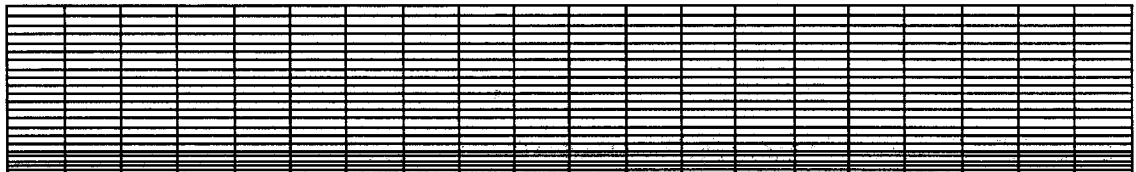
FIGURE 33 PATRAN mesh for 192-ply composite lay-up.

Convective boundaries were selected for all the outer surfaces of the mesh. The damming

material on the outer edges of the laminate was neglected in the heat transfer analysis. The

simulation was run on a Silicon Graphics 4D/320 VGX workstation. Four selected nodal

temperatures were plotted along with the corresponding measured temperatures as a func-

tion of time. Four of these temperature profiles are shown in Figures 34 -37.
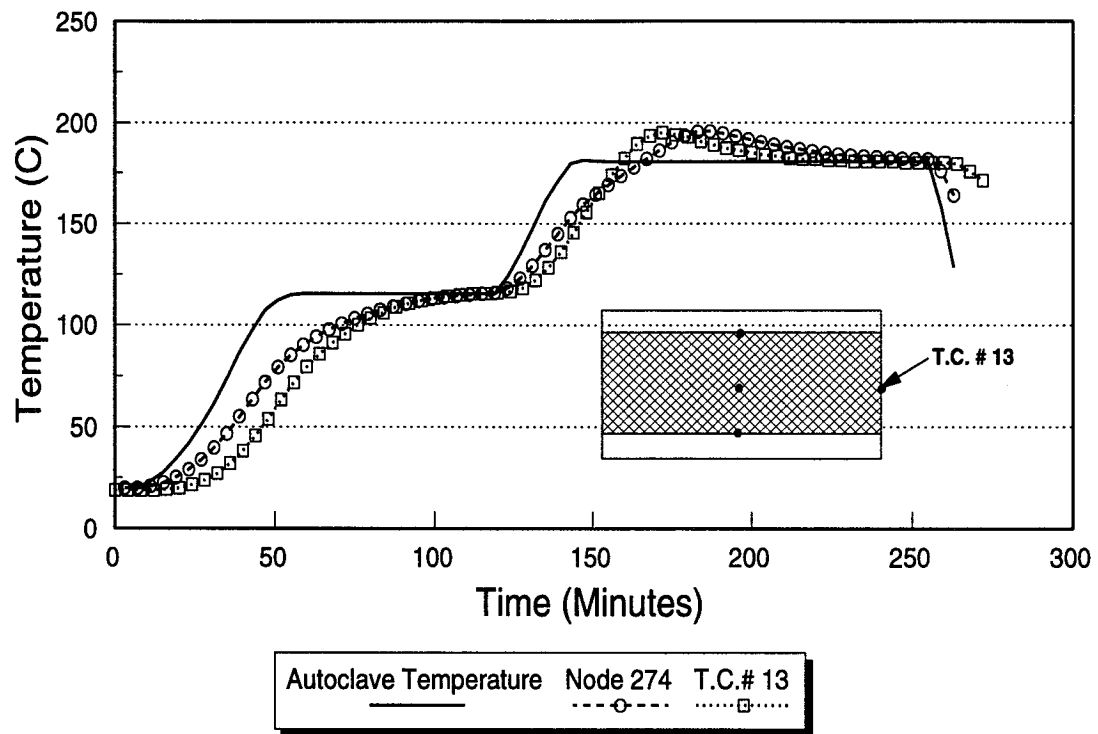
FIGURE 34 Predicted versus measured temperatures, 192-ply laminate, outside edge.
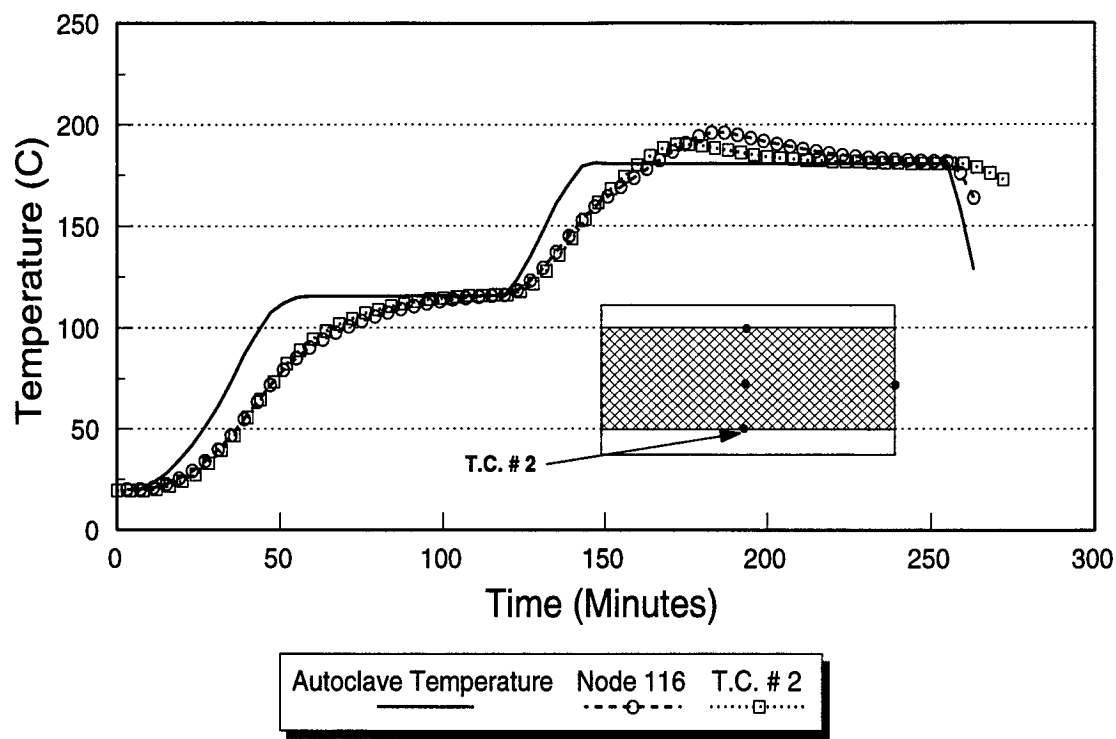
FIGURE 35 Predicted versus measured temperatures, 192-ply panel, bottom center.
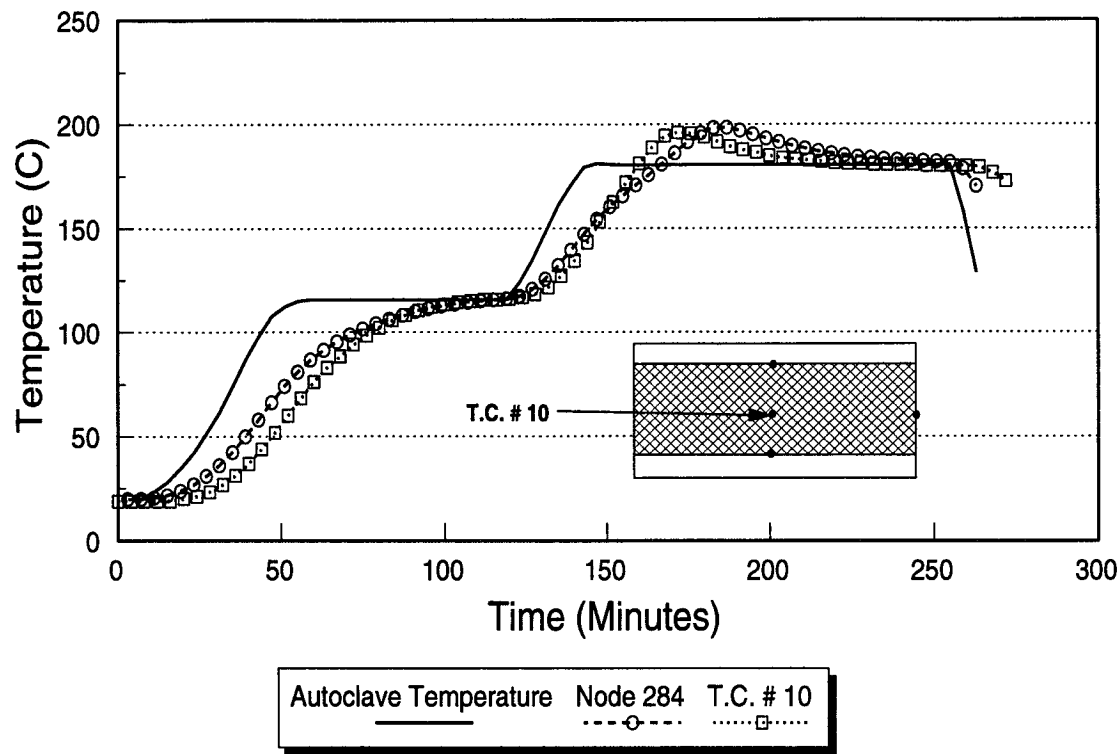
FIGURE 36 Predicted versus measured temperatures, 192-ply panel, middle center.
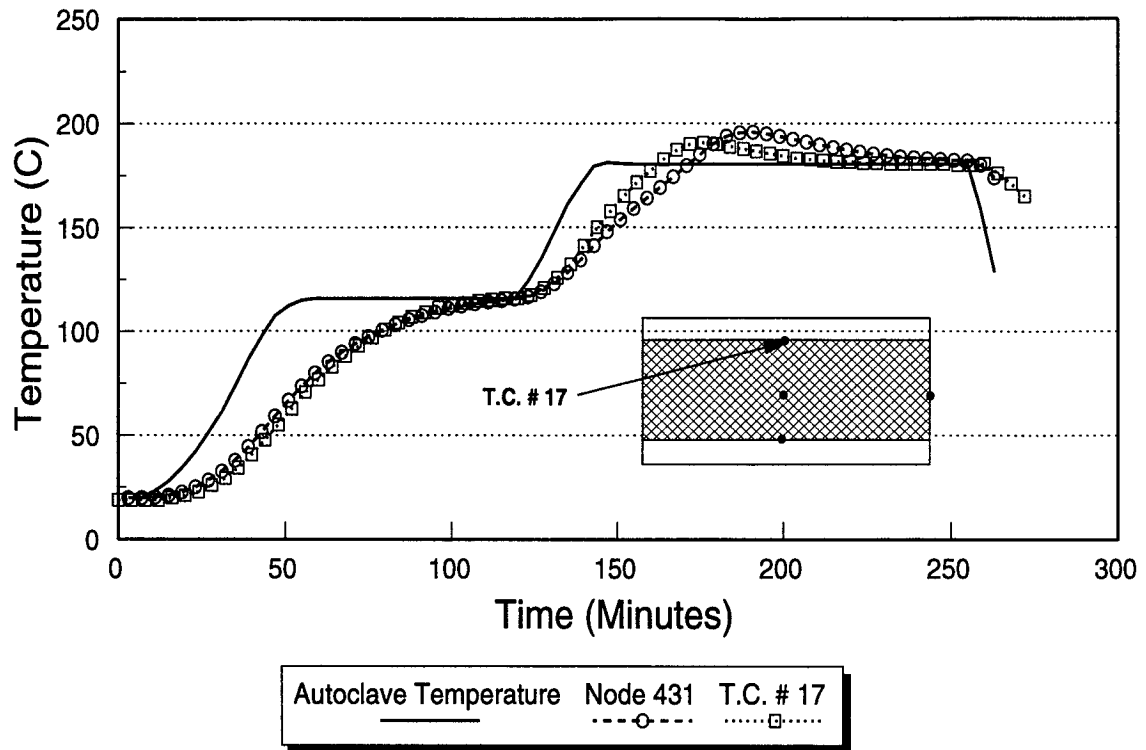
FIGURE 37 Predicted versus measured temperatures, 192-ply panel, middle top.

In Figure 34, the temperature profile predicted by the heat transfer submodel is compared with the measured temperature profile for a location at the center of the laminate. As can be seen in the Figure, the predicted and measured profiles match reasonably well at this location. There is some temperature variation at the beginning of the intermediate hold. Also, the exothermic overshoot predicted by the heat transfer submodel occurred at a later time than that which was actually measured. Figure 35 shows the predicted and measured temperature profiles for the bottom-center of the laminate. The agreement between the measured and calculated temperatures is good except in the region of the exotherm. The predicted and measured temperature profiles for the middle-center and middle-top loca-

tions in the laminate are shown in Figures 36 and 37, respectively. The agreement between the predicted and measured values in these Figures is similar to those described above.

The difference in the measured and calculated temperatures at the beginning of the intermediate hold at the middle and outside edge of the laminate can be partially explained by the fact that the thermal properties of the damming materials were not included in the model. The damming materials would act as an insulator and would slow the heat transfer into the composite laminate. This would partially explain the slightly higher temperatures predicted during the initial ramp to the intermediate hold.

The calculated exothermic peak lags the measured exothermic peak during the curing cycle and may be due to the slightly different temperature history of the resin system during the early stages of the cure cycle or a variation in the specified initial degree of cure of the resin system prior to the start of the cure cycle. A value of 0.05 was used as an initial degree of cure in this analysis.

At the upper and lower surfaces of the laminate, the temperature profiles predicted by the model matched the experimental values well. The convective heat transfer coefficient used in the simulation model was the value calculated by Loos for a one-dimensional thermal model. The same heat transfer coefficient was assumed in the two-dimensional RTM simulation model for the right and left sides of the laminate. The actual heat transfer coefficient present on the side surfaces could have been different in the experiment. Therefore, one would expect good agreement between the experiment and measured temperatures along the vertical mid-plane of the laminate, with less agreement horizontally across the panel. The RTM simulation results exemplify this behavior.

Overall the predictions of the heat transfer model in this case were satisfactory. A closer agreement in the predicted and final values could be attained by adding the effects of the

damming materials on the edges of the model and adjusting the initial degree of cure for the model. However, as far as demonstrating the capability of the heat transfer submodel to accurately predict the temperature profiles for a reacting composite lay-up with convective boundaries and subjected to a transient temperature profile, this effort proved sufficient.

CHAPTER 8

Stiffened Panel Simulation

The previous chapter addressed the verification of the resin transfer molding simulation model. In this chapter the results of the resin transfer molding simulation of the blade stiffened panel, introduced in Chapter 3, will be discussed. The blade stiffened panel simulation provides an example of how a comprehensive resin transfer molding computer model can be utilized in the manufacture of complex shape composite structures. A discussion of the boundary conditions required for simulation of the stiffened panel fabrication, as well as the PATRAN pre-processing and the simulation results, are presented in this chapter.

As described in Chapter 3, the stiffened panel is manufactured by the resin infusion process. This process is a variation of the resin transfer molding process and involves placing a degassed hot melt resin film of a predetermined thickness onto the surface of the tool plate. Next a stitched fabric preform is placed on top of the resin film, and the remaining tooling details are assembled. The tooling/part assembly is then placed in a vacuum bag and cured under elevated temperature and pressure in an autoclave.

The objective of the resin transfer molding simulation of this blade stiffened part was to demonstrate the utility of such a processing model in the manufacturing of a realistic subscale wing panel. In order to achieve that goal quantities such as resin viscosity, degree of cure, compaction, and flow infiltration time must be predicted accurately and with a minimum of computational resources.

Modeling of this structure began with the selection of a region of the tooling assembly to be analyzed. A single blade on the outer edge of the three blade tooling assembly was selected for modeling. The region was selected due to the proximity of the edges of the part/tool assembly. By having three separate faces present in this region any temperature gradients due to differences in boundary conditions would be magnified in the part/tool assembly. Also by selecting only one stiffener, the computational requirements would be greatly reduced. The chosen region is depicted in Figure 38.
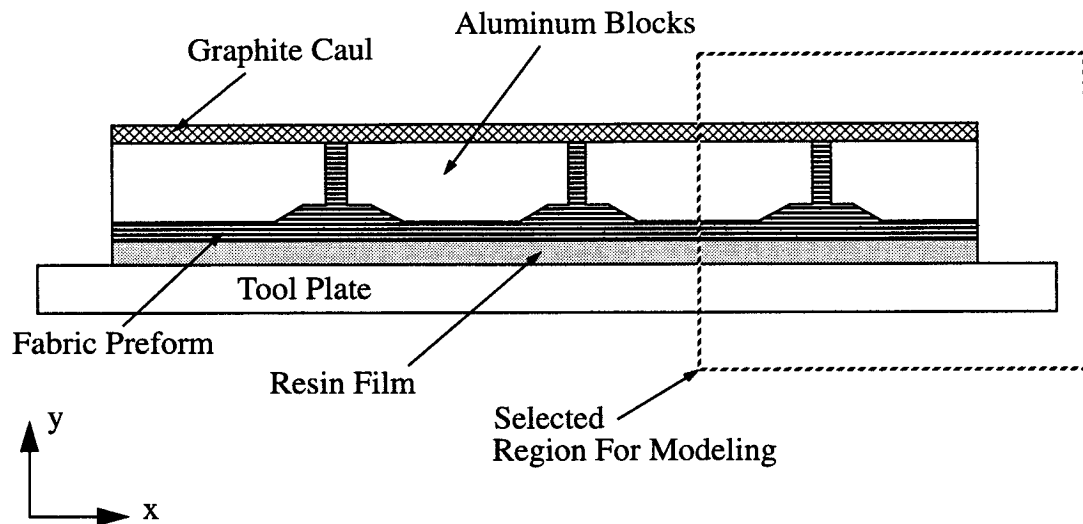
FIGURE 38 Region of tooling assembly selected for modeling.

The left-hand edge of the selected region was treated as an axis of symmetry. Although this was not a true axis of symmetry, the simulation results obtained from this model still provided valuable information about processing. A more detailed schematic representation of the selected region is given in Figure 39. The tooling consists of two aluminum blocks and shims, a graphite or aluminum caul sheet, and an aluminum base plate. The resin film and stitched graphite preform are also shown in Figure 39.

Once the region of interest had been established, the next phase of modeling the single blade and tooling assembly was to calculate and obtain the necessary material constants and boundary conditions. The determination of the necessary input for the simulation model is described in the following section.
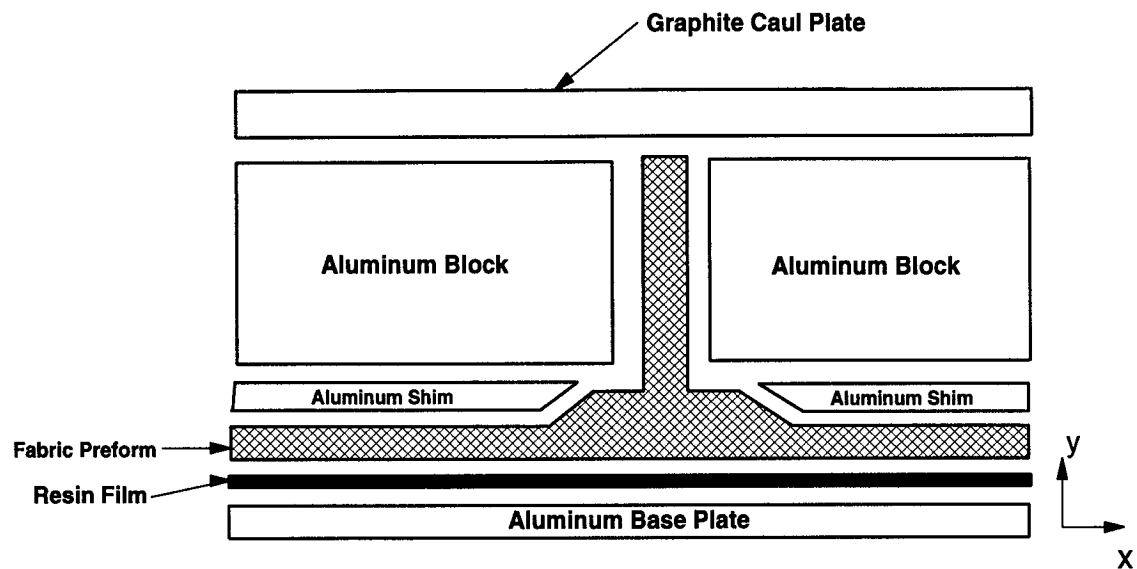
FIGURE 39 Schematic of selected single blade region.

8.1 Simulation Model Input

Accurately modeling the processing of the blade stiffened panel requires a complete description of the material constants and boundary conditions present during the manufacturing process. The flow, heat transfer, and compaction submodels all require input in the form of relevant material constants and boundary conditions. These material constants and boundary conditions will be discussed for each of the three submodels.

8.1.1 Flow Model Input

The simulation of the resin flow movement through the stitched graphite preform requires that the permeability of the fabric medium, the viscosity of the resin, and the applied resin pressure be specified. Each of these input parameters for the flow submodel will be described below.

In the processing of the blade stiffened panel, Hercules 3501-6 hot melt epoxy resin is pre-heated, degassed, and formed into the desired film thickness prior to manufacture. The resin film melts at elevated temperature and infiltrates the preform upon application of pressure. The thermosetting epoxy resin is a reactive material that is undergoing a chemi-cal cross-linking. Hence, the viscosity of the resin is a function of temperature and time, and the temperature history of the resin must be known to accurately predict the viscosity behavior. The viscosity submodel requires that the initial resin degree of cure specified. The heat transfer and kinetics submodels were used to predict the advancement of the resin during the initial degassing and forming stages. Figure 40 illustrates the temperature profile and viscosity changes that took place during fabrication of a Hercules 3501-6 resin film. As can be seen, the resin viscosity dropped rapidly with increasing temperature and then obtained a constant value below 10 Pa•s. The length of time that the resin system was exposed to elevated temperature during degassing and forming was relatively short, and therefore the advancement of the resin system was small. The degree of cure value pre-dicted by the kinetics submodel at the end of the resin film manufacturing was 0.02. This value was then used as the initial degree of cure for the stiffened blade processing cycle.
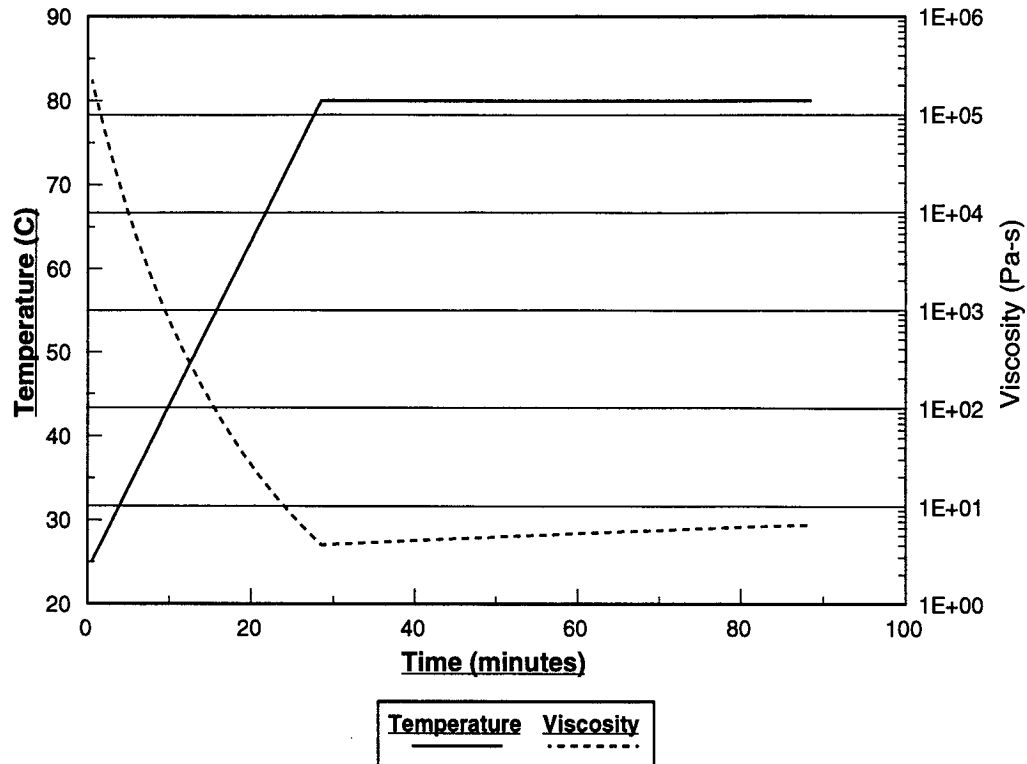
FIGURE 40 Temperature/Viscosity profiles for resin film manufacturing.

Once the initial degree of cure is known the kinetics submodel predicts viscosity changes in the resin during the remainder of the processing cycle. This viscosity information is stored for each element during the processing cycle.If a particular elemental viscosity was to reach a very high magnitude during the latter part of the processing cycle with a correspondingly high degree of cure, the resin would then be considered to have reached gelation or vitrification, and the flow solution would no longer be needed for that element.

Solution of the resin flow model requires that the permeabilities of the fabric preform be specified. In order to obtain this information, samples of the fabric being used in the manufacture of the blade stiffened panel were obtained and the permeabilities of those fabrics were measured.

The preform consisted of a stitched 54-ply graphite fabric skin and a stitched blade. The blade was formed from a stitched 72-ply graphite fabric which was folded and then stitched to the skin. Each of the preform materials had a quasi-isotropic stacking sequence. The stitching in the preform materials played an important role in compacting the material to the desired thicknesses for placement into the tooling assembly. The compaction directly influences the permeability of the fabric. Therefore in order to predict the infiltration of resin into the blade stiffened preform the values of permeability must be determined as a function of porosity or compaction of the preform. By looking at the cross section of the stitched preform a decision was made to characterize the preform permeabilities in only the through-the-thickness and in-plane (perpendicular to the stitching direction) directions. The reasons for this decision included the limited availability of preform specimens to test and also the number of directions in which flow could occur in the preform.

The permeabilities of the stitched fabric preforms were measured in test fixtures designed for in-plane and through-the-thickness permeability measurement. Figure 41 shows schematics of the in-plane and through-the-thickness permeability fixtures. Each of the fixtures was placed in an Instron testing machine so that different compaction loadings might be applied. The measurement of permeability was accomplished by placing a specimen in the test fixture and compacting the specimen to a desired fiber volume fraction. The specimen was held at the selected fiber volume fraction while a test fluid (water) was allowed to pass through the fully saturated specimen. Measurements of flow rate were made at several values of pressure drop across the test specimen. These values were recorded and then the specimen was compacted to a new fiber volume fraction and the procedure repeated.
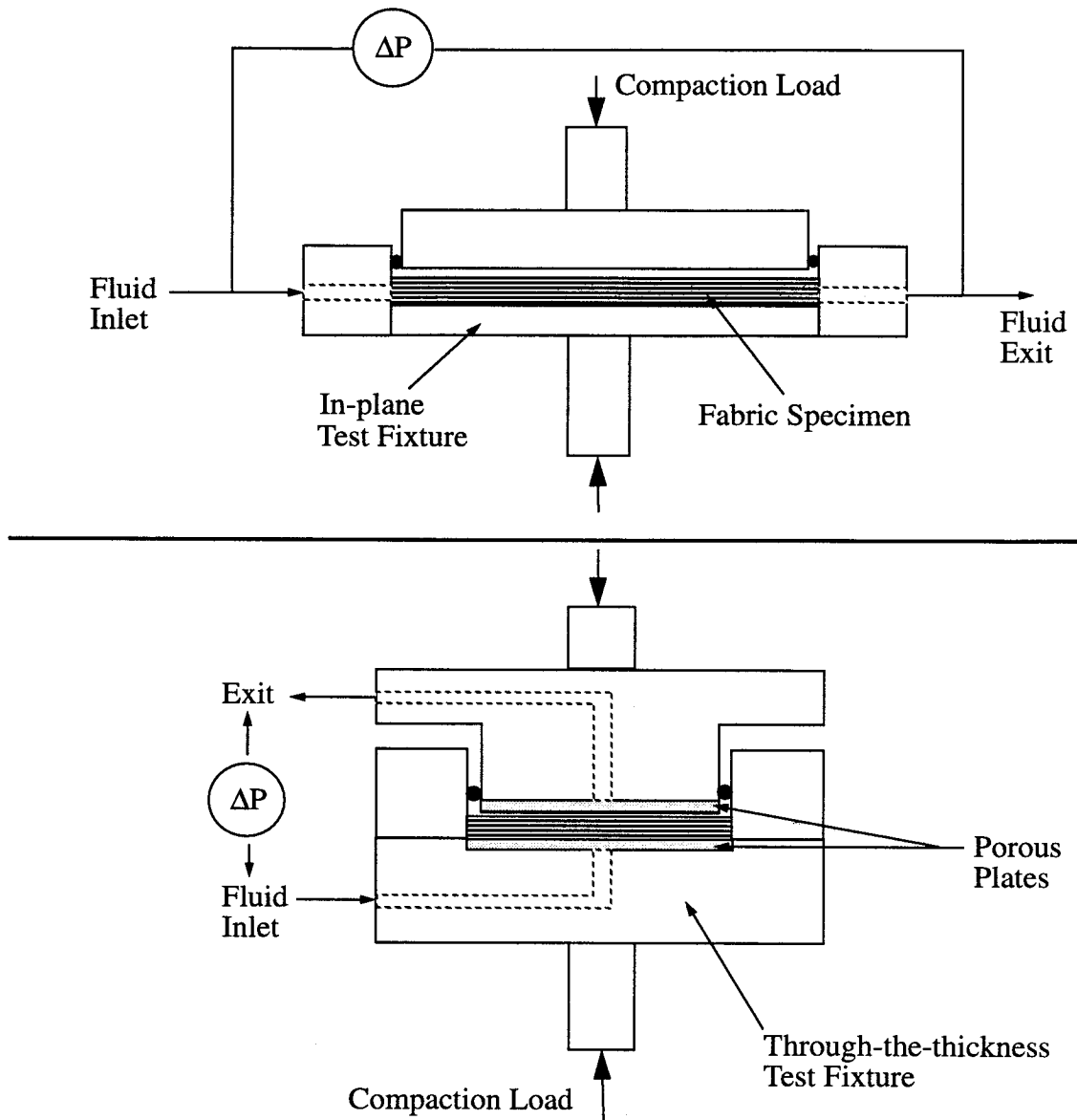
FIGURE 41 In-plane and through-the-thickness permeability test fixtures.

A curve was then generated of the flow rate versus pressure drop at different fiber volume or compaction loadings. A typical curve is shown in Figure 42.
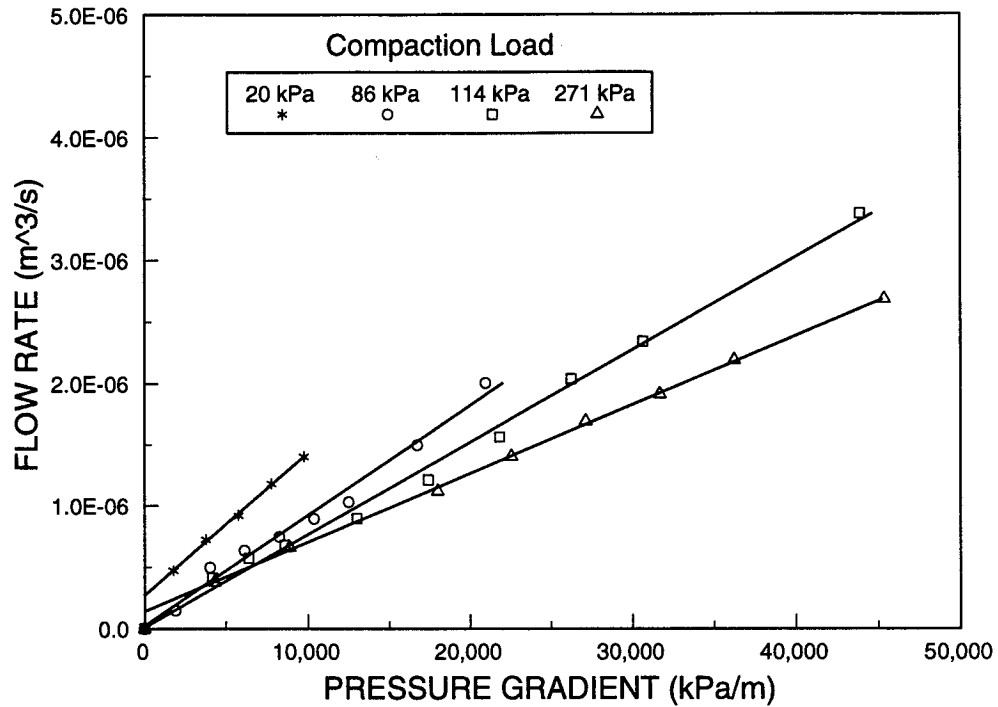
FIGURE 42 Typical pressure drop versus flow rate plot.

As can be seen from Figure 42, the pressure drop versus flow rate curves are reasonably linear and for the most part pass through or close to the origin. These results demonstrate that for this particular specimen Darcy's law is valid. Therefore, the permeability may be determined by taking the slope of each line. If the viscosity of the test fluid and the cross sectional area of the sample are known, the permeabilities may be calculated from the following relation

$$k = \frac{\mu \, (Slope)}{A} \tag{8-1}$$

where μ is the viscosity of the test fluid, the Slope is the slope of the flow rate versus pressure gradient plot, and A is the cross sectional area of the test specimen.

The permeabilities of the 54-and 72-ply stitched materials were measured by the method described above for fiber volume fractions in the range of 55% to 75%. Measurements of both in-plane and through-the-thickness permeability were made for the 72-ply preforms. However, the 54-ply material was only measured in the through-the-thickness direction due to the limited amount of material available. The in-plane permeability of the 54-ply material was not needed to complete the analysis of the blade stiffened panel. The permeabilities as a function of fiber volume fraction for the 54-and 72-ply stitched materials are shown in Figure 43. The lines passing through each set of data points represents a power law regression of the data. In order to account for the permeability changes as a function of the fiber volume fraction these power law regressions were input into the simulation model. Each power law function was used to describe an individual component of the permeability tensor. The assignment of the measured permeabilities to different components of the permeability tensor used in the resin flow model will be discussed in Section 8.2 .

One additional point should be made concerning the fabric permeabilities used in this analysis. The values used in the simulation model do not account for the effects of a partially saturated media. The assumption here is that the measured steady state fully saturated permeabilities are valid for all of the resin saturated elements in the model.

The remaining data needed to complete the input of the flow submodel includes the initial and boundary conditions for the infiltration process. The most significant of these is the treatment of the resin film used in the processing of the blade stiffened panel. At the beginning of the cycle the resin film has a specified initial thickness.
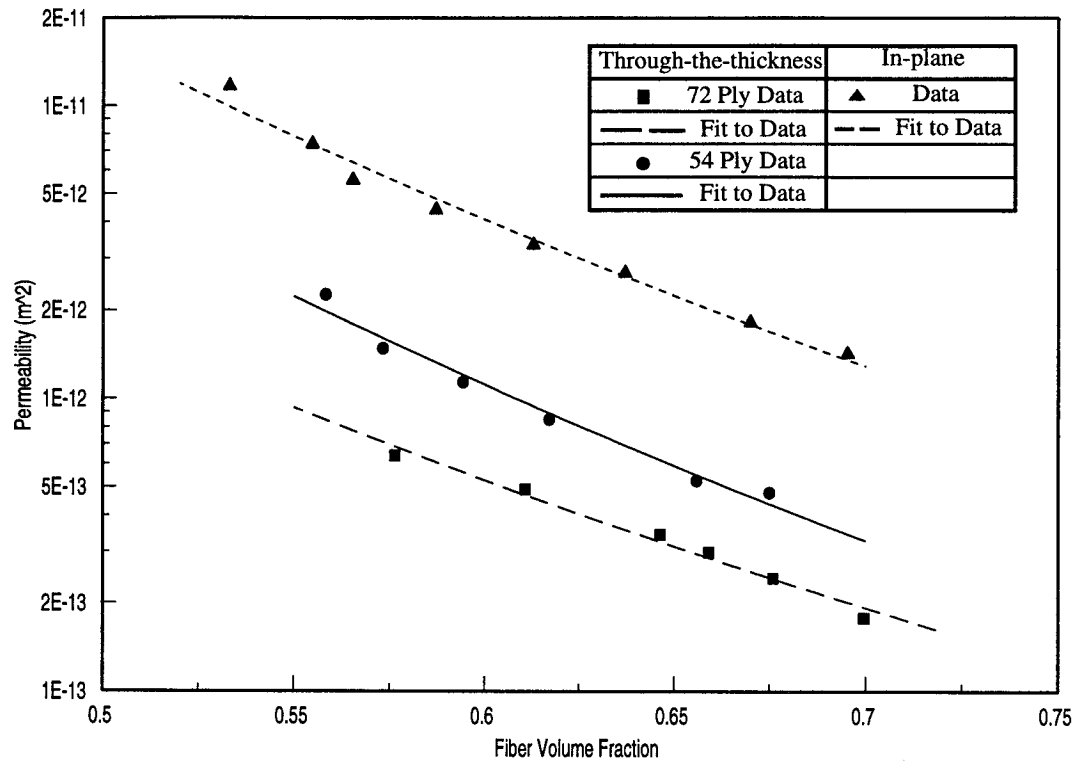
FIGURE 43 Measured permeabilities for 54-and 72-ply stitched preform materials.

As the temperature and pressure increase during the curing cycle, the resin softens and begins to infiltrate the fabric preform. At some point during the cycle, the thickness of the resin film decreases to zero as all the resin will have infiltrated into the fabric preform. In the simulation model, the resin film thickness initially is ignored. The simulation begins by specifying the thickness (usually one layer of elements) of the preform that is completely infiltrated by resin. In effect a constant supply of resin is assumed at the interface between the fabric preform and the resin film. A routine within the flow submodel tracks the amount of resin passing through the interface nodes and thus allows for the calculation of the resin film thickness required to completely fill the preform as well as the final part resin mass.

Figure 44 details the boundary conditions used in the simulation of the single blade stiff-ened preform. Along the surface of the skin which comes in contact with the baseplate a fluid pressure equal to the autoclave compaction pressure was specified. This provided the driving force behind the resin flow movement. A full vacuum was assumed inside the fabric preform and zero pressure was specified for all the unsaturated regions of the fabric preform. This provided the boundary condition at the resin flow front. Once again for this analysis the effects of surface tension and capillary pressure on the resin flow front were ignored. Resin flow through the tooling was prevented by specifying that the pressure gradient normal to the wall be zero.
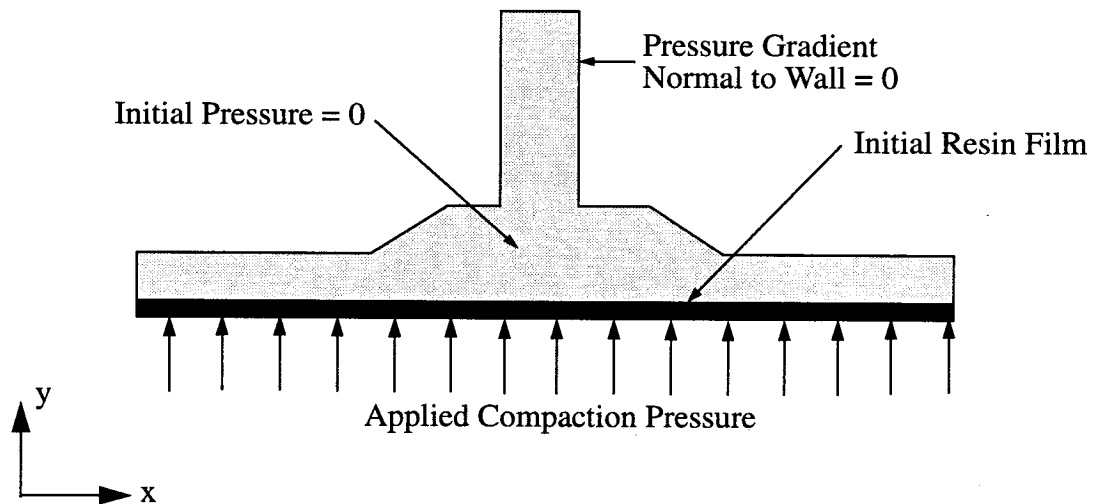
FIGURE 44 Flow submodel boundary conditions for single blade stiffener.

The parameters described above include all the material constants, initial, and boundary conditions necessary for input into the flow submodel.

8.1.2   Heat Transfer Model Input

In order to simulate the temperature changes taking place within preform and tooling assembly during the curing process, the values of the thermal conductivity, density, and specific heat must be known for each of the tooling materials as well as the fabric preform and resin. In addition to these material constants, a convective heat transfer coefficient must be found for any convective boundaries present in the model. Finally, the autoclave temperature cure cycle must be specified.

The effect of temperature on the thermal conductivity, density, and specific heat of the materials present in the single blade tooling assembly was neglected and the material properties were assumed to remain constant over the temperature range prescribed in the cure cycle. One purpose of the simulation model was to determine the optimum temperature cycle necessary for the manufacture of advanced composite materials. Along these lines, two cycles were analyzed during this study. The first temperature cycle analyzed was the original cycle used by MDA-West during the manufacturing of the three blade stiffened panel. The second cycle used in the analysis was developed after manufacturing the part, using with original cycle resulted in partial resin infiltration of the fabric preform. A more detailed discussion of these cycles will be presented later in this chapter. Figure 45 shows the original temperature curing cycle. The modified or extended cycle is shown in Figure 46. For the two cases analyzed, the autoclave temperatures represented in the Figures were used as the input temperature profile. A constant room temperature of 25 °C was specified throughout the tooling assembly as the initial temperature.
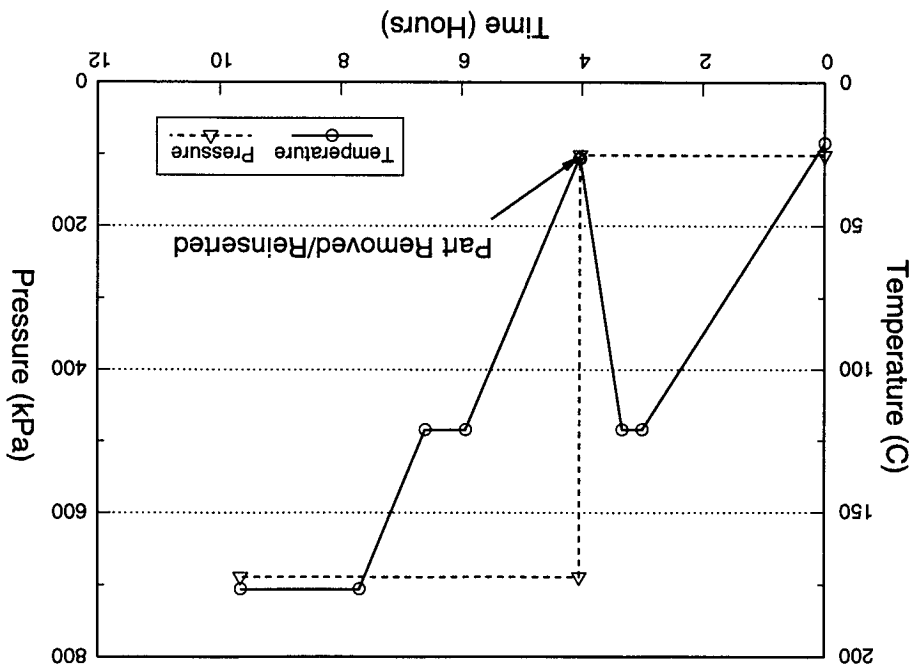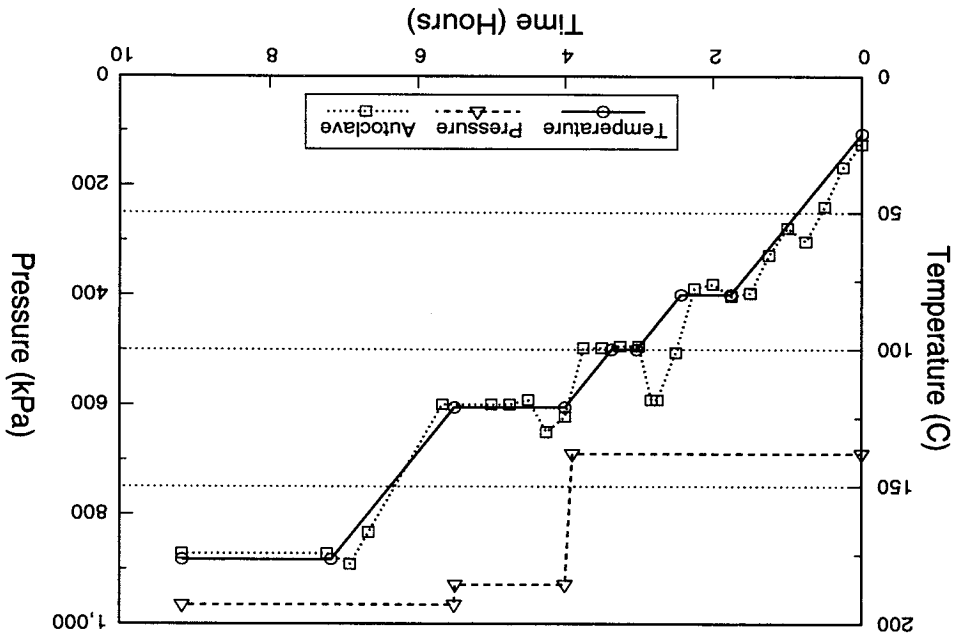
The thermal conductivities, densities, and specific heats for the tooling, preform, and resin materials are given in Table 6 . These properties were obtained either from handbook values [17], as in the case of the aluminum and steel tooling blocks, or from calculations made using the rule of mixtures model, as in the case of the graphite caul sheet. The thermal conductivity for the dry graphite preform was determined from an effective thermal conductivity model for a porous split phase material developed by Russell [18]. The expression used in these calculations was

$$
K = K_s \left[\frac{\left(\phi^{\frac{2}{3}} + \frac{K_s}{K_p} \left(1 - \phi^{\frac{2}{3}} \right) \right)}{\left(\phi^{\frac{2}{3}} - \phi + \frac{K_s}{K_p} \left(1 - \phi^{\frac{2}{3}} + \phi \right) \right)} \right] \cdot
\tag{8-2}
$$

where K_s and K_p are the thermal conductivities of the solid and porous phase, respectively, and ϕ is the porosity of the fabric preform.

TABLE 6 Material properties for single blade stiffened heat transfer model.

Materials	Density (kg/m^3)	Specific Heat (J/kg•°K)	Thermal Conductivity (W/m•°K)
Steel	7.8498E+03	4.6055E+02	4.50E+01
Aluminum	2.7074E+03	8.7085E+02	2.02E+02
Resin	1.2600E+03	1.2560E+03	1.674E-01
Fiber	1.7900E+03	7.1176E+02	2.597E+01
Graphite Caul/Saturated Preform (Transverse)	1.5980E+03	1.1589E+03	7.772E-01

TABLE 6 Material properties for single blade stiffened heat transfer model.

Materials	Density (kg/m^3)	Specific Heat (J/kg·°K)	Thermal Conductivity (W/m·°K)
Graphite Caul/Saturated Preform (Longitudinal)	1.5980E+03	1.1589E+03	1.694E+01
Unsaturated Preform (Transverse)	1.157E+03	4.626E+02	1.938E+00
Unsaturated Preform (Longitudinal)	1.157E+03	4.626E+02	7.260E+00

The boundary conditions used in the single blade stiffened model are outlined in Figure 47. An adiabatic boundary was specified along the left side of the tooling assembly. This boundary was chosen so that only one end blade would be simulated. Selecting this region would allow for the study of the suspected higher gradients in temperature in this region as well as reducing the computational resources required for the simulation. The remaining boundaries were modeled as convective boundaries. The tooling assembly was normally covered with four layers of insulating material as well as the teflon release and bagging films. Four layers of insulating cloth were also placed under the tooling plate. Rather than attempt to include these layers directly into the finite element mesh, the thermal resistance from these materials was included in the estimation for the heat transfer coefficient used on the convective boundaries. A value of 20 W/m^2·°K was used for the convective heat transfer coefficient on all three convective surfaces. It was assumed that this value remained constant throughout the curing process.

These material parameters represent the necessary input parameters for the heat transfer submodel. A description of the pre-processing mesh used in the heat transfer analysis will be addressed latter in this chapter.
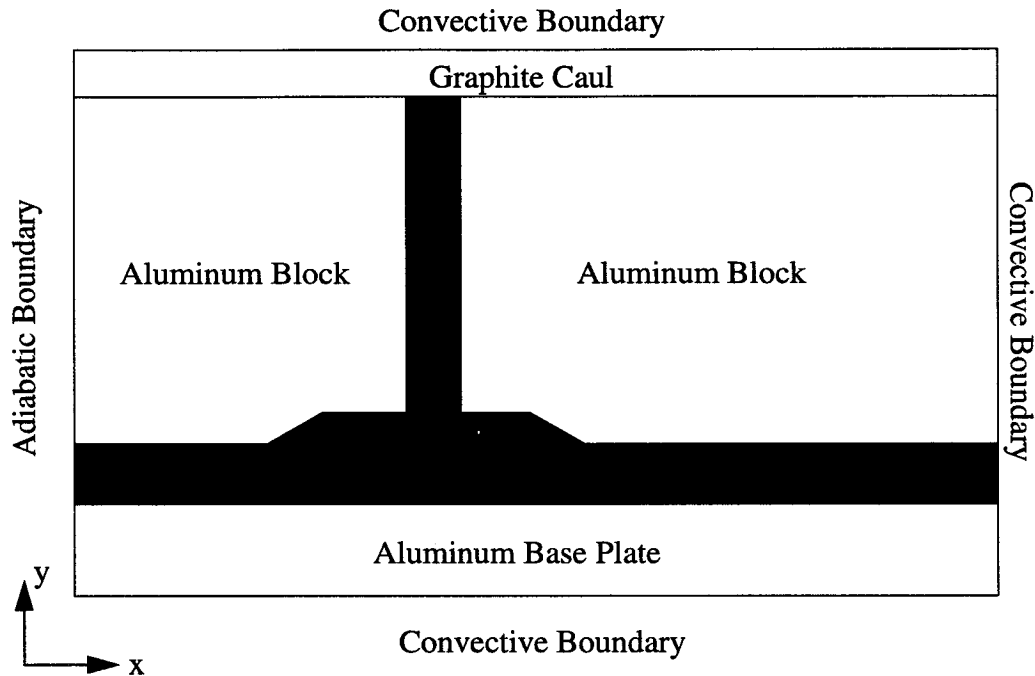
FIGURE 47 Schematic of boundary conditions for heat transfer model.

8.1.3 Compaction Model Input

The input required for the compaction submodel included the applied compaction pressure profiles, the material stiffenesses of the various tooling and preform components, the initial fiber volume fraction of the preform material, and the boundary conditions. A description of the values necessary to model the compaction behavior of the single blade stiffened panel are included in this section.

The compaction or deflection behavior of the tooling assembly can be caused by either an externally applied pressure or by the internal expansion of the tooling components due to increases in temperature during the processing cycle. The externally applied compaction is induced from the autoclave atmosphere during the processing cycle. The pressure cycles used in the single blade stiffener processing can be seen in Figures 45 and 46. Although there were several pressure cycles used by MDA-West, these two cycles represented the extremes of the pressure range and therefore were chosen for analysis. As can be seen in Figure 45, the original pressure cycle included depressurizing the autoclave, removing the part/tool assembly for inspection, replacing the assembly, and repressurizing the auto-clave. The extended cycle shown in Figure 46 allowed for an intermediate ramp in pressure before the final value of pressure was applied. These applied pressure profiles were input into the compaction model on the surfaces shown in Figure 48.
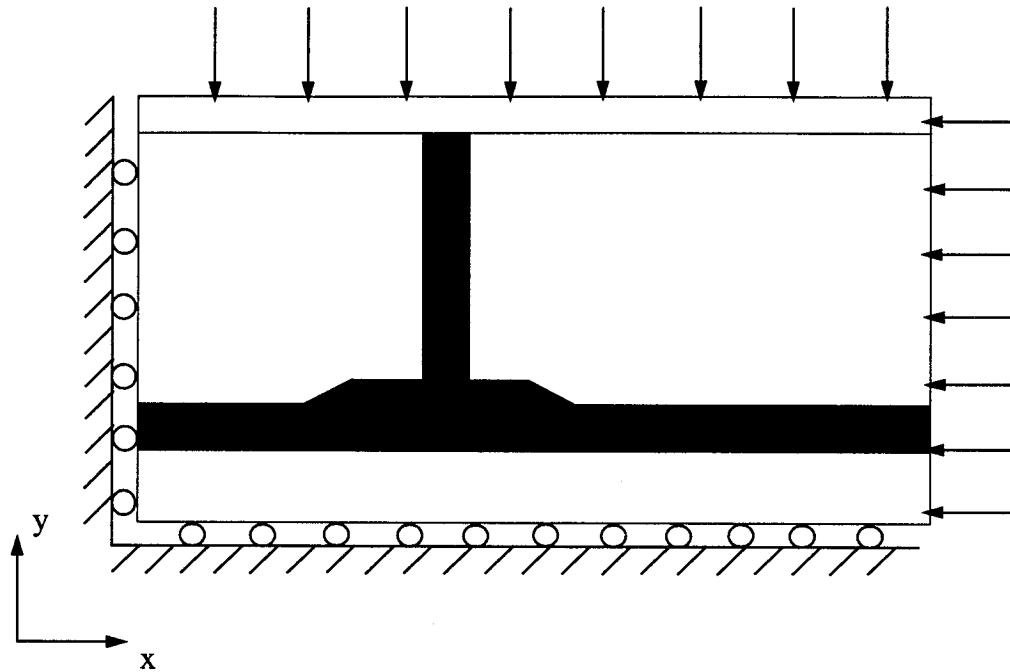
FIGURE 48 Applied pressures and deflections in compaction model.

The elevated autoclave pressures were applied on the top and right sides of the single

blade tooling assembly as is shown in Figure 48. The left edges of the tooling assembly

were allowed to move in the y direction, while motion was restricted in the x direction.

Motion was restricted in the y direction for the lower surface of the tooling assembly,

while deflections were allowed in the x direction. These boundary conditions were chosen

to best match the relative motion of the tooling/preform components during the processing

cycle.

Elastic constants for each of the materials used in the preform/tooling assembly are

required in order to solve the plane strain equations incorporated into the compaction sub-

model. As a first approximation all the materials were considered to linearly elastic and isotropic except the fabric preform. The elastic constants for the fabric preform were obtained by performing a through-the-thickness compaction experiment on the dry preform at a strain rate of 5.29×10^{-4} cm/min. The load versus deflection result from the compaction experiment were then used to calculate the fiber volume fraction versus compaction pressure plot show in Figure 49. The fiber volume fraction was calculated using the known areal weight and density of the fabric and the volume of the test fixture chamber. The compaction pressure was determined from the applied load and the cross sectional area of the specimen. The result of this experiment for a 72-ply stitched specimen is shown in Figure 49 and illustrates the non-linear nature of the preform compaction as a function of fiber volume fraction. The compaction data were recalculated to give the an elastic modulus versus volume change or dilatation, shown in Figure 50. The dilatation or volume change was taken directly from the fiber volume fraction calculation described above. The instantaneous modulus of the material was calculated by taking the slope load-deflection curve and assuming Hooke's law applies for the material at that instant in time. After each time step in the compaction submodel a new dilatation change was calculated for each element by averaging the changes in the nodal control volumes. This dilatation change was then input into a curve fit for the modulus vs. dilatation for the stitched preform (see Figure 50) and a new modulus was calculated for that element. The new value of modulus for that element was used to calculate a new elastic material constant. In this manner the nonlinear preform compaction behavior was included in the simulation.
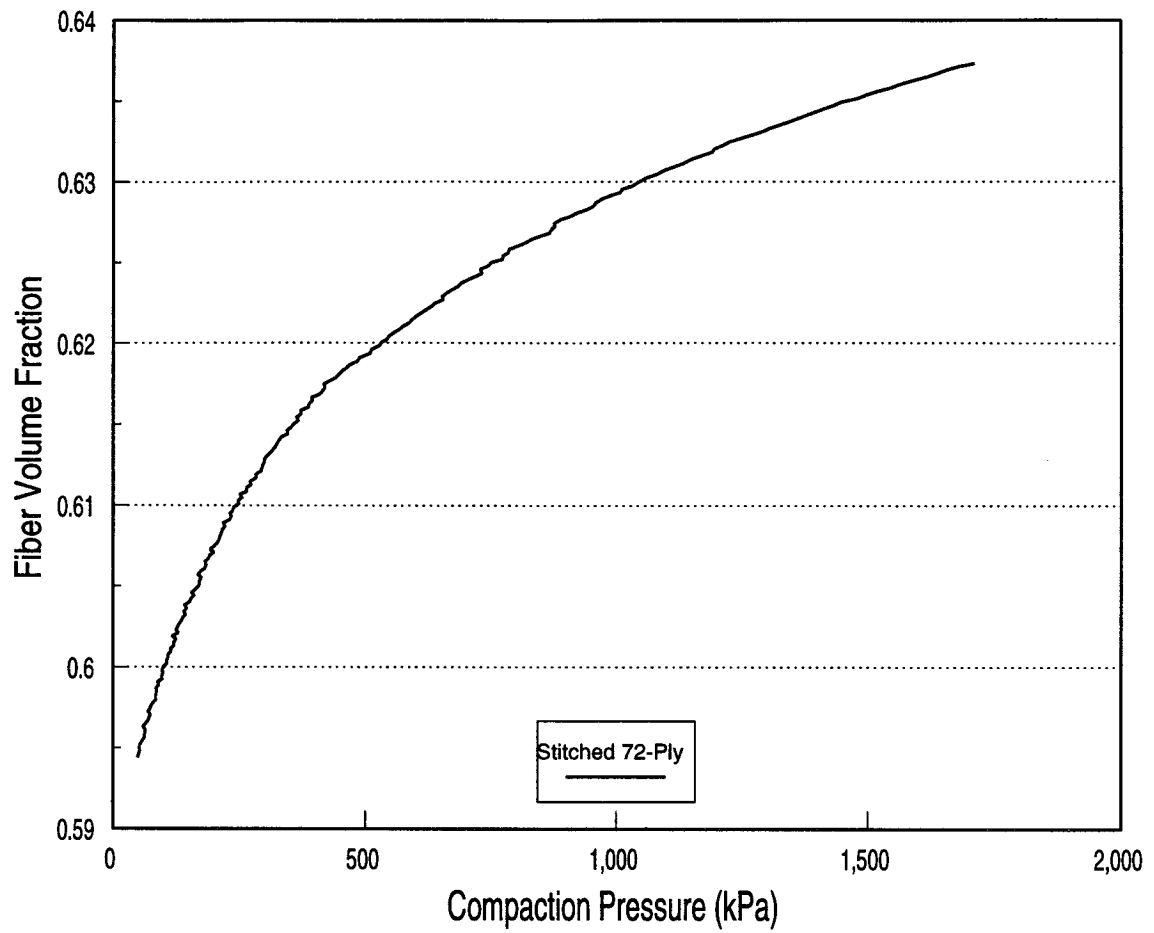
FIGURE 49 Compaction behavior of 72-ply stitched preform.
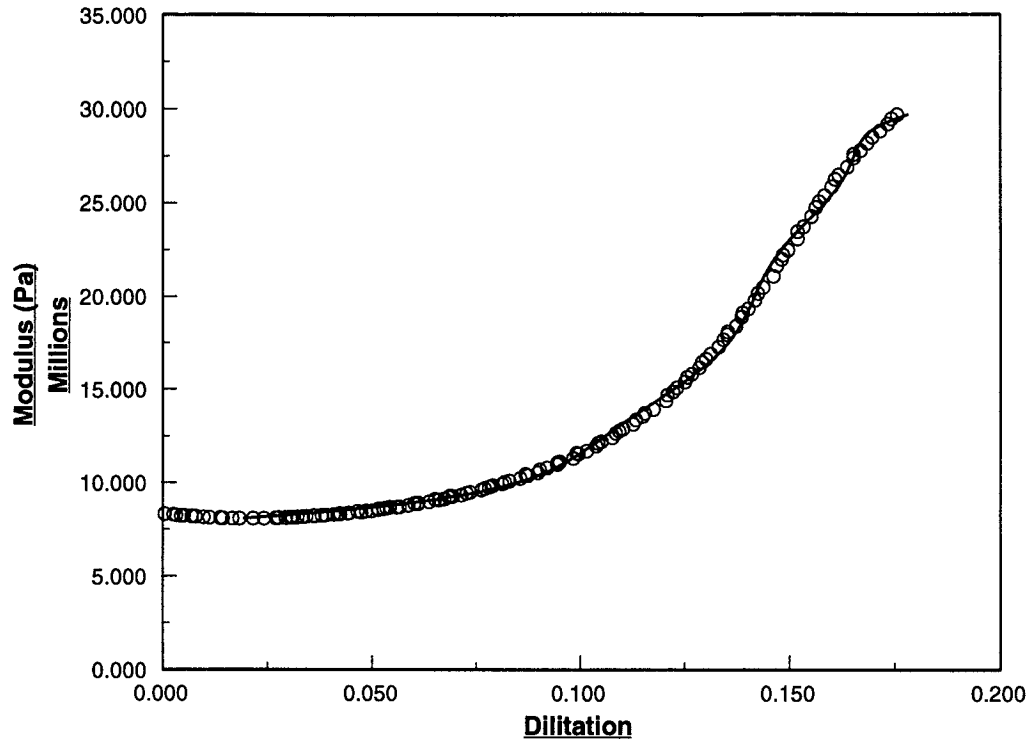
FIGURE 50 Modulus versus dilation for stitched preform material.

The elastic material constants used in the single blade stiffened panel model are shown in Table 7 . Also included in Table 7 are the thermal expansion coefficients used for the various preform and tooling materials. The thermal expansion coefficients were included in the input file for the heat transfer submodel.

TABLE 7 Material constants used in compaction model.

Material	C_{11}	C_{12}	C_{22}	C_{33}	α (1/°C)	Modulus (Pa)	ν
Aluminum	1.226E11	5.25E10	1.226E11	0	23.6E-06	7.2E10	0.33
Graphite Preform	Curve Fit	Curve Fit	Curve Fit	0	0	Curve Fit	0.26
Carbon Tool Plate	1.272E11	4.24E10	1.272E11	0	0	1.06E11	0.26

8.2 PATRAN Pre-Processing Model

The previous section discussed the material constants and boundary conditions that were used in the simulation of the single blade stiffened panel. In this section the input of the geometry of the single blade stiffened panel tooling assembly into the PATRAN pre-processor will be discussed. The PATRAN model was created in three separate stages. Each of these steps generated one of the three input files necessary for the simulation model. The overall dimensions of the single blade stiffened tooling assembly are shown in Figure 51.
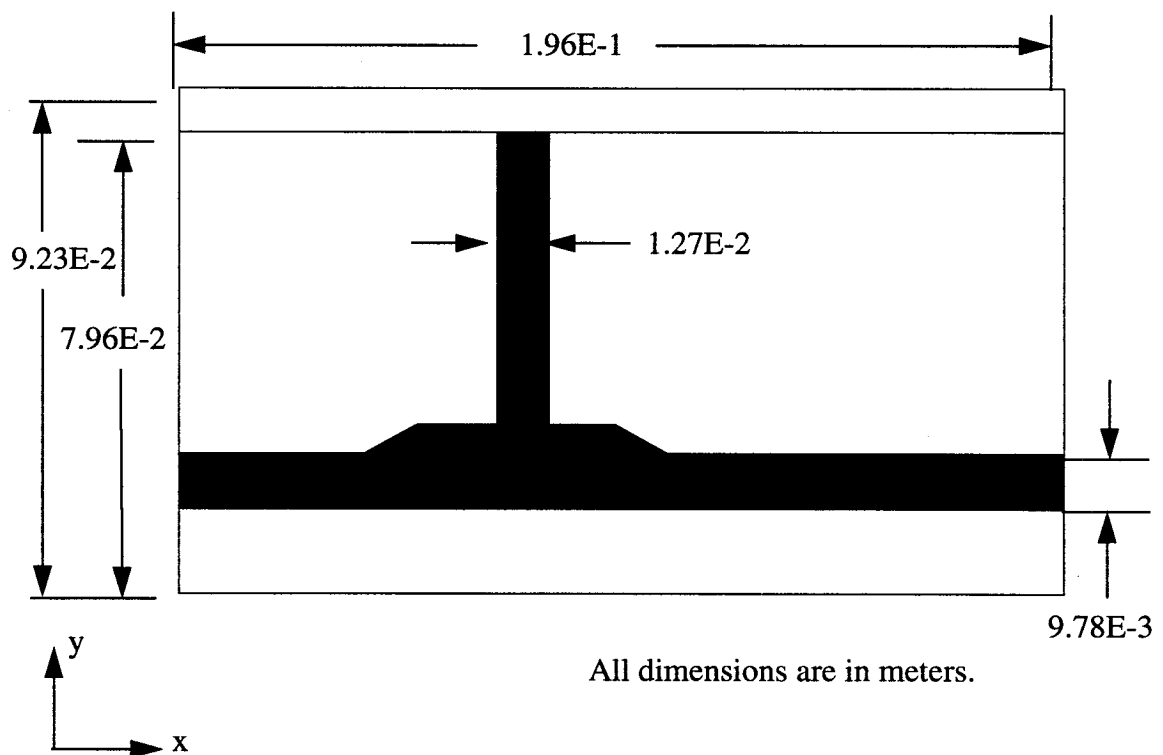
FIGURE 51 Overall dimensions of single blade tooling assembly.

8.2.1   PATRAN Flow Model

The first of step is the creation of a PATRAN generated model for the flow submodel. The geometry modeled in this step only contains the saturated preform region of the tooling assembly (The shaded region in Figure 51). An important consideration was the inclusion of the resin film region into the model. As discussed earlier the resin film region consisted of filled elements within the initial preform geometry model. The generated mesh for the preform region is shown in Figure 52. The mesh consisted of 98 linear quadrilateral elements and 131 nodes. A relatively course mesh was used to limit the amount of computational resources needed for the full simulation.
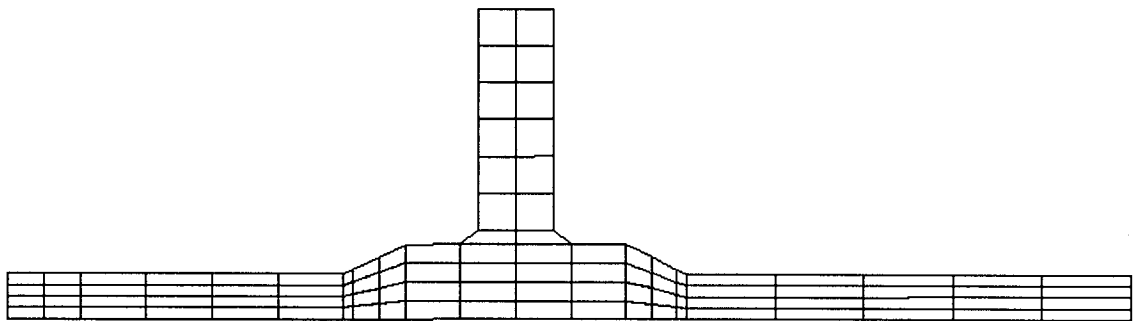
FIGURE 52   PATRAN mesh of preform region.

Two different regions within the mesh were used for the assignment of material property information. These two regions are shown in Figure 53. Different permeability tensors were required in these two regions. The orientations of the stitched preform material dictated the values assigned to the components of the permeability tensors in each of the regions. The blade section required in-plane permeabilities to be used in the y direction and through-the-thickness permeabilities in the x direction. The directions in the skin region (light colored region in Figure 53) were reversed.
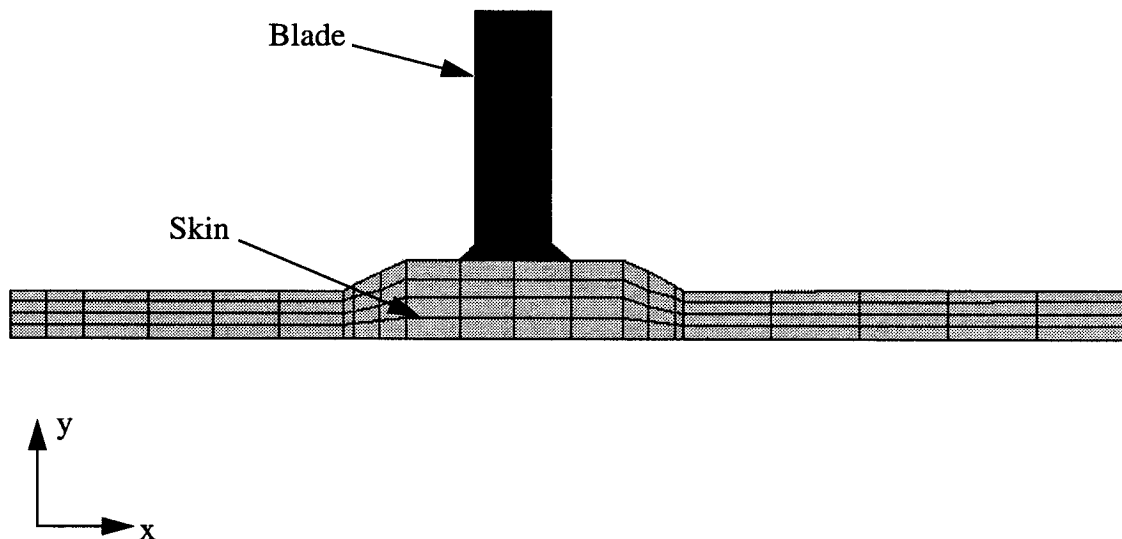
FIGURE 53 Material property regions for PATRAN flow model.

The material property and boundary condition information were entered into the PATRAN flow model as described in Section 8.1.1 . Once this was completed a PATRAN neutral file was produced which contained all the necessary information for the flow submodel.

8.2.2 PATRAN Heat Transfer Model

The PATRAN heat transfer model was the next of the three input files created. The region modeled in this effort was the entire preform and tool assembly. This PATRAN generated mesh was created by starting with the mesh used in the flow submodel. The various tooling components were created around the preform region of the model. A mesh was again constructed from quadrilateral elements containing 330 nodes and 293 elements. The mesh used in the heat transfer input file is shown in Figure 54.
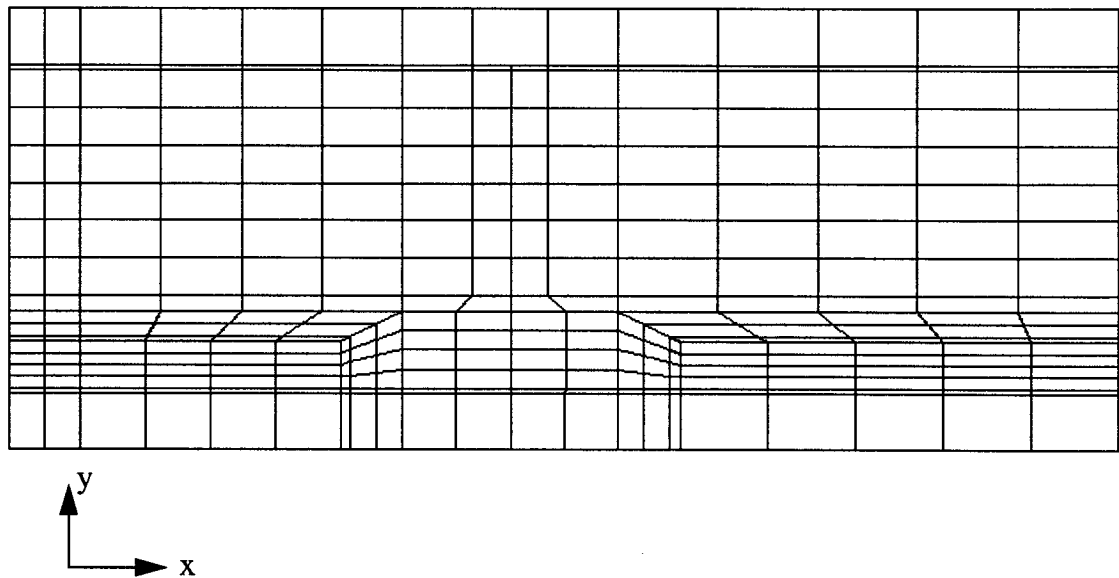
FIGURE 54 PATRAN mesh for entire preform tooling assembly.

Material properties were assigned in four different regions of the preform/tooling assembly. Figure 55 illustrates where the four regions were defined within the PATRAN mesh. The fabric preform was again divided into two separate regions as in the flow submodel.
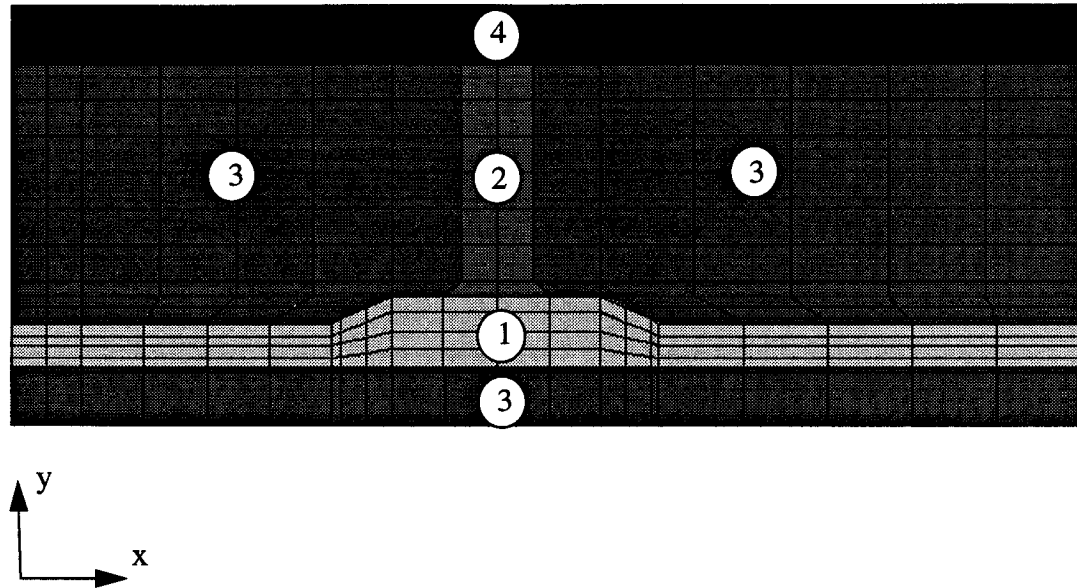
FIGURE 55 Material property regions for the PATRAN heat transfer model.

The convective and adiabatic conditions were again added to the PATRAN model as described in Section 8.1.2 . Once these boundary conditions and material properties were input into the PATRAN model a neutral file was created which contained the necessary input for the heat transfer submodel.

8.2.3   PATRAN Compaction Model

The final input file required for the simulation of the single blade stiffened panel was the compaction neutral file. The region of the preform/tooling assembly which was represented in the compaction model was the same as that used for the heat transfer submodel (Figure 54). The mesh used in the compaction input file contained the same number and type of elements as in the heat transfer file. However, in an effort to simulate sliding of the

tooling components during the compaction process and due to thermal expansion of the components, a small thin row of elements were include along the surfaces that experience sliding. In the tooling assembly, the relative sliding between the graphite caul sheet and the aluminum blocks underneath it, for example, were represented by giving the small row of elements a stiffness comparable to the graphite caul sheet in the y-direction and a value of stiffness in the x-direction of 1% of the y-direction stiffeness. The row of elements would deform easily in the x direction, thus simulating the sliding between these two surfaces. Elements with similar properties were placed at appropriate interfaces between the preform and the various tooling components. Figure 56 shows the four different regions of material properties used in the compaction model. Also depicted are the regions included to represent the sliding of the tooling components.
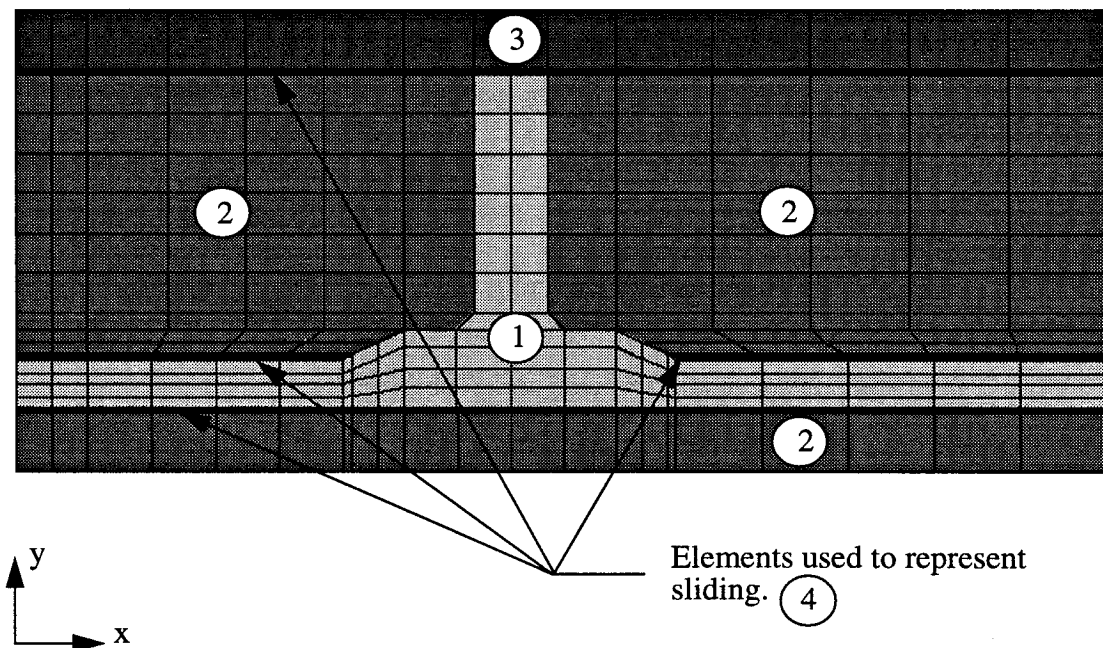
FIGURE 56 Material property regions for compaction model.

The material constants and boundary conditions described in Section 8.1.3 were included in the PATRAN model, and a neutral file was generated. This file, the neutral files for the flow and heat transfer models, and an initialization file, which included the temperature and pressure cure cycle information, comprised the input required for the simulation model. A sample of these input files are included in the Appendix to this document.

8.3   Single Blade Panel Simulation Results

The previous sections of this chapter have described the necessary input for the RFI simulation of the single blade stiffened panel. Presented in this section will be the simulation results from panels fabricated with the original cure cycle and the extended cure cycle. Also included will be the results of a parametric study done to observe the effects of compaction pressure on the total infiltration time of the single blade stiffened panel.

8.3.1   Original Cure Cycle

The original cure cycle, shown in Figure 45, was used by MDA-West in their initial attempts to fully saturate the stitched graphite preform. Complete infiltration meant that the resin would have to flow from the bottom of the stitched preform to the very tip of the blade assisted only by the compaction pressure generated in the autoclave and the vacuum present during the entire curing process. The original cycle included a portion where the tooling was disassembled in order to find any dry regions in the preform. Resin was added to the dry regions and the resin rich areas on the bottom section of the preform were eliminated. This method resulted in incomplete infiltration of the fabric preform.

As a starting point, the simulation program was run with the original cycle. The model was run on the CRAY Y-MP at NASA Langley research center in Hampton, VA. Computational time required was 1020 CPU seconds. The output from the simulation model is contained in several PATRAN results files as well as one listing file. The PATRAN results files were used to generate a series of contour plots of various processing parameters at selected times during the cure cycle. The listing file contains a complete numerical output of the processing variables as a function of processing time.

A contour plot of the model predicted resin infiltration profile is shown in Figure 57. As can be seen, the model predicts that the resin will infiltrate up to the intersection between the blade and the skin of the preform. The total infiltration time at that point is about 5.4 hours. This incomplete infiltration had been observed during the actual processing of the blade stiffened panel. The final flow front location predicted by the simulation model was found to be relatively close to that observed in the processing laboratory. The reason behind the incomplete infiltration was the lack of sufficient time during the low viscosity region of the curing cycle when the applied pressure was sufficient for resin movement. The degree of advancement in the resin system caused the resin viscosity to build up to a level higher than was sufficient for resin movement at the applied compaction pressure after the part was reinserted into the autoclave (see Figure 45). The degree of cure profile at 1.7 hours into the cycle is shown in Figure 58. It is evident from this profile that there was a significant difference in the state of advancement of the resin at this point in the processing cycle. An 85% difference in the degree of cure in the resin saturated regions of the preform was predicted. Although the magnitude of the degree of cure is small at this point this variation in the degree of cure could have a large effect on the length of time a minimum viscosity can be held once higher temperatures are reached later in the cycle. These effects were somewhat masked by the small amount (45minutes) of hold time at interme-

diate temperature in the original cycle (see Figure 45). By ramping the temperature quickly (< 1hour) from the intermediate hold, all of the resin saturated regions reached gelation rapidly.

A = 5.4 hours
B = 3.8 hours
C = 2.3 hours
D = 0.7 hours

Final Flow Front Location
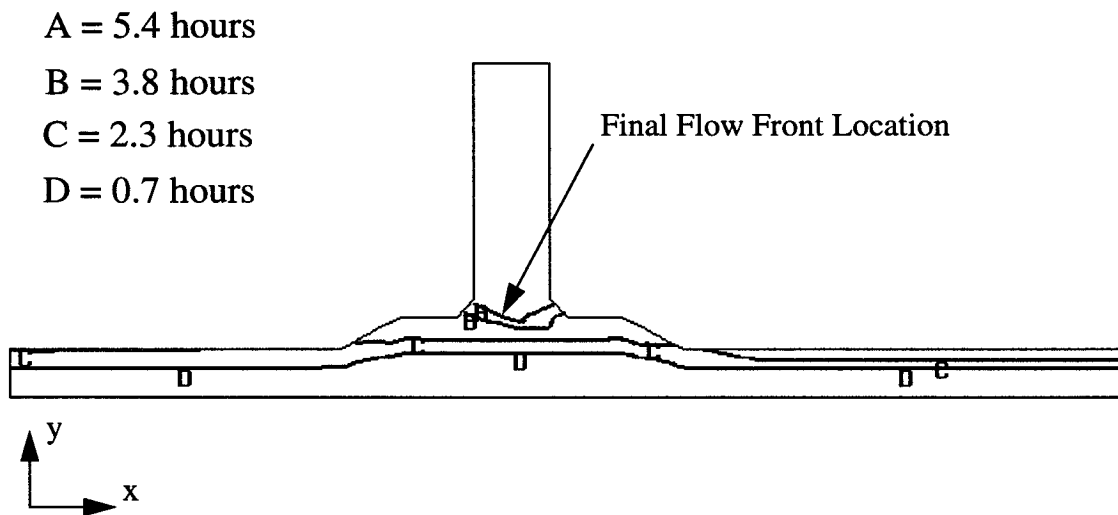
FIGURE 57 Flow front versus infiltration time for the original cure cycle.

A = 0.054

B = 0.038

C = 0.023

D = 0.008
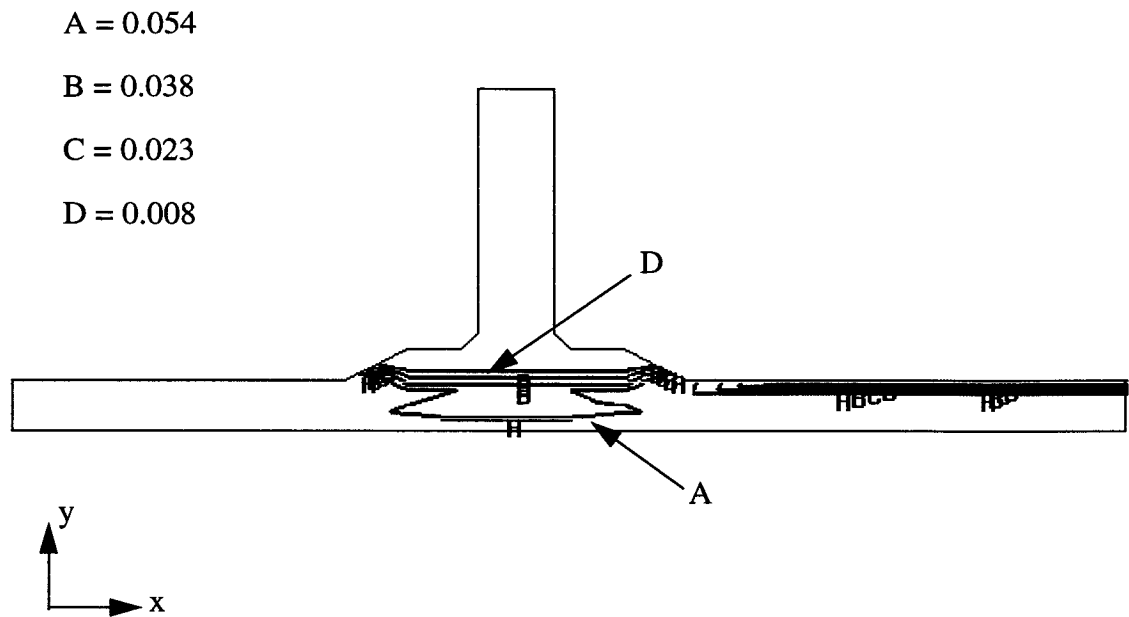
FIGURE 58 Degree of cure contours at 1.7 hours in the original cure cycle.

A = 119.1 °C   B = 114.3 °C   C = 110.0 °C   D = 107.2 °C
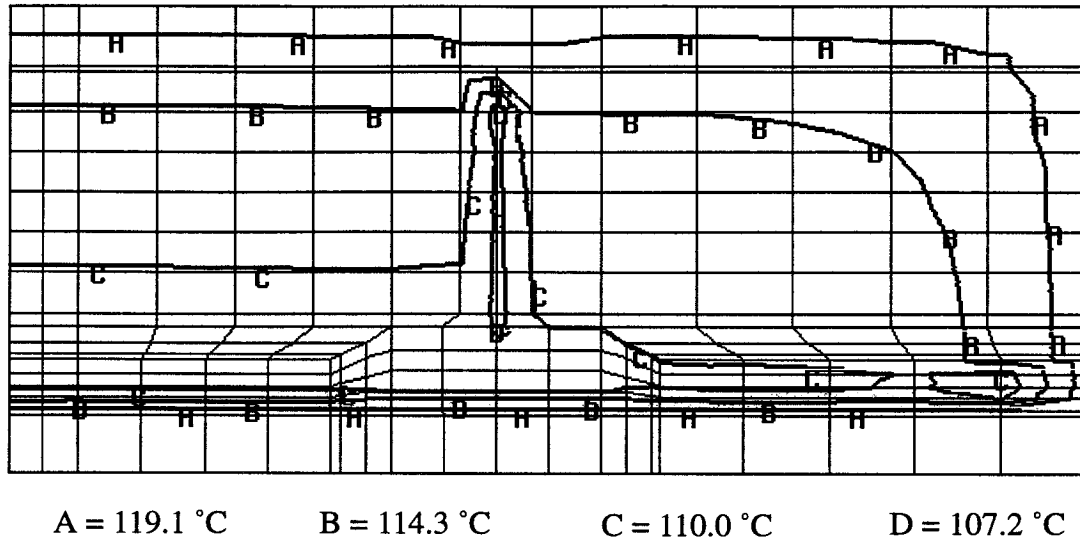
FIGURE 59 Temperature contours at 2.1 hours in the original cure cycle.

The main cause of the gradients in degree of cure are the differences in temperature history seen by different parts of the saturated preform. The temperature profile in the tooling assembly at 2.1 hours is shown in Figure 59. The temperature profile illustrates the flow of heat in the tooling assembly. The trends in the heat flow can clearly be seen in the heat transfer profiles. The fabric preform obviously did not conduct heat as rapidly as the surrounding tooling. Due to the graphite caul sheet used in the tooling assembly, the heat was supplied mainly through the side and bottom surfaces of the tooling assembly. This behavior was somewhat offset by the lower heat transfer coefficients present on those surfaces due to the larger amount of fiberglass insulation placed along those surfaces.

The compaction behavior of the tooling assembly is shown in Figure 60. The dashed lines indicate the original undeformed shape of the tooling assembly. Solid lines in Figure 60 represent the exaggerated deformed shape of the tooling assembly at the maximum compaction pressure of 689 kPa. The deformed shape shown in the Figure has been exaggerated 30% to allow for the viewing of the displacements. The amount of compaction on the blade stiffener section of the preform was small compared with the compaction of the skin section. This illustrates the importance of having a tightly stitched preform in the blade region in achieving the desired final fiber volume fraction. The tight stitching provides some measure of pre-compaction and thus the compaction required by the aluminum blocks to achieve the target fiber volume fraction is reduced.
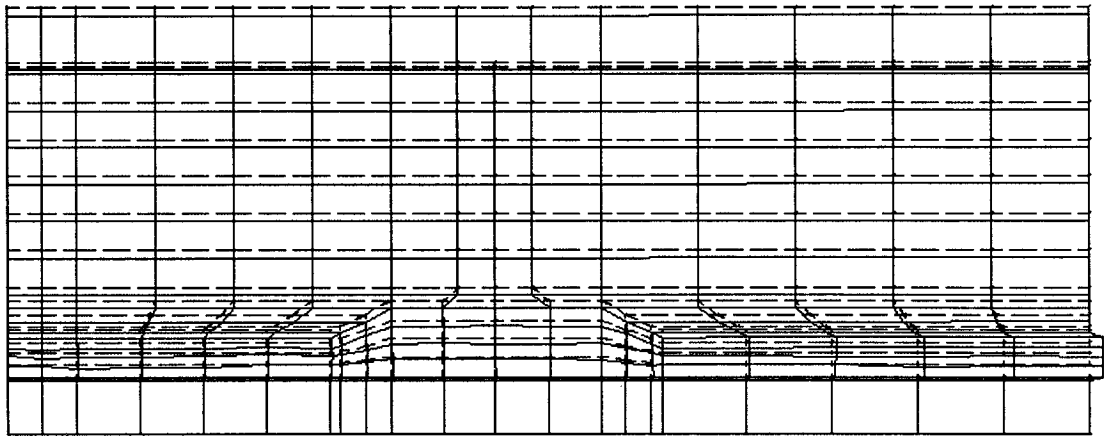
FIGURE 60 Predicted compaction behavior for the original cure cycle.

These results show some of the capabilities of the simulation model. However, as is evident from the simulation results, the original cycle used by MDA-West in the manufacture of these parts by the resin infusion process was unacceptable. Another processing cycle had to be developed to allow for the complete infiltration of the blade stiffened preform during processing.

8.3.2   Extended Cure Cycle Results

Due to the incomplete infiltration exhibited in the stiffened panels with the original cure cycle, an alternative cycle was developed based on some of the insight gained from the simulation effort done on the early cure cycle. A multiple step extended cycle (Figure 46) was developed, allowed the resin viscosity to remain at a minimum level for a significantly longer period of time than the original cycle. The multiple steps effectively lowered the heating rate used in the tooling assembly. A longer minimum viscosity provided additional time for resin to flow to the top of the blade. In addition, a pressure of 690 kPa was applied at the beginning of the cure process and the pressure was increased in steps to a final value of 897 kPa (see Figure 46). It was proposed that with these additional changes to the cycle the resin should completely infiltrate the preform.

The simulation with the extended cycle was run on the Cray Y-MP at NASA Langley research center and required a total of 1121 CPU seconds. The output files generated were the same as those discussed in the previous section. The temperature input for the extended cure cycle was taken directly from autoclave thermocouple data reported by MDA-West. Pressure cycle input was also taken from the pressure profiles measured during the manufacturing of the blade stiffened panel.

Figure 61 is a plot of the model predicted temperatures at various locations in the carbon preform as a function of time. The results illustrate that the location nearest the outer edge of the tooling assembly (Node 100) is predicted to react the fastest to changes in the auto-clave temperature. The remaining nodal locations within the preform are predicted to track each other closely during the processing cycle. It is interesting to note that although location 130 is close to the outer surface of the part, the low thermal conductivities of the graphite caul and the bagging materials are predicted to keep the temperature close to the interior preform temperatures. Note that only the initial heating portion of the cycle was simulated to reduce the required computational resources, and because after the laminate reaches the final hold, significant variations in the processing parameters trail off.
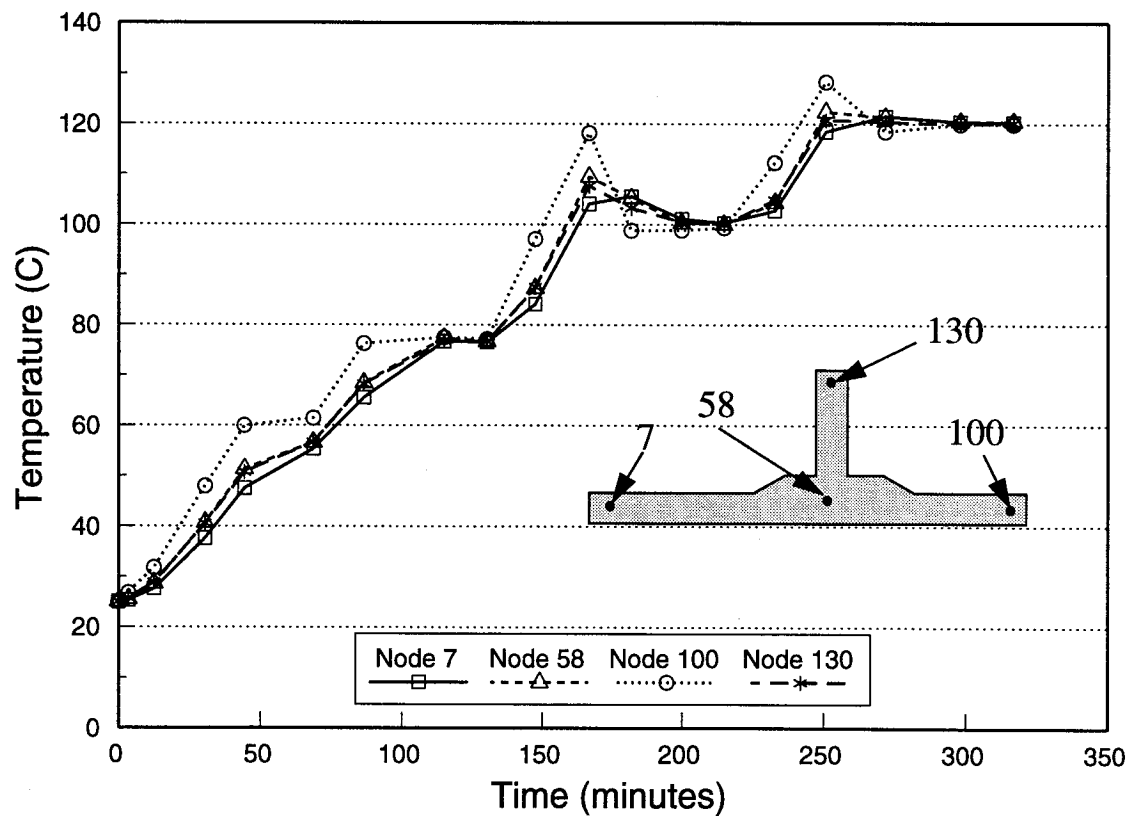
FIGURE 61 Predicted temperature profile for extended cure cycle.

A viscosity profile for the extended cure cycle is shown in Figure 62. As designed the extended cure cycle maintains low viscosity in the resin system for an extended length of time. A viscosity of less than 10 Pa•s is predicted to be maintained for over 150 minutes during the processing of the panel.
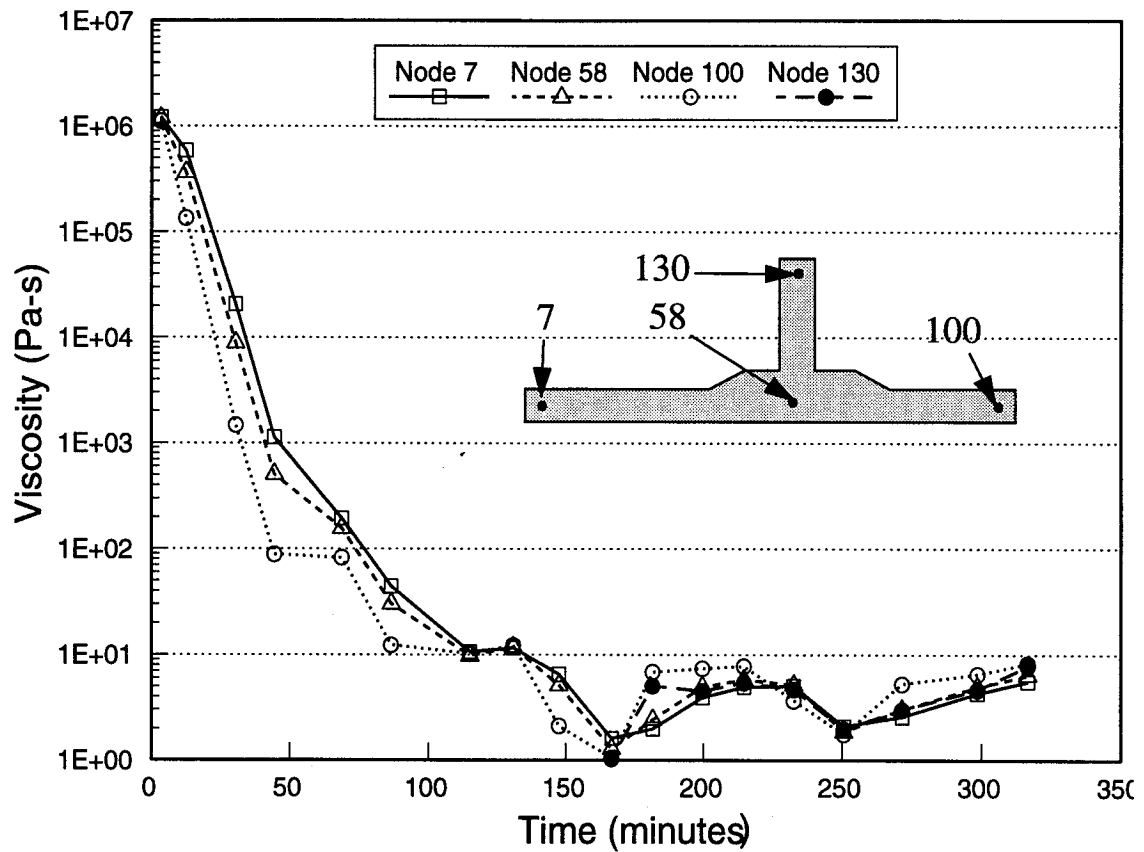
FIGURE 62 Predicted viscosity profile for the extended cure cycle.

The degree of cure profiles which were predicted with the extended cure cycle are shown in Figure 63. As can be seen in the figure, as with the temperature and viscosity, the degree of cure is predicted to have a small variation due to location within the preform. Due to the slow heating rate, the degree of cure of the resin system is still relatively low after processing for 5.3 hours.
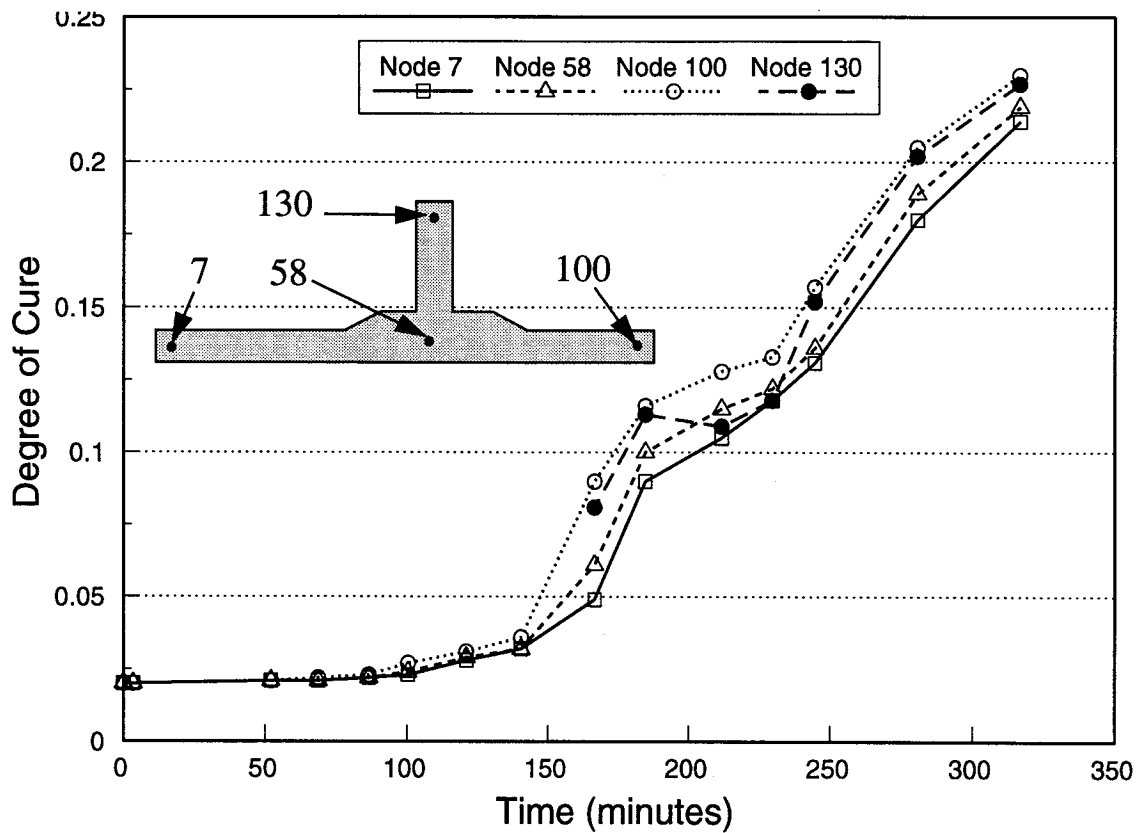
FIGURE 63 Predicted degree of cure profile for the extended cure cycle.

A series of contour plots were made at 160 minutes into the extended cure cycle. This value of time was selected due to the fact that the largest predicted variation in many of the processing variables occurred around this time in the cure cycle. This variation is due

to the large fluctuation in autoclave temperature at this point (see Figure 46). Figure 64 represents the predicted flow front locations at values of time proceeding 160 minutes in the cure cycle. As can be seen from the figure, the flow front locations are predicted all the way to the top of the blade. Actually the single blade preform was predicted by the simulation model to be completely infiltrated at 156 minutes into the cycle.

A = 155.0 minutes
B = 140.5 minutes
C = 109.3 minutes
D = 78.0 minutes
E = 15.6 minutes
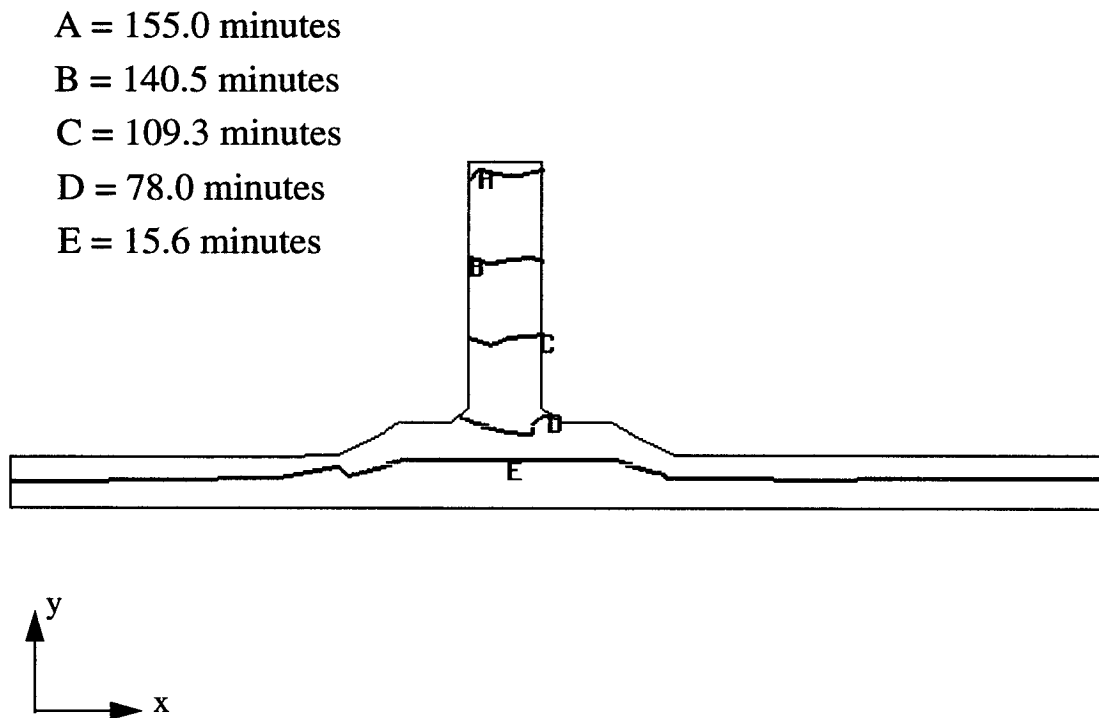
FIGURE 64 Predicted flow front versus infiltration time for the extended cure cycle.

The temperature contours at 160 minutes into the cycle are shown in Figure 65. The predicted temperature profiles again demonstrate the small variations in temperature present during the long, slow heating portion of the extended cure cycle. It is also interesting to

note that the temperature contours predicted at 160 minutes illustrate the effects of the autoclave temperature decreasing during a slight overshoot of the set point during the ramping portion of the cycle. This overshoot produced a local maximum in the temperature inside the tooling components. The tooling blocks in the center sections had not yet reached the local maximum when the autoclave temperature began decreasing. Therefore, these are the coolest regions shown. However, in the regions near the outer edge of the tool, the temperature had begun to react to the decreasing autoclave temperatures and were decreasing from the local maximum. These regions had an intermediate value in temperature. The remaining regions of the tooling assembly, like the intersection of the blade and the skin, had not yet begun to react to the decreasing temperature due to their location and the fact that some heat was being generated in the preform due to chemical reactions. These regions were predicted to show the highest temperatures at 160 minutes into the cycle. It should be noted that although there was some variation in temperature, the predicted magnitude of this difference was only about 7°C.

A = 113 °C   B = 111 °C   C = 108 °C   D = 106 °C
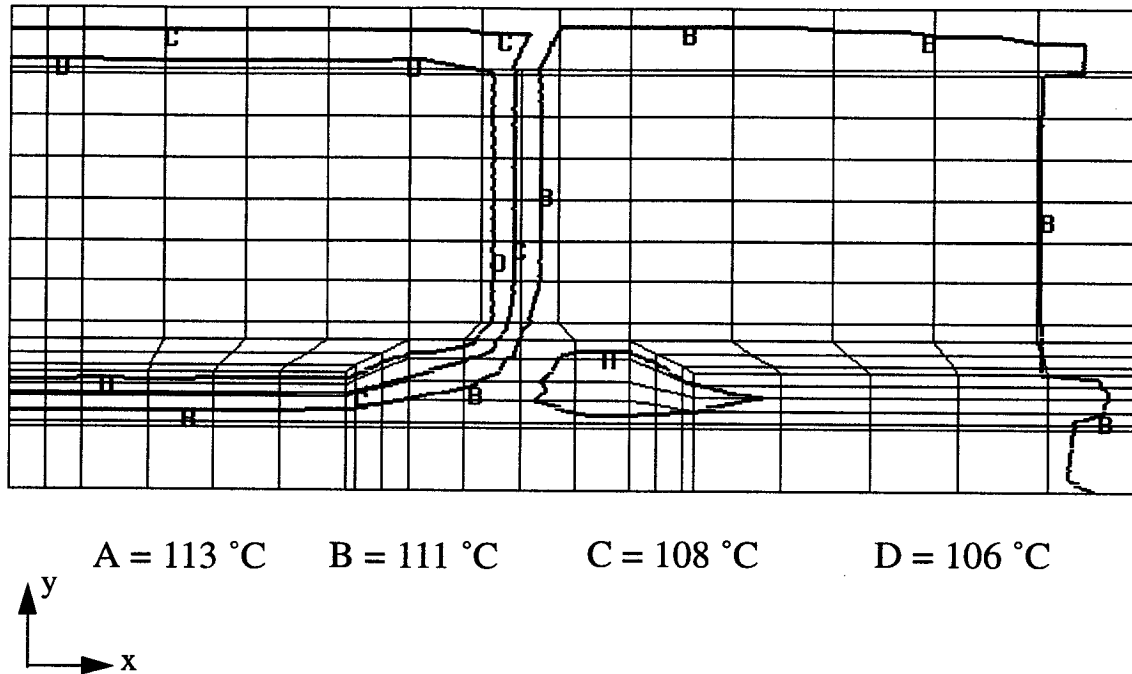
FIGURE 65 Predicted temperature contours at 160 minutes into the extended cure cycle.

The variation in the predicted viscosities and degree of cure are shown in Figure 66 and 67, respectively. Once again the variation in these processing variables at 160 minutes into the cycle is small due to the predicted uniformity in temperature history throughout the fabric preform.

The deflections predicted by the extended cure cycle simulations were very similar to those in the original cycle. The magnitudes of the deflections were slightly greater due to the increase in pressure applied. The deformed geometry plot is shown in Figure 68.

A = 1.9 Pa•s   B = 1.7 Pa•s   C = 1.6 Pa•s   D = 1.4 Pa•s
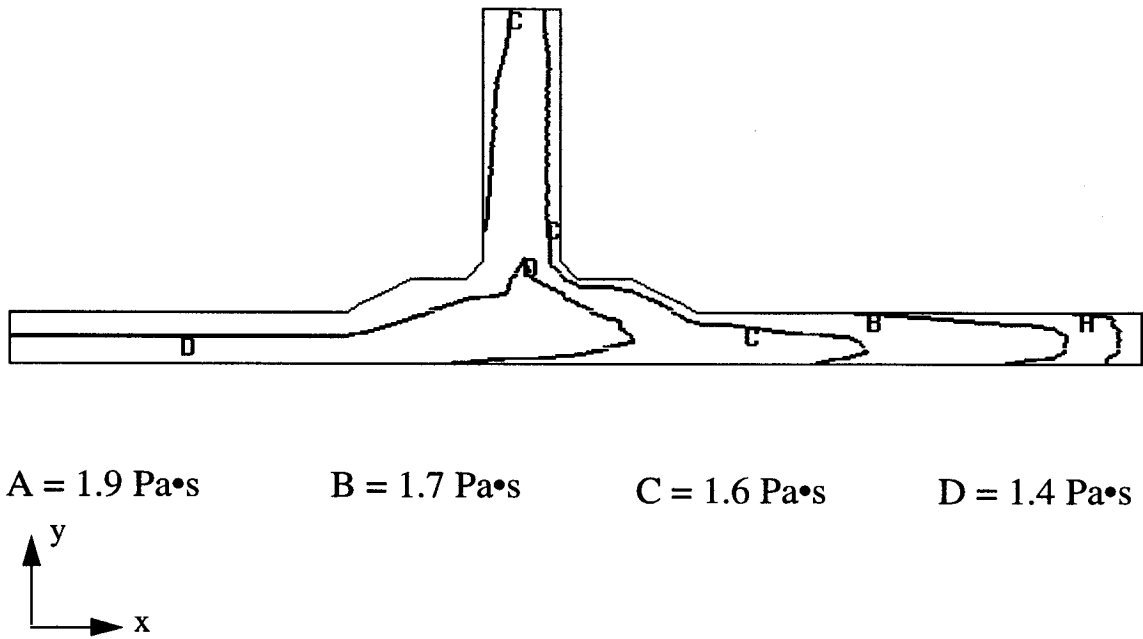
FIGURE 66 Predicted viscosity contours at 160 minutes into the extended cure cycle.

A = 0.1   B = 0.09   C = 0.08   D = 0.06
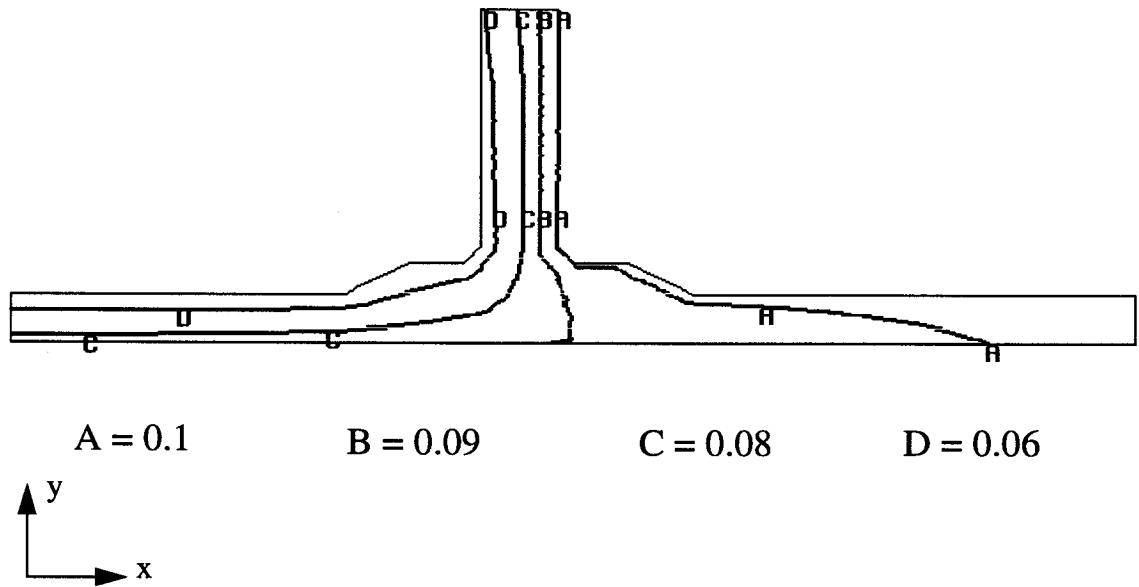
FIGURE 67 Predicted degree of cure contours at 160 minutes into the extended cure cycle.
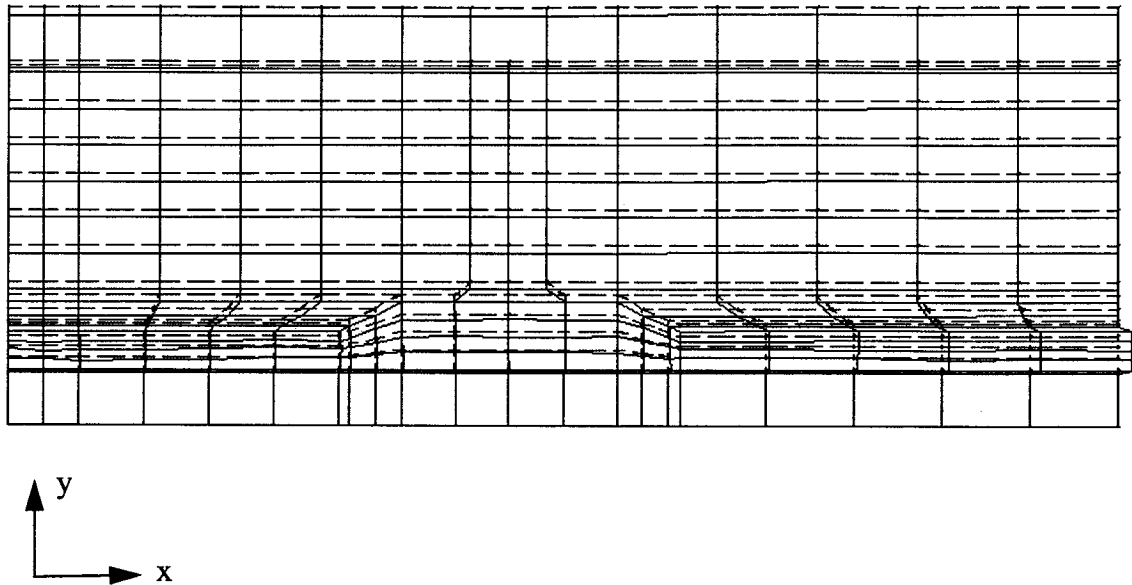
FIGURE 68 Predicted compaction behavior for the extended cure cycle.

The results of the extended cure cycle modeling effort provide an example of the utility of the computer simulation of the resin infusion process. The computer simulation was able to provide a detailed estimate of the important processing parameters. The interactions between these processing variables could then be studied to help optimize the processing cycle. An effort was made to utilize the processing model for just such a study. A series of computer simulations were preformed with the input parameters from the extended cure cycle. The objective of this parametric study was to gain some insight into the effects of autoclave pressure on the fabric preform infiltration. Therefore all other processing variables were held constant while the maximum autoclave pressure was allowed to vary. The results of the parametric study are plotted in Figure 69. The simulations predicted that complete infiltration of the fabric preform could be attained with a minimum pressure of 172 kPa. The infiltration time required to achieve complete infiltration of the preform var-

ied with applied pressure in a nonlinear fashion. This reduction in applied compaction pressure would have a corresponding drop of 3% in the fiber volume fraction of the final laminate.
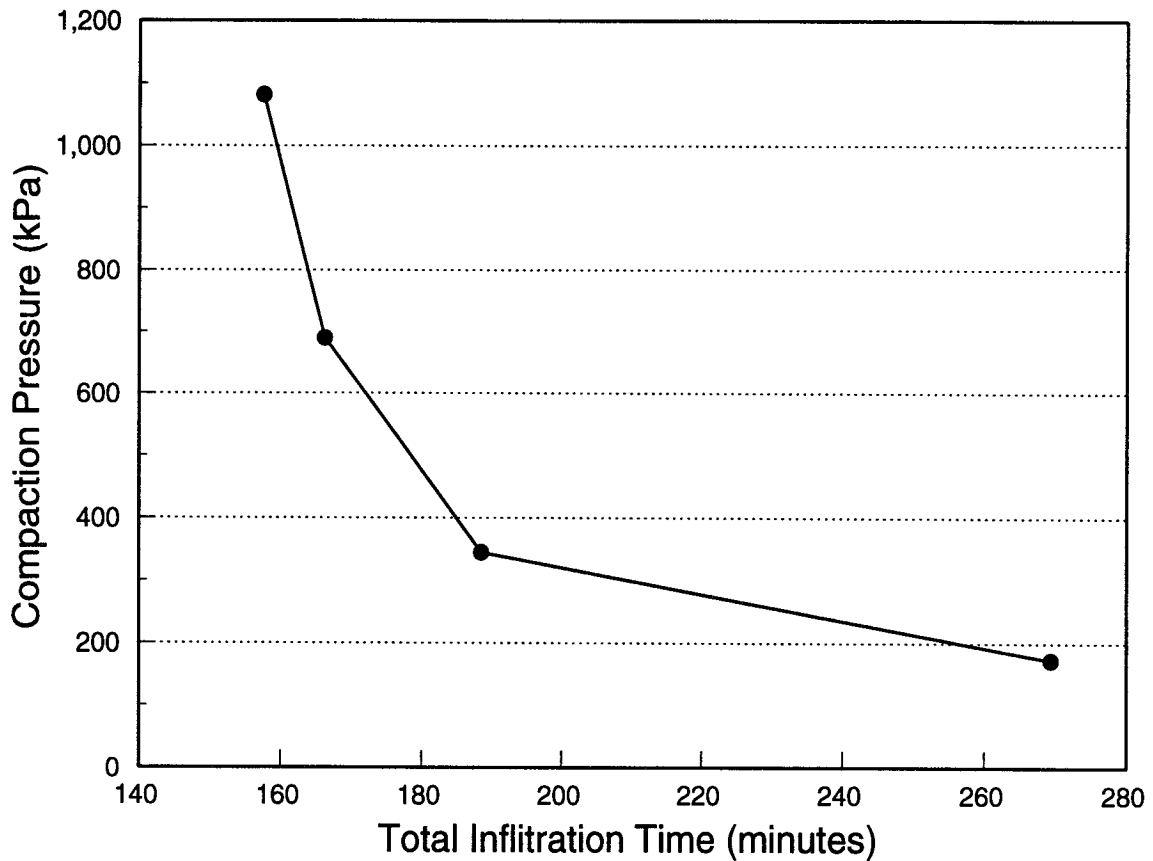
FIGURE 69 Predicted compaction pressure versus infiltration time.

The results presented in this chapter represent an initial effort in the simulation of the manufacture of a blade stiffened panel by the resin film infusion process. The utility of the simulation model was examined. Simulation results for two different cure cycle were presented along with a detailed discussion of the boundary conditions and material constants necessary. The construction of the PATRAN pre-processing model was addressed as well as the use of PATRAN for producing contour plots of the processing variables. Also

included in the discussion in this chapter was a parametric study of the effects of compaction pressure on the fabric preform infiltration time.

CHAPTER 9

Conclusions and Future Work

9.1 Conclusions

This study has shown that it is possible to develop a computer simulation model capable of providing the aircraft structure and tool designers with a method of predicting the infiltration and curing behavior of an advanced composite material component. A two-dimensional simulation model was developed which predicts the resin flow inside the fabric preform, the heat transfer in the tooling assembly, and the compaction behavior of the tooling assembly. The computer simulation model also demonstrated the capability to predict the resin kinetics and viscosity, the final part dimensions, and the completed component fiber volume fraction.

Infiltration was described by Darcy's law for a Newtonian fluid flowing through a porous medium. A finite element control volume approach was utilized for predicting the moving boundary behavior of the resin front. The heat transfer in the fabric preform and tooling was analyzed with a transient finite element model which included the effects of convection on the tooling surfaces. The compaction behavior of the preform and tooling assembly was described by a plane strain elasticity analysis. A finite element model was used to solve these equations. All of these solutions were coupled together in a quasi-steady state non-linear fashion inside the computer code.

Simulation model verifications were carried out on individual components of the computer model. The resin flow sub-model was verified by a comparing model predictions with experimental data reported in literature and two-dimensional visualization studies performed for a center-port injection of a flat plate. The heat transfer model was verified by comparing the model predicted temperature distribution with the temperature distribution measured during cure of a thick section composite laminate. The compaction model verification was limited to the comparison of the final part dimensions with those calculated with the model.

Computer simulations were performed with two resin infusion cycles for a single blade stiffened composite panel. The simulation model results were used to assist in the development of an alternative cure cycle for manufacture of a three blade stiffened panel. The results demonstrated the importance of a sufficient minimum viscosity region in the cycle in order to allow the resin to completely infiltrate the fabric preform of the structure. Predictions of the viscosities and degree of cure profiles within the single blade stiffened panel illustrated the uniformity of these parameters during the curing cycle.

Work performed in this study helped to emphasize the importance of the use of computer simulation in the advanced composite manufacturing processes. Computer simulation of the resin infusion process will allow engineers to make critical design decisions prior to the costly production of large scale composite tooling and components. The simulation models provides a method for the detailed study of the processing variables and allows informed decisions to be made.

This work provides a foundation on which future processing simulation models can be built. Tools such as this simulation model add to the current scientific understanding of the resin film infusion and resin transfer molding manufacturing processes and are an important part of making composite materials a cost-effective alternative to traditional aircraft materials.

9.2 Future Work

Although many of the necessary processing variables could be estimated using the techniques in this study, several important refinements need to be made to simulation model. As demonstrated in the verification portion of this study, the effects of surface tension, a no-slip boundary condition, preform saturation, and possibly the capability to handle non-Newtonian fluids all need to be included in the flow model for a more accurate flow front prediction. In the area of heat transfer a study to address the effects of convective heating needs to be carried out to determine its importance in the resin infusion process. Finally, anisotropic material behavior should be incorporated into the compaction model.

An additional area of future work would include an effort to extend the two-dimensional simulation model into three dimensions. The utility of the model would be greatly increased with this extension. This would inevitably increase the computational resource

requirements significantly. Therefore an important area of work in the future will be in finding more efficient algorithms to solve the domain problems contained within the computer code.

References

[1] Robertson, F.C. "Resin Transfer Moulding of Aerospace Resins-A Review." *British Polymer Journal,* Vol. 20, pp. 417-426, (1988).

[2] Harlow, F.H. and Welch, J. E., "Numerical Calculations of Time-Dependent Viscous Incompressible Flow of Fluid with a Free Surface." *Physics of Fluids,* Vol. 8, pp. 2182-2189, (1965).

[3] Takashi and Takaaki, "Computer Aided Mold Design for Injection Molding.", *Technology Japan*, Vol. 19, pp. 38-45, (1986).

[4] Tucker, C. L., *Fundamentals of Computer Molding for Polymer Processing,* Hanser Publishing, New York, 1989.

[5] Lin, R., Lee, L.J., and Liou, M.J., "Nonisothermal Mold Filling in Resin Transfer Molding and Structural Reaction Injection Molding.", *ANTEC*, pp. 815-818, (1991).

[6] Fracchia, C.A., Castro, J., and Tucker, C.L., "A Finite Element/Control Volume Simulation of Resin Transfer Molding.", *Proceedings of the American Society for Composites- Fourth Technical Conference,* pp. 157-166, (1989).

[7] Coulter, J.P. and Guceri, S.I., "Resin Impregnation During the Manufacturing of Composite Materials Subject to Prescribed Injection Rate." *Journal of Reinforced Plastics and Composites,* Vol. 7, No. 3, pp. 200-219, (1987).

[8] Um, M.K. and Lee, W.I., "Numerical Simulation of the Resin Transfer Molding Process Using Boundary Element Methods." *Proceedings of the 35th International SAMPE Symposium,* pp. 1905-1916, (1990).

[9]   Coulter, J.P., Smith, B.I., and Guceri, S.I., "Experimental and Numerical Analysis of Resin Impregnation During the Manufacturing of Composite Materials." *Journal of Reinforced Plastics and Composites,* Vol. 9, pp. 209-217, (1988).

[10]   Young, W.B., Rupel, K., Han, K., Lee, L.J., and Liou, M.J., "Analysis of Resin Injection Molding In Molds With Preplaced Fiber Mats. II: Numerical Simulation and Experiments of Mold Filling." *Polymer Composites,* Vol. 12, No. 1, pp. 30-38, (1991).

[11]   Chiou, P. and Letton, A., "Reaction Kinetics and Chemoviscosity of a Thermoset Exhibiting Complex Curing Behavior." *Proceedings of the American Society for Composites*, Fourth Technical Conference, pp. 157-166, (1989).

[12]   Weideman, M.H., Loos, A.C., Dexter, H.B. and Hasko, G.H., "An Infiltration/Cure Model for Manufacture of Fabric Composites by the Resin Infusion Process." *Virginia Tech Center for Composite Materials and Structures, Report No. CCMS-92-05,* Virginia Tech, (1992).

[13]   Reddy, J.N., *An Introduction to the Finite Element Method,* McGraw Hill Book Company, New York, (1984).

[14]   Somanath, N. and Loos, A.C., "A Finite Element Cure Model and Cure Cycle Optimization for Composite Structures." *Virginia Tech Center for Composite Materials and Structures, Report No. CCMS-88-14,* Virginia Tech, (1988).

[15]   Loos, A.C., MacRae, J.D., Hammond, V.H., Kranbuehl, D.E., Hart, S.M., Hasko, G.H., and Markus, A.M., "Analytical Modeling and Sensor Monitoring for Optimal Processing of Advanced Textile Structural Composites by Resin Transfer Molding."

Third NASA Advanced Composite Technology Conference, NASA-CP-3178, pp. 231-261, (1992).

[16] Loos, A.C., and Springer, G.S., "Curing of Epoxy Matrix Composites." *Journal of Composite Materials,* Vol. 17, pp. 135-169, (1983).

[17] Incropera, F.P. and DeWitt, D.P., *Fundamentals of Heat Transfer,* John Wiley and Sons, New York, (1981).

[18] Russell, H.W., "Principles of Heat Flow in Porous Insulation." *Journal of American Ceramic Society,* Vol. 18, p. 1, (1935).

[19] Bruschke, M.V. and Advani, S.G., "A Finite Element/Control Volume Approach to Mold Filling In Anisotropic Porous Media." *Polymer Composites,* Vol. 11, No. 6, pp. 398-405, (1990).

[20] Osswald, T.A. and Tucker, C.L., "Compression Mold Filling Simulation for Non Planar Parts." *International Polymer Processing V,* pp. 79-87, (1990).

[21] Li, S. and Gauvin, R., "Numerical Analysis of the Resin Flow in Resin Transfer Molding." *Journal of Reinforced Plastics and Composites,* Vol. 10, pp. 314-327, (1991).

[22] Coulter, J.P. and Guceri, S. I., "Resin Impregnation During Composite Manufacturing: Theory and Experimentation." *Composites Science and Technology,* Vol. 35, pp. 317-330, (1991).

[23] Bear, J., Braester, C. and Menier, P.C., "Effective and Relative Permeabilities of Anisotropic Porous Media." *Transport in Porous Media 2,* D. Reidel Publishing Company, pp. 301-306, (1987).

Appendix

This appendix contains the necessary input files for the resin film infusion model. The initialization, flow, thermal, and compaction input files as shown.

"INITIALIZATION FILE"

26000.0	cycle ending time (seconds)
1	number of temp. cycles
26	number of points in temp cycle
0.0 25.0	time(seconds) temp(C)
900.0 33.3	
1800.0 47.7	
2700.0 60.5	
3600.0 55.5	
4500.0 65.5	
5400.0 79.4	
6300.0 80.5	
7200.0 76.1	
8100.0 77.7	

9000.0 101.1
9900.0 118.3
10200.0 118.3
10800.0 98.8
11700.0 98.8
12600.0 99.4
13500.0 99.4
14400.0 124.4
15300.0 130.0
16200.0 118.3
17100.0 120.0
18000.0 120.0
20400.0 120.0
24000.0 166.6
24900.0 178.3
26000.0 174.4
3   number of points in pressure cycle
0.0 1.0   time(seconds) pressure(Pa)
600.0 1066618.0
26000.0 1066618.0
0.70   Maximum fiber volume fraction
0.47   porosity
8.0E-6   fiber diameter
2   number of permeability tensors
0.300E+020.000E+000.000E+00   permeability tensor K11,k12,k13,k22,k23,k33
0.000E+002.500E+000.000E+00
0.000E+000.000E+000.000E+00
2.500E+000.000E+000.000E+00
0.000E+003.000E+020.000E+00
0.000E+000.000E+000.000E+00
1.0   number of cycle flags

"FLOW INPUT FILE"
25 0 0 1 0 0 0 0 0
PANEL FLOW MODEL INPUT
26 0 0 1 131 98 2 0 0
 TEST RUN
 1 1 0 2 0 0 0 0 0   nodal coordinates

```
0.000000000E+00 0.126999998E-01 0.000000000E+00
1G 6 0 0 000000
 1 2 0 2 0 0 0 0 0
0.635000039E-02 0.126999998E-01 0.000000000E+00
1G 6 0 0 000000
 1 3 0 2 0 0 0 0 0
0.127000008E-01 0.126999998E-01 0.000000000E+00
1G 6 0 0 000000
 1 4 0 2 0 0 0 0 0
0.000000000E+00 0.151447495E-01 0.000000000E+00
1G 6 0 0 000000
 1 5 0 2 0 0 0 0 0
0.635000039E-02 0.151447495E-01 0.000000000E+00
1G 6 0 0 000000
 1 6 0 2 0 0 0 0 0
0.127000008E-01 0.151447495E-01 0.000000000E+00
1G 6 0 0 000000
 1 7 0 2 0 0 0 0 0
0.000000000E+00 0.175895002E-01 0.000000000E+00
1G 6 0 0 000000
 1 8 0 2 0 0 0 0 0
0.635000039E-02 0.175895002E-01 0.000000000E+00
                   .
                   .
                   .
                   .
                   .
                   .
                   .
 2 1 4 2 0 0 0 0 0                          element connectivity
 4 0 2 0 0.000000000E+00 0.000000000E+00 0.000000000E+00
 1 2 5 4
 2 2 4 2 0 0 0 0 0
 4 0 2 0 0.000000000E+00 0.000000000E+00 0.000000000E+00
 2 3 6 5
 2 3 4 2 0 0 0 0 0
 4 0 2 0 0.000000000E+00 0.000000000E+00 0.000000000E+00
 4 5 8 7
 2 4 4 2 0 0 0 0 0
```

```
4 0 2 0 0.000000000E+00 0.000000000E+00 0.000000000E+00
5 6 9 8
2 5 4 2 0 0 0 0 0
4 0 2 0 0.000000000E+00 0.000000000E+00 0.000000000E+00
7 8 11 10
2 6 4 2 0 0 0 0 0
4 0 2 0 0.000000000E+00 0.000000000E+00 0.000000000E+00
8 9 12 11
2 7 4 2 0 0 0 0 0
4 0 2 0 0.000000000E+00 0.000000000E+00 0.000000000E+00
10 11 14 13
```

.

.

.

.

.

.

.

```
3 1 5 20 0 0 0 0 0                        material properties
 0.000000000E+00 0.000000000E+00 0.000000000E+00 0.000000000E+00
0.000000000E+00
 0.000000000E+00 0.000000000E+00 0.500000000E+01 0.000000000E+00
0.000000000E+00
 0.000000000E+00 0.000000000E+00 0.000000000E+00 0.000000000E+00
0.124900004E-11
 0.000000000E+00 0.000000000E+00 0.703799996E-11 0.000000000E+00
0.000000000E+00
 0.000000000E+00 0.000000000E+00 0.000000000E+00 0.000000000E+00
0.000000000E+00
 0.000000000E+00 0.000000000E+00 0.000000000E+00 0.000000000E+00
0.000000000E+00
 0.000000000E+00 0.000000000E+00 0.000000000E+00 0.000000000E+00
0.000000000E+00
 0.000000000E+00 0.000000000E+00 0.000000000E+00 0.000000000E+00
0.000000000E+00
 0.000000000E+00 0.000000000E+00 0.000000000E+00 0.000000000E+00
0.000000000E+00
 0.000000000E+00 0.000000000E+00 0.000000000E+00 0.000000000E+00
0.000000000E+00
```

0.000000000E+00 0.000000000E+00 0.000000000E+00 0.000000000E+00
0.000000000E+00
  0.000000000E+00 0.000000000E+00 0.000000000E+00 0.000000000E+00
0.000000000E+00
  0.000000000E+00 0.000000000E+00 0.000000000E+00 0.000000000E+00
0.000000000E+00
  0.000000000E+00 0.000000000E+00 0.000000000E+00 0.000000000E+00
0.000000000E+00
  0.000000000E+00 0.000000000E+00 0.000000000E+00 0.000000000E+00
0.000000000E+00
  0.000000000E+00 0.000000000E+00 0.000000000E+00 0.000000000E+00
0.000000000E+00
  0.000000000E+00 0.000000000E+00 0.000000000E+00 0.000000000E+00
0.000000000E+00
  0.000000000E+00 0.000000000E+00 0.000000000E+00 0.000000000E+00
0.000000000E+00
  0.000000000E+00 0.000000000E+00 0.000000000E+00 0.000000000E+00
0.000000000E+00
  0.000000000E+00

.
.
.
.
.
.
.

10 1 1 1 1 0 0 0 0   pressure boundary conditions
  0.101352000E+06
10 2 1 1 1 0 0 0 0
  0.101352000E+06
10 3 1 1 1 0 0 0 0
  0.101352000E+06
10 4 1 1 1 0 0 0 0
  0.101352000E+06
10 5 1 1 1 0 0 0 0
  0.101352000E+06
10 6 1 1 1 0 0 0 0
  0.101352000E+06
10 7 1 1 1 0 0 0 0

0.0000000000E+00
10 8 1 1 1 0 0 0 0

. . . . . .

fill factors

15 1 1 1 1 0 0 0 0
0.1000000000E+01
15 2 1 1 1 0 0 0 0
0.1000000000E+01
15 3 1 1 1 0 0 0 0
0.1000000000E+01
15 4 1 1 1 0 0 0 0
0.1000000000E+01
15 5 1 1 1 0 0 0 0
0.1000000000E+01
15 6 1 1 1 0 0 0 0
0.1000000000E+01
15 7 1 1 1 0 0 0 0
0.0000000000E+00
15 8 1 1 1 0 0 0 0
0.0000000000E+00
15 9 1 1 1 0 0 0 0
0.0000000000E+00

. . . . . .

.9900100000

end of file

"THERMAL INPUT FILE"
25 0 0 1 0 0 0 0 0
TEMPERATURE MODEL INPUT PANEL6
26 0 0 1 330 293 5 0 0

Appendix

29-JUN-91 15:12:10 2.4
1 1 0 2 0 0 0 0 0   nodal coordinates
0.000000000E+00 0.126999998E-01 0.000000000E+00
1G 6 0 0 000000
1 2 0 2 0 0 0 0 0
0.635000039E-02 0.126999998E-01 0.000000000E+00
1G 6 0 0 000000
1 3 0 2 0 0 0 0 0
0.127000008E-01 0.126999998E-01 0.000000000E+00
.
.
.
.
.
.

2 1 4 2 0 0 0 0 0   element connectivity
4 0 2 0 0.000000000E+00 0.000000000E+00 0.000000000E+00
1 2 5 4
2 2 4 2 0 0 0 0 0
4 0 2 0 0.000000000E+00 0.000000000E+00 0.000000000E+00
2 3 6 5
2 3 4 2 0 0 0 0 0
4 0 2 0 0.000000000E+00 0.000000000E+00 0.000000000E+00
4 5 8 7
2 4 4 2 0 0 0 0 0
4 0 2 0 0.000000000E+00 0.000000000E+00 0.000000000E+00
5 6 9 8
2 5 4 2 0 0 0 0 0
.
.
.
.
.
.

3 1 5 20 0 0 0 0 0   material properties
0.000000000E+00 0.000000000E+00 0.000000000E+00 0.000000000E+00
0.000000000E+00

0.000000000E+00 0.185203000E+07 0.500000000E+01 0.000000000E+00
0.000000000E+00

0.000000000E+00 0.000000000E+00 0.000000000E+00 0.000000000E+00
0.733290005E+00

0.000000000E+00 0.000000000E+00 0.733290005E+00 0.000000000E+00
0.000000000E+00

0.000000000E+00 0.000000000E+00 0.000000000E+00 0.000000000E+00
0.000000000E+00

0.000000000E+00 0.000000000E+00 0.000000000E+00 0.000000000E+00
0.000000000E+00

0.000000000E+00 0.000000000E+00 0.000000000E+00 0.000000000E+00
0.000000000E+00

0.000000000E+00 0.000000000E+00 0.000000000E+00 0.000000000E+00
0.000000000E+00

0.000000000E+00 0.000000000E+00 0.000000000E+00 0.000000000E+00
0.000000000E+00

0.000000000E+00 0.000000000E+00 0.000000000E+00 0.000000000E+00
0.000000000E+00

0.000000000E+00 0.000000000E+00 0.000000000E+00 0.000000000E+00
0.000000000E+00

0.000000000E+00 0.000000000E+00 0.000000000E+00 0.000000000E+00
0.000000000E+00

0.000000000E+00 0.000000000E+00 0.000000000E+00 0.000000000E+00
0.000000000E+00

0.000000000E+00 0.000000000E+00 0.000000000E+00 0.000000000E+00
0.000000000E+00

0.000000000E+00 0.000000000E+00 0.000000000E+00 0.000000000E+00
0.000000000E+00

0.000000000E+00 0.000000000E+00 0.000000000E+00 0.000000000E+00
0.000000000E+00

0.000000000E+00 0.000000000E+00 0.000000000E+00 0.000000000E+00
0.000000000E+00

0.000000000E+00 0.000000000E+00 0.000000000E+00 0.000000000E+00
0.000000000E+00

0.000000000E+00 0.000000000E+00 0.000000000E+00 0.000000000E+00
0.000000000E+00

0.000000000E+00

.

.

.

.
.
.

10 1 1 1 1 0 0 0 0   initial temperatures
 0.250000000E+02
10 2 1 1 1 0 0 0 0
 0.250000000E+02
10 3 1 1 1 0 0 0 0
 0.250000000E+02
10 4 1 1 1 0 0 0 0
 0.250000000E+02
10 5 1 1 1 0 0 0 0
 0.250000000E+02
10 6 1 1 1 0 0 0 0
 0.250000000E+02
10 7 1 1 1 0 0 0 0
 0.250000000E+02
10 8 1 1 1 0 0 0 0
 0.250000000E+02
10 9 1 1 1 0 0 0 0
 0.250000000E+02
10 10 1 1 1 0 0 0 0
 0.250000000E+02
10 11 1 1 1 0 0 0 0
 0.250000000E+02

.
.
.
.
.
.
.

17 69 1 2 1 0 0 0 0   convection coefficients
0 01100000
 0.200000000E+07
17 74 1 2 1 0 0 0 0
0 01100000

```
   0.200000000E+07
17 79 1 2 1 0 0 0 0
0 01100000
   0.200000000E+07
17 84 1 2 1 0 0 0 0
0 01100000
   0.200000000E+07
17 170 1 2 1 0 0 0 0
0 01100000
   0.200000000E+07

   .

   .

   .

   .

18 69 1 2 1 0 0 0 0                    temperature cycle flags
0 01100000
   0.100000000E+01
18 74 1 2 1 0 0 0 0
0 01100000
   0.100000000E+01
18 79 1 2 1 0 0 0 0
0 01100000
   0.100000000E+01
18 84 1 2 1 0 0 0 0
0 01100000
   0.100000000E+01
18 170 1 2 1 0 0 0 0
0 01100000
   0.100000000E+01

   .

   .

   .

   .

99 0 0 1 0 0 0 0 0                     end of file
```

"COMPACTION INPUT FILE"
```
25 0 0 1 0 0 0 0 0
```

COMPACTION MODEL P6 #2

26 0 0 1 330 293 4 0 0

10-JUL-91 14:17:54 2.4

1 1 0 2 0 0 0 0 0   nodal coordinates

0.000000000E+00 0.126999998E-01 0.000000000E+00

1G 6 0 0 000000

1 2 0 2 0 0 0 0 0

0.635000039E-02 0.126999998E-01 0.000000000E+00

1G 6 0 0 000000

1 3 0 2 0 0 0 0 0

0.127000008E-01 0.126999998E-01 0.000000000E+00

1G 6 0 0 000000

1 4 0 2 0 0 0 0 0

0.000000000E+00 0.151447495E-01 0.000000000E+00

.

.

.

.

.

.

2 1 4 2 0 0 0 0 0   element connectivity

4 0 1 0 0.000000000E+00 0.000000000E+00 0.000000000E+00

1 2 5 4

2 2 4 2 0 0 0 0 0

4 0 1 0 0.000000000E+00 0.000000000E+00 0.000000000E+00

2 3 6 5

2 3 4 2 0 0 0 0 0

4 0 1 0 0.000000000E+00 0.000000000E+00 0.000000000E+00

4 5 8 7

2 4 4 2 0 0 0 0 0

4 0 1 0 0.000000000E+00 0.000000000E+00 0.000000000E+00

5 6 9 8

2 5 4 2 0 0 0 0 0

4 0 1 0 0.000000000E+00 0.000000000E+00 0.000000000E+00

7 8 11 10

2 6 4 2 0 0 0 0 0

4 0 1 0 0.000000000E+00 0.000000000E+00 0.000000000E+00

8 9 12 11

.
.
.
.
.

3 1 5 20 0 0 0 0 0   element properties
 0.000000000E+00 0.000000000E+00 0.000000000E+00 0.000000000E+00
0.000000000E+00
 0.000000000E+00 0.000000000E+00 0.500000000E+01 0.000000000E+00
0.000000000E+00
 0.000000000E+00 0.000000000E+00 0.000000000E+00 0.000000000E+00
0.191474000E+08
 0.672450000E+07 0.000000000E+00 0.191474000E+08 0.000000000E+00
0.620990000E+07
 0.000000000E+00 0.000000000E+00 0.000000000E+00 0.000000000E+00
0.000000000E+00
 0.000000000E+00 0.000000000E+00 0.000000000E+00 0.000000000E+00
0.000000000E+00
 0.000000000E+00 0.000000000E+00 0.000000000E+00 0.000000000E+00
0.000000000E+00
 0.000000000E+00 0.000000000E+00 0.000000000E+00 0.000000000E+00
0.000000000E+00
 0.000000000E+00 0.000000000E+00 0.000000000E+00 0.000000000E+00
0.000000000E+00
 0.000000000E+00 0.000000000E+00 0.000000000E+00 0.000000000E+00
0.000000000E+00
 0.000000000E+00 0.000000000E+00 0.000000000E+00 0.000000000E+00
0.000000000E+00
 0.000000000E+00 0.000000000E+00 0.000000000E+00 0.000000000E+00
0.000000000E+00
 0.000000000E+00 0.000000000E+00 0.000000000E+00 0.000000000E+00
0.000000000E+00
 0.000000000E+00 0.000000000E+00 0.000000000E+00 0.000000000E+00
0.000000000E+00
 0.000000000E+00 0.000000000E+00 0.000000000E+00 0.000000000E+00
0.000000000E+00
 0.000000000E+00 0.000000000E+00 0.000000000E+00 0.000000000E+00
0.000000000E+00

0.000000000E+00 0.000000000E+00 0.000000000E+00 0.000000000E+00
0.000000000E+00
0.000000000E+00 0.000000000E+00 0.000000000E+00 0.000000000E+00
0.000000000E+00
0.000000000E+00 0.000000000E+00 0.000000000E+00 0.000000000E+00
0.000000000E+00
0.000000000E+00

.

.

.

.

.

6 238 1 2 0 0 0 0 0   initial pressures
01001000000110000 2
-0.101352000E+06
6 239 1 2 0 0 0 0 0
01001000000110000 2
-0.101352000E+06
6 240 1 2 0 0 0 0 0
01001000000110000 2
-0.101352000E+06
6 241 1 2 0 0 0 0 0
01001000000110000 2
-0.101352000E+06
6 242 1 2 0 0 0 0 0
01001000000110000 2
-0.101352000E+06

.

.

.

.

.

8 1 1 2 0 0 0 0 0   initial displacements
0100000
0.000000000E+00
8 4 1 2 0 0 0 0
0100000

0.000000000E+00
8 7 1 2 0 0 0 0
0100000
0.000000000E+00
8 10 1 2 0 0 0 0
0100000
0.000000000E+00

.

.

.

.

99 0 0 1 0 0 0 0 0   end of file

BIBLIOGRAPHIC DATA SHEET	1. Report No. CCMS-95-01, VPI-E-94-09	2.		3. Recipient's Accession No.
4. Title and Subtitle Development and Verification of a Resin Film Infusion/Resin Transfer Molding Simulation Model for Fabrication of Advanced Textile Composites				5. Report Date December 1994
				6.
7. Author(s) John Douglas MacRae, Alfred C. Loos, H. Benson Dexter, Jerry W. Deaton, Gregory H. Hasko				8. Performing Organization Rept. No. VPI-E-94-09, CCMS-95-01
9. Performing Organization Name and Address Virginia Polytechnic Institute and State University Department of Engineering Science and Mechanics Blacksburg, VA 24061-0219				10. Project/Task/Work Unit No.
				11. Contract/Grant No. NAG-1-343
12. Sponsoring Organization Name and Address Mechanics of Materials Branch National Aeronautics and Space Administration Langley Research Center Hampton, VA 23681-0001				13. Type of Report & Period Covered Interim Report 99 January 1992 - December 1994
				14.

15. Supplementary Notes

16. Abstract

The objective of this study was to develop a two-dimensional computer model for the simulation of the resin transfer molding/ resin film infusion processing of advanced composite materials. This computer simulation model is designed to provide aircraft structure and tool designers with a method of predicting the infiltration and curing behavior of a composite material component. For a given specified cure cycle, the computer model can be used to calculate the resin infiltration, resin viscosity, resin advancement, heat transfer within the component/tool assembly during processing and preform compaction. Formulations of the resin flow problem are given using the finite element/control volume technique based on Darcy's Law of flow through porous media. This technique allows for the efficient numerical calculation of the advancing resin front within the preform materials. The heat transfer in the fabric preform and tooling is analyzed using a transient finite element method which included the effects of convection on the tooling surfaces. Compaction behavior of the tooling assembly is analyzed using a simplified isotropic form of the plane elasticity equations. All of these solutions were coupled together in a quasi-steady state non-linear fashion inside the computer code. Simulation model verifications were carried out on individual components of the computer model. A verification of the flow model is carried out by a comparison with experiments reported in literature as well as two dimensional visualization studies performed for a center-port injection of a flat plate. The heat transfer model was verified using the experimental results of a thick section composite laminate processing. Verification of the compaction model were limited to the comparison of the final part dimensions. Two computer simulations were performed on two resin infusion cycles of a single blade-stiffened composite panel. The simulation model results of the two cycles were used to assist in the development of an alternative cycle for the composite manufacturing of a three blade stiffened panel. The results demonstrated the importance of a sufficient minimum viscosity region in the cycle in order to allow the resin to completely infiltrate the fabric preform of the structure. Predictions of the viscosities and degree of cure profiles within the single blade stiffened panel illustrated the uniformity of these parameters during the curing cycle.

17. Key Words and Document Analysis.   17a. Descriptors

RTM, resin transfer molding/resin film infusion, porous media flow, textile preforms, finite element/control volume, composite material processing, preform compaction

17b. Identifiers/Open-Ended Terms

17c. COSATI Field/Group

18. Availability Statement	19. Security Class (This Report) UNCLASSIFIED	21. No. of Pages 174
	20. Security Class (This Page) UNCLASSIFIED	22. Price